POLITECNICO DI MILANO

Scuola di Ingegneria Industriale e dell'Informazione

Corso di Laurea Magistrale in Ingegneria Biomedica

DEVELOPMENT OF A MULTISENSORY ACQUISITION SYSTEM FOR FLS TRAINING ASSESSMENT

Relatori: Prof. Elena De Momi

Prof. Marc Garbey

Correlatori: Prof. Ahmet Omurtag

Guillaume Joerger, PhD

Tesi di Laurea Magistrale di:

Andrea Panaccio (Matr. 853459)

Anno Accademico 2016/2017

RINGRAZIAMENTI

I miei ringraziamenti vanno alla professoressa Elena De Momi per la disponibilità e per avermi proposto questo progetto di tesi dandomi la possibilità di confrontarmi con una realtà americana importante come lo Houston Methodist.

I would like to thank my advisor Prof. Marc Garbey, Scientific Director from the Center for Computational Surgery of Houston Methodist, for the help, expertise and inexhaustible enthusiasm and Prof. Ahmet Omurtag for the always prompt availability despite the distance. I want to thank also Guillaume for the good advices and the constant help, Stefano for the introduction to the American life, Joseph, a very good friend, Shannon, Juliette, Remi, Adeline, Louis, Anne-Cecile, Aman and all the others from the lab for the nice experience.

A special thanks to Monika without which these seven months wouldn't have been the same and to Nicolas, Heidi, Pierre, Juliane, Claudia, Martina and all the other people I met for the great time spent together.

Agli amici in Italia, da Cesena a Milano passando da quelli storici di Bagna e dintorni che ancora oggi, dopo tanto tempo, fanno parte della mia vita. In particolare a Enri, mio coinquilino, Sara e Augusto per le avventure, le risate e le difficoltà che abbiamo condiviso in quest'ultimo periodo di studi a Milano, felicissimo di concludere questo percorso assieme così come era cominciato.

Infine ma non per importanza alla mia famiglia, per avermi sempre sostenuto nelle mie scelte, aiutandomi nei momenti di difficoltà ed avermi spinto a dare sempre il massimo senza mai staccare il piede dall'acceleratore.

TABLE OF CONTENTS

LIST OF FIGURES

LIST OF TABLES

Abstract

Background and purpose. Laparoscopic surgery is a very common surgical procedure whose benefits for the patient and the relative low cost make it preferable respectively to open surgery and robotic surgery. However, it constitutes also a challenge for the surgeons due to the required training in order to archive a good proficiency. The training is a very important part of each learning program, in particular in the surgical field where it is a key point to be efficient in the OR later on. Previous studies report as surgeons are exposed to a large number of stressors. Despite it was proved that stressful condition can affect the performance, there are still a low number of medical trainings which encompass this aspect in their leaning module unlike fields such as military and civil aviation. Previous studies on stress, anxiety, mental load have shown how they can be estimated from an analysis of physical (e.g. eye gaze, movement, pupil size) and physiological (e.g. heart and brain activities) measurements which can be measured with non-invasive and unobtrusive sensors. However, the analysis of these signal cannot disregard an evaluation of the performance itself.

This work was focused on the practical part of the Fundamental of Laparoscopic Surgery (FLS) educational program offered by SAGES and ACS and mainly diffused in the US and Canada. The study aims at the development of a multisensory acquisition system for an evaluation of the FLS performance. In particular, the purpose is to realize a system which encompasses different devices and algorithms that allow to extract information of different nature describing the status and the behaviours of the subject during the performance. These information were used to conduct a preliminary analysis on a subset of data and constitute the input for future studies aimed at the identification of parameters which allow to extend the evaluation of the FLS performance to the physiological and stress conditions. This project of thesis was conducted at the Center for Computational Surgery (Department of Surgery, Houston Methodist, Houston, TX) during an internship of six months.

Material and methods. A new FLS scoring metric, based on the evaluation of the video of the performance, was created to overcome the limits of the standard FLS metric. However, this kind of metric is not able to provide information about the subject behaviour and the physiological and mental demands during the task.

There is not an a-priori specific sensor that can be used to detect the stress and the mental load. Therefore, it was decided to include in this first version of the platform a large gamma of sensors providing different kind of information. They encompass the use of video-cameras, Smart Trocars, Eye Tracking (ET), physiological monitoring through Smart Cloth (Hexoskin) and EEG. The acquisition system makes use of a GUI realized in Matlab and of the software of the devices.

The Matlab GUI ensured to display a real-time video from the camera inside the trainer box and allowed to acquire videos from the four cameras with a maximum frame rate of 5Hz.

The extraction and the synchronization among signals from the different devices was done offline with Matlab making use of the Unix (posixtime) timescale.

A new version of the image analysis algorithm for the Smart Trocars to reconstruct the 2D movement of the tool was implemented to face particular luminosity conditions of the room. Moreover, an algorithm for the detection of the blinking was developed based on a multimodal analysis of EEG and ET data allowing to overcome the limits of the analysis conducted on the single devices.

1. Laparoscopic tool 2D motion: The algorithm for the estimation of the 2D motion of the laparoscopic tool consists in an image analysis of the video made by the camera located on the side of the trocar. The camera points toward the ceiling where some flat black square-shape panels were attached. Each square can be identified from its inside white pattern. The algorithm recognizes the squares in each frame and extracts their features points (i.e. corners and centroids). Corresponding points in subsequent frames were given in input to an ICP registration algorithm to estimate the roto-translational transform frame by frame.
2. Blinking detection: The algorithm for the blinking detection was based on a multimodal analysis of ET and EEG data. In the ET data analysis, the time intervals of eyes non captured by the device with a duration lower than 400 ms were considered blinking candidates. From the EEG data, an amplitude and spectral analysis were conducted on the signals coming from Fp1 and Fp2 electrodes which are located on the front over the eyes. The final blinks were identified comparing the candidates obtained from the analysis of single devices.

The system was tested on 12 healthy subjects subdivided into three categories of different expertise level: 4 Beginners who were not from the surgical field, 5 Residents and 3 Experts from the Houston Methodist Hospital.
The experimental protocol comprises a resting phase followed by the performance of three selected tasks of the FLS module (Peg Transfer, Precision Cutting and Suture with Intracorporeal Knot) during which the Attentional Tunnelling concept was tested through the use of external sounds. The GUI was used during the acquisition mainly to manage the information of the participant, the video acquisitions (from the face camera, 2 trocars' cameras and the laparoscopic camera), the serial communication with the trigger box of the EEG and to keep track of the time references of all the events along each task.
The ET was used to retrieve information about the eyes, the dry EEG for the brain activity through 19 electrodes on the scalp (10-20 system) and the Smart Cloth for the heart and respiratory activities.
Reports on a subset of signals were created for each subject with two purposes: to find particular trends or reaction to specific events within a subject and to compare the data among different subjects.
They encompass mainly graphs of some selected signals from the ET and the Smart Cloth, their mean, std and mean variation. In particular, they are the eyes gaze, the pupil dimension, the blinking rate, the Heart Rate, the Breathing Rate, the NN intervals, the Tidal Volume.
The videos of the performances were observed to keep track of the time occurrence of specific events such as actions (e.g. grasp or release an object), phases (e.g. completion of ¼ of cutting of the circle) or errors (e.g. drop of an object). Using specific symbols, all these events plus the blinking and the sound occurrences were reported on the graphs.

Validations and Results. A series of tests were conducted to validate the new algorithm for the 2D reconstruction of the motion of the tool showing a registration error of the ICP of a maximum of 4 pixels in good quality images. However, the method is strongly affected by the presence of blur in the image which causes an increase of the error.
The videos of the frontal camera were used as ground truth to validate the algorithm for the blinking detection. Tests have shown that the algorithm is able to detect all the blinks in standard conditions but its accuracy decreases in the analysis of performances which are strongly affected by movement artifacts.

The usage of the new scoring metric were useful to highlight differences among subject with different expertise level by simply evaluating the performance video.
From the preliminary analysis on subgroup of signals (mainly from ET and smart cloth), it was noticed that the ET is a valuable source of information to describe the level of focus highlighting differences among categories and the blinking rate, which is low during exercises, increases in moments of major difficulty. In some subjects, an increase of the Tidal Volume irregularity was recognized during difficult situations.
Even if the pupils size was found to increase from rest to task, their dimension remain constant during the exercise. Large part of the heart activity signals from the Hexoskin smart cloth were found to be affected by errors detected by the device itself.

Discussion and Conclusions. The study proposed an acquisition setup and some algorithms to retrieve a large quantity of information of different nature from the FLS training in a non-invasive and unobtrusive way. The system received good feedbacks from all the surgical experts who tried it. The algorithm for the blinking detection allowed a more robust identification of the blinks with respect to the analysis conducted on the single devices. The algorithm for the reconstruction of the 2D motion of the tool can be used to estimate the entity of the movement frame by frame.
The observations on the reports suggested that ET and respiration data could contain signals of interest. Moreover, an improvement of the platform is required due to the inefficacy of the sound as trigger of the Attentional Tunnelling and to the low quality of about 1/3 of the cardiac data. This study could be extended by a future in depth analysis of all the signals to find relevant parameters which can be included in the evaluation of the FLS program.

Sommario

Background e scopo. La chirurgia laparoscopica è una pratica molto comune i cui benefici per il paziente e il relativo basso costo la rendono preferibile alla chirurgia aperta e robotica. Tuttavia, essa costituisce anche una sfida per i chirurghi in quanto, per raggiungere una buona competenza, è necessario un adeguato allenamento. Il training infatti è una parte molto importante di ogni programma di apprendimento, in particolare nel campo chirurgico dove è un punto chiave per aumentare l'efficienza in Sala Operatoria. Studi precedenti sottolineano come i chirurghi siano esposti ad un gran numero di fattori di stress.

Nonostante sia stato dimostrato che una condizione di stress può influire sulle performance, sono ancora pochi i training in medicina che tengono in considerazione questo aspetto nel loro programma a differenza di quanto avviene in campi come il militare e l'aviazione civile. Studi precedenti su stress, ansia e carico mentale hanno mostrato come essi possano essere stimati a partire dall'analisi di segnali fisici (es. sguardo, movimento, dimensione delle pupille) e fisiologici (es. attività cardiaca e cerebrale) che possono essere misurati tramite sensori non invasivi e non ostruttivi. Tuttavia l'analisi di questi segnali non può prescindere da una valutazione della performance stessa.

Questo lavoro è stato incentrato sulla parte pratica contenuta nel programma di "Fundamental of Laparoscopic Surgery" (FLS) offerto da SAGES e ACS e principalmente diffuso in US e Canada. Lo studio mira allo sviluppo di un sistema di acquisizione multi-sensore per la valutazione delle prestazioni in FLS. In particolare, lo scopo è quello di realizzare un sistema che comprende vari strumenti e algoritmi che permettono di estrarre informazioni di diversa natura descriventi lo stato e i comportamenti del soggetto durante la performance. Queste informazioni sono state utilizzate per condurre un'analisi preliminare su un sottogruppo di dati e costituiscono l'input per studi futuri finalizzati all'identificazione di parametri che consentano di estendere la valutazione delle prestazioni di FLS alle condizioni fisiologiche e di stress. Questo progetto di tesi è stato condotto presso il Center for Computational Surgery (Department of Surgery, Houston Methodist, Houston, TX) durante un tirocinio di sei mesi.

Materiali e metodi. Una nuova metrica per la valutazione dei task di FLS, basata sull'esaminazione del video della performance, è stata realizzata per superare i limiti della

metrica standard del programma FLS. Tuttavia essa non è in grado di fornire informazioni sul comportamento del soggetto e le sue richieste fisiologiche e mentali durante l'attività.
Non vi è un sensore specifico che possa essere usato a-priori per stimare lo stress o il carico mentale. Perciò, è stato deciso di includere in questa prima versione della piattaforma una larga gamma di sensori che forniscono diversi tipi di informazioni. Essi comprendono un Eye Tracker (ET), uno Smart Cloth, l'EEG, gli Smart Trocars e diverse telecamere. Il Sistema di acquisizione fa uso di una GUI che è stata realizzata in Matlab e dei software dei vari device. L'interfaccia in Matlab garantisce il real-time del video della camera all'interno del box e permette l'acquisizione video da tutte e 4 le telecamere con una frame rate massima di 5Hz. L'estrazione e la sincronizzazione tra segnali di differenti strumenti è stata eseguita offline usando Matlab facendo uso della scala temporale Unix (posixtime).
Una nuova versione dell'algoritmo di image-analysis per gli Smart Trocar è stata realizzata per far fronte alle condizioni di luminosità della stanza in cui sono stati condotti i test.
Inoltre, al fine di detettare il blinking, è stato sviluppato un algoritmo basato sull'analisi multimodale dei dati di EEG e ET che ha consentito di superare i limiti dell'analisi fatta con i singoli dispositivi.

1. Moto 2D del tool laparoscopico: L′algoritmo per la stima del moto 2D dello strumento laparoscopico consiste in un image-analysis del video prodotto dalla camera posizionata a lato di ciascun trocar. La camera punta verso il soffitto sul quale sono stati posizionati vari poster a forma di quadrato nero. Ogni quadrato può essere identificato dal suo pattern bianco interno. L′algoritmo riconosce i quadrati in ciascun frame ed estrae i loro punti caratteristici (cioè i vertici e i centroidi). Punti corrispondenti in frame successivi sono stati dati in input ad un algoritmo di registrazione ICP per stimare la trasformata di roto-traslazione frame per frame.
2. L′algoritmo per la detezione del blinking è basato su un′analisi multimodale dei dati di ET e EEG. Nell′analisi dei dati dell′ET, gli intervalli di tempo in cui gli occhi non sono stati catturati dal device, con una durata inferiore ai 400ms, sono stati considerati possibili candidati di blink. Un′analisi in ampiezza e un′analisi spettrale sono state condotte sui segnali dell′EEG provenienti dagli elettrodi Fp1 e Fp2 posizionati sulla fronte sopra agli occhi dei partecipanti. I blink finali sono stati identificati comparando i candidati ottenuti dalle analisi dei singoli devices.

Il sistema è stato testato su 12 soggetti sani suddivisi in tre categorie di diverso livello di esperienza: 4 Principianti (Beginners) non provenienti dal campo chirurgico, 5 Specializzandi (Residents) e 3 Esperti (Experts) provenienti dallo Houston Methodist Hospital.

Il protocollo sperimentale comprende una fase di riposo seguita da tre esercizi del programma di FLS (Peg Transfer, Precision Cutting and Suture with Intracorporeal Knot) durante i quali è stato testato il concetto di Attentional Tunneling utilizzando suoni esterni.

L'interfaccia è stata utilizzata durante l'acquisizione principalmente per gestire le informazioni del partecipante, per l'acquisizione di video (da una videocamera frontale, le due camera dei trocar e la camera laparoscopica), per la comunicazione seriale con il trigger box dell'EEG e per tener traccia dei rifermenti temporali di determinati eventi che caratterizzano ciascun esercizio.

L'ET è stato usato per ottenere informazioni relative agli occhi, il Dry EEG per l'attività cerebrale attraverso 19 elettrodi sullo scalpo (sistema 10-20) e lo Smart Cloth per l'attività cardiaca e per quella respiratoria.

Per ogni soggetto è stato creato un report su un sottogruppo di segnali con un duplice scopo: trovare particolari trend o reazioni a specifici eventi e confrontare dati tra diversi soggetti.

Il report di ogni soggetto comprende principalmente grafici di alcuni segnali selezionati dall'ET e dallo Smart Cloth, la loro media, deviazione standard e variazione media. In particolare, quelli di maggior interesse, sono la posizione dello sguardo sullo schermo, la dimensione delle pupille, la blinking rate, la frequenza cardiaca, la frequenza respiratoria, gli intervalli NN e il volume d'aria corrente (Tidal Volume). I video delle performance sono stati osservati per tener traccia dell'occorrenza temporale di specifici eventi quali azioni (es. afferrare e rilasciare oggetti), fasi (es. completamento di ¼ del taglio del cerchio) o errori (es. caduta di un oggetto). Tutti questi eventi con l'aggiunta del blinking e dell'occorrenza del suono sono stati aggiunti ai grafici usando una determinata simbologia.

Validazioni e risultati. Una serie di test è stata condotta per validare il metodo per la ricostruzione 2D del moto del tool ottenendo un massimo errore di registrazione dell'algoritmo di ICP di 4 pixel per immagini di buona qualità. Tuttavia, il metodo è fortemente affetto dalla presenza di sfocatura nell'immagine che causa un incremento dell'errore.

I video della camera frontale sono stati usati come ground truth per validare l'algoritmo per la detezione dei blinks. I test hanno mostrato come l'algoritmo sia capace di detettare tutti in blink in condizioni standard ma che la sua accuratezza cala nell'analisi di performance fortemente affette da artefatti da movimento.
L'utilizzo della nuova metrica di valutazione è stato utile per evidenziare le differenze tra soggetti con un diverso livello di esperienza semplicemente analizzando i video delle performance.
Dall'analisi preliminare su un sottogruppo di segnali (principalmente da ET e Smart Cloth) si è notato che l'ET è una valida fonte di informazione per descrivere il livello di focus del soggetto evidenziando differenze tra le varie categorie e che la blinking rate, che in generale è bassa durante gli esercizi, tende ad aumentare nei momenti di maggiore difficoltà. In alcuni soggetti è stato riscontrato anche un incremento dell'irregolarità del Tidal Volume durante situazioni complicate. Sebbene sia stato notato un incremento della dimensione delle pupille dalla fase di riposo rispetto la fase degli esercizi, questa è poi rimasta constante durante il task. Larga parte dei segnali relativi all'attività cardiaca è stata caratterizzata dalla presenza di vari errori rilevati dallo stesso device.

Discussione e conclusioni. Lo studio propone un setup di acquisizione e alcuni algoritmi per estrarre una grande quantità di informazioni di diversa natura dal training di FLS in maniera non invasiva e non ostruttiva. Il sistema ha ricevuto feedback positivi dei vai esperti chirurgici che hanno avuto modo di provarlo. L'analisi multimodale dell'algoritmo per la detezione del blinking permette una sua più robusta identificazione rispetto all'analisi condotta sui singoli device. L'algoritmo per la ricostruzione 2D del moto dello strumento può essere usato per stimare l'entità del movimento frame per frame.
Le osservazioni sui report suggeriscono che i dati respiratori e dell'ET possano contenere segnali di interesse. Inoltre hanno evidenziato come sia necessario un miglioramento della piattaforma data l'inefficacia del suono come trigger dell'Attentional Tunnelling e la bassa qualità di circa 1/3 dei dati relativi all'attività cardiaca. Questo studio potrà essere esteso da studi futuri riguardanti una profonda analisi di tutti i segnali ottenuti al fine di trovare parametri che possano essere inclusi nella valutazione del programma FLS.

Chapter 1 Introduction

Laparoscopy has experienced a significant growth since the nineties becoming a very common surgery procedure. As can be seen from a recent statistical report of Eurostat [1] for the period 2009-14, among a selection of five surgical operations and procedures which have become more frequent, four of these concern laparoscopic techniques. In the United States, according to iData Procedure Tracker, it has been estimated an amount of 3.5 million laparoscopic procedures performed in the US across 12 procedure types and it has been determined that the three States that have the highest number of laparoscopic procedures performed are California, Texas and Florida [2].

Section 1.1 presents a background about laparoscopy and its pro and cons compared to other techniques.

Section 1.2 introduces a laparoscopic training diffused in the USA (FLS) and the concept of stress.

1.1 Laparoscopy background

Laparoscopy is a surgical procedure used to examine the organs inside the abdomen. It can be used for both diagnostic and operational purposes.

It is also referred to as minimally invasive surgery and it is a popular alternative to open surgery due to the considerable reduction of recovery time, pain, scaring, and complications. The performance is conducted with the assistance of laparoscope (camera) and several thin instruments.

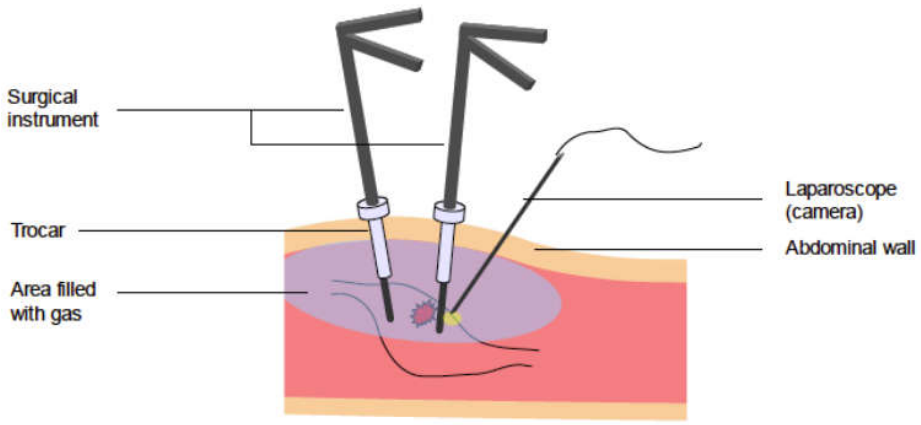

Figure 1.1: A laparoscopic procedure [3]

On the contrary of a conventional open surgery, the surgeon makes small incisions (up to 1.5 cm) on the abdomen of the patient and plastic tubes called Trocars are placed through these incisions (Figure 1.1). Gas, usually carbon dioxide, is injected within the cavity to achieve a better manipulation of the tools and visualization of the organs.

The camera captures a video of the organs inside the abdomen and its stream is sent to a monitor. Therefore, the video-camera becomes the surgeon's eyes in laparoscopy surgery, since the surgeon uses the image from the camera positioned inside the patient's body to perform the procedure [3].

Implementation of laparoscopic surgery has had a significant impact on surgical outcomes, mainly by increasing the speed of postoperative recovery and subsequent discharge from the hospital.

Laparoscopic surgery has introduced lots of advantages for the patients with respect to the corresponded open surgery procedure [4].

The Pro of a conventional open surgery procedure mainly concerns the possibility to directly interact with the structures inside the abdomen:

- The surgical procedure takes place under the direct vision of the surgeon
- The structures and tissues involved in the procedure can be directly seen, touched and manipulated.

But it presents also lots of cons as:

- Large wounds on the abdomen to access the organs.
- Long time to heal
- It causes ongoing pain during recovery
- It leave large scars on the abdomen

The introduction of laparoscopic surgery [3], [5], being a minimally invasive procedure, has brought many advantages such as:

- Smaller surgical scars
- Reduced blood loss during surgery
- Less pain following surgery
- Shorter hospital stay
- Faster return to normal activity
- Reduced risk of infection.

But this procedure presents also disadvantages/challenges for the surgeon such as:

- Special training required due to the fact that the procedure is completely different from an open surgery one.
- Indirect access to the organ: no more direct touch but only through the instruments.
- Lower mobility: limited to the fixed rotational points (incisions)
- The lack of depth perception: during laparoscopy the surgeon has to rely only on the video provided by the laparoscopic camera. The first change regard the fact that the surgeon has to watch a screen instead of the subject and the second is that he has to obtain depth information based on 2D images.

Despite the introduction of Laparoscopy, the research in this field has not been abandoned. Lots of effort has been made to overcame its limitations, especially in the robotic field. The 'Da Vinci' Surgical System is a perfect example of robotic device that has been introduced as the next advance in minimally invasive surgery to overcome the technical limitations of a standard laparoscopy [6].

A robotic scenario with the 'Da Vinci' can be observe in Figure 1.2 where the surgeon sits at a console and uses hand controls to manipulate the robotic arms located at the patient's side, rather than holding and manipulating the tools themselves as in a standard laparoscopic surgery.

Figure 1.2: The left image represents an example of robotic surgery scenario with the master console, the robotic arms and the surgical assistant. The right image represents a focus of the master console itself

As in a laparoscopic procedure, the surgeon makes an incision in the abdominal cavity for the insertion of an endoscope. After expanding the abdominal cavity with carbon dioxide gas for accurate visualization and operative manipulation, three additional small incisions are made to place narrow tubes used for interchangeable instruments. The robotic arms are

located on the patient side (slave side) together with a surgical assistant or/and nurse and the surgeon sits at the control console (master side) located in the room. One or two additional small tubes are often placed for the surgical assistant to use. If the surgeon console is not located in the same room of the patient, the procedure is named Telerobotic surgery, or remote robotic surgery [7].

The benefits [7]–[9] of robotic surgery are:

- Short recovery: As in any laparoscopic procedure, robotic surgery usually leads to a quicker recovery and less post-operative pain compared to open-incision surgery.
- 3D view: the endoscope is composed by 2 cameras which provide a 3D view of the intern of the patient.
- Increased surgeon control: In laparoscopic surgery, each hand controls one instrument or the camera (a total of two items at the same time). On the other hand, in robotic surgery, the surgeon controls all camera movements and three instruments (four items).
- 'Scaling' of the movement: large movements of the surgeon in the master console correspond to small movements of the robotic instruments. This added precision is particularly useful with the system's magnified view avoiding erroneous and dangerous movements.
- Wrist-like movements: they tip of the instruments move like a human wrist. This provides greater range of motion, more precision and a more intuitive movement.

However, robotic surgery has to deal with two main problems: the cost-effectiveness of the procedures which are higher [10] in comparison to standard laparoscopy and the lack of a full haptic information on which research is focusing the attention.

For these reasons, standard laparoscopy is still widely diffused. Overall, minimally invasive surgery has brought lots of benefits for the patients with respect to open surgery procedures but it constitutes a challenge for the surgeons due to the required training in order to archive a good proficiency.

This work deals with the training required for standard laparoscopy.

1.2 Introduction to the FLS training and to the stress concept

In 1997, The Society of American Gastrointestinal and Endoscopic Surgeons (SAGES) created an educational program called "The Fundamentals of Laparoscopic Surgery" (FLS). FLS is an education module aimed to teach the fundamental knowledge and skills required in a basic laparoscopic surgery. It includes hands-on skills training and knowledge

components. The content of FLS is appropriate for surgical trainees as well as practicing surgeons [11].

Prior the advent of the FLS program, learning laparoscopic surgical techniques was a haphazard affair for many surgeons. At the beginning, everybody were sure about the value of the technique but there were two main problems: first, the low availability of prepared teachers and second, the differences in the training formant provided though industry-founded courses. Usually, surgeons were used to attend courses and then go back to the hospital and get credentials but the obtained knowledge was very inhomogeneous [12].

The goal of the FLS program was to create a training program different from a regular educational test where you just passively go into a room and observe things, or in which you do random operations on animals. On the contrary, FLS is highly structured, and it comprises a verification part to ensure to have some basis to decide if give or not a diploma to the candidate. In this way, minimum standards of cognitive and technical skills were established. FLS measurements have been considered to be highly reliable and valid measures of laparoscopic skill [13]. The FLS program has become a standard of validated surgical training for residency education in America.

In the modern surgical practice, two of the main crucial elements are the quality and safety of the performance in the Operating Room and, therefore, of the patient outcome. It has been highlighted as the performance can be affected by technical skill as well as nontechnical skills which include communication, teamwork and decision making [14].

“In a medical or biological context stress is a physical, mental or emotional factor that causes bodily or mental tension. Stresses can be external (from the environment, psychological, or social situations) or internal (illness, or from a medical procedure)..” [15].

It is true that some Emotional stress can lead to an improvement of the performance by enhancing concentration, focus, alertness and efficiency of action, but when stress is too high, performance is compromised.

Despite this belief, the evaluation of performances in stressful training conditions is still not so common in the surgical field. This lack could lead to have surgeons which are poorly prepared for the complex demands of the real operative environment.

Chapter 2 State of the art and Aim of the work

The following Chapter presents in what consists the FLS training program, the principal measurements of stress and the aim of the work.
Section 2.1 describes the FLS educational training program while Section 2.2 reports some studies related to it.
Section 2.3 provides a comprehensive overview about the common measures of stress and Section 2.4 explores its impact on the performance.
Section 2.5 explains the aim of the work and Section 2.6 presents its structure.

2.1 FLS training program

The "Fundamentals of Laparoscopic Surgery" (FLS) training program has been created by SAGES in 1997. It is an education module aimed to teach the fundamental knowledge and skills required in a basic laparoscopic surgery and it includes hands-on skills training and knowledge components.
The final exam comprises two tests:

- A cognitive test consisting of multiple-choice questions. It is computer-based and it is designed to evaluate the knowledge and the application of the basic fundamentals of laparoscopy together with clinical judgment and intra-operative decision-making.
- A manual skills test consisting of five simulation exercises aimed to teach the most common psychomotor skills necessary for basic laparoscopic surgery. They are non-procedure specific and they are used both for training and final assessment.

Both components of the test have been carefully designed and examined by experts within the field of laparoscopic surgery. Only physicians (MD, DO, or MBBS or equivalent) are eligible to take the FLS test. It is equivalent to say that this program is directed only to surgical residents, fellows and practicing physician [16]. Just to clarify, Residents are physicians who want to pursue a specialization training in a hospital or clinic under the direct or indirect supervision of an attending physician. Residency training may be followed by fellowship. Anyway, the unstructured practical tasks of which it is composed, allow it to be directed not only to general surgeons, but also to urologists, gynaecologists, or thoracic surgeons practicing minimally invasive surgery.

But why a practicing surgeon would need the FLS Program? Nowadays, it is more and more common that physicians are asked to provide certification to demonstrate their abilities. In this sense, the FLS program meets the need providing an accredited certification to a successful participant.

The program content has also been endorsed by the American College of Surgeons (ACS) and is a joint educational offering of SAGES and ACS. FLS is also CME (Continuing Medical Education) accredited and since October 1, 2012 the issued certification is not valid indefinitely. In fact, it must be recertified every 10 years by successfully complete again the entire test. So, the FLS program has become a standard of validated surgical training for residency education in US and Canada. In 2014 it has been estimated that since the its introduction, more than 9,000 surgical residents, fellows, and practicing physicians have successfully completed the FLS program [12]. Moreover, the program is not only confined in US and Canada but it has been asked and used from other groups worldwide.

This work has been focused on the practical surgical tasks that are part of the module. They encompass several deconstructed surgical tasks that the trainee must complete within the allotted time span and with a good accuracy to be considered proficient [17].

The FLS manual skills program consists of 5 tasks of increasing complexity (Figure 2.1). They are:

- Peg Transfer
- Precision Cutting (for the sake of simplicity: Circle Cut)
- Ligating Loop
- Suture with Extracorporeal Knot (for the sake of simplicity: Extracorporeal Knot)
- Suture with Intracorporeal Knot (for the sake of simplicity: Intracorporeal Knot)

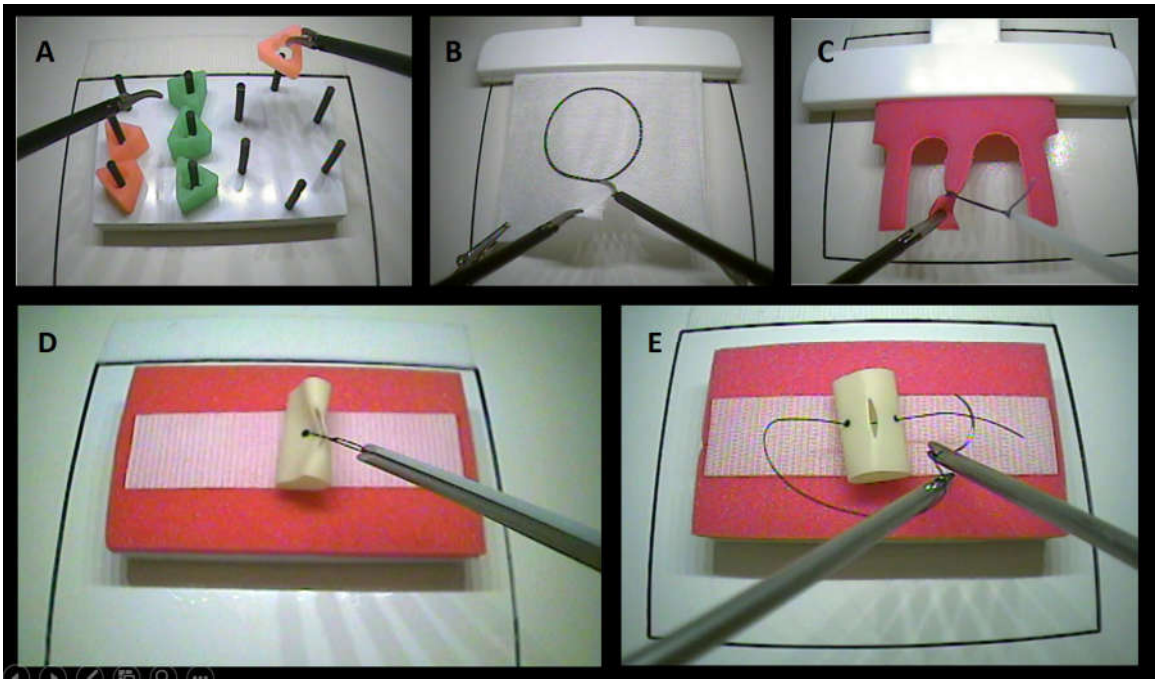

Figure 2.1: FLS manual tasks: (A) Peg Transfer, (B) Precision Cutting, (C) Ligating Loop, (D) Suture with Extracorporeal Knot and (E) Suture with Intracorporeal Knot [17]

All these tasks are part of the final evaluation and must be performed once during the test. Each task must be completed within a maximum time and a proper scoring formula based upon a combination of time and accuracy measures is defined. High scores are related to completion of the exercise performed efficiently and without errors. If you don't complete the exercise within the maximum time, you will be asked to stop and the assigned score for the exercise will be zero. Moreover, the completion of the exercise doesn't guarantee a passing score for the specific task. The scores for the tasks are normalized so that they contribute equally to the total manual skills assessment score.

The trainee can practice and he will perform the final exam using a physical simulator called FLS trainer box. As can be observed in Figure 2.2A, it consists in an open box that simulates the patient abdomen with an internal camera instead of using a laparoscope and two holes on the top for the insertion of the tools. On the base, there is a marked square with a Velcro strips in the center in which the scenario for the specific exercise can be set up with all the required accessories (Figure 2.2B). The internal camera can be tilt in order to include the whole area inside the black contour but it cannot be moved during the exercise. Its stream is sent to a movable monitor that together with the base of the platform can be regulate in height based on how tall is the subject.

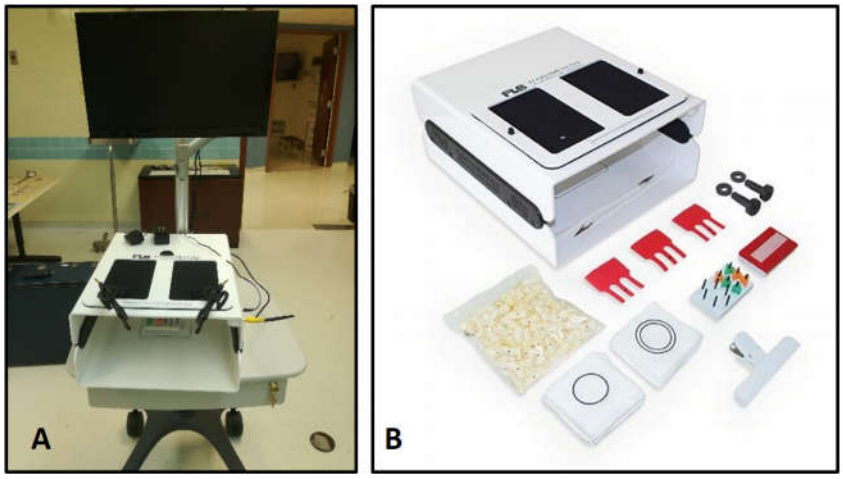

Figure 2.2: (A) FLS trainer box with TV monitor, (B) FLS accessories

A description of each single task will follow [17].

Task One: Peg Transfer

The aim of this test is to develop depth perception and visual-spatial perception in a monocular viewing system and the coordinated use of both the dominant and nondominant hands [18].

A pegboard must be placed in the center of the marked square attached to the Velcro strip. The pegboard is made by 12 pegs, organized into groups of 6 which form 2 different patterns (Figure 2.1A). All the six colored ring objects should be aligned on the group of pegs on the same side of the board as the subject non-dominant hand (it is not important which is the pattern in which they are placed). The task consists into grasp each object with the Non-dominant hand and transfer the object mid-air to the dominant hand. Then, the object must be placed on one of the six pegs on the opposite side of the pegboard. It is not important the order in which the objects are transferred or the peg in which they are placed. During the transportation of the object, the board or pegs cannot be used for assistance. Once all six objects have been transferred to the opposite side of the board, the process is reversed: first the object is grasped with the dominant hand, transferred mid-air to the non-dominant hand, and placed on the original side of the pegboard. It is not important to put the object in its original position. Penalties are assessed for no mid-air transfer, for object dropped outside the field of view or in general for not retrievable objects. In case the subject is not able to retrieve it, he can continue the exercise until the end. Moreover, if he can retrieve the object, he must pick it up with the same hand it was dropped with and continue the exercise. Timing for this task begins when you touch the first object and it ends when you release the last one.

Task Two: Precision Cutting

The aim of this test is to learn the concept of traction and the need to use the nondominant hand to provide a convenient working angle for the dominant hand, all within the constraints of fixed trocar positions [18].

The two-ply gauze must be placed into the jumbo clip with the folded edge on the opposite side of it as it is shown in Figure 2.1B The circle marker must be facing up and the alligator clips are used to secure the bottom corners of the gauze and suspend it. The Maryland dissector is used to provide traction to the gauze, placing it at the best possible angle to the cutting hand. Then, using the endoscopic scissors in the other hand, the trainee has to cut into the gauze and then along the pre-marked circle until it is completely removed from the 4x4 gauze piece. He must start cutting from the edge of the gauze and he can switch hands with your instruments at any time during the task. Only the upper layer is scored and a penalty is assessed for any cuts deviating from the line demarcating the circle, whether made inside or outside the marked circle. If the gauze comes out of the jumbo clip during the task, the subject can finish the exercise but he cannot reaffix it. Timing ends when the marked circle is completely cut off.

Task Three: Ligating Loop

A foam organ must be placed into the jumbo clip with the three appendages hanging out the bottom of the clip as shown in Figure 2.1C. The trainee must introduce the pretied ligating loop (endoloop) through one trocar, while controlling a tubular structure (foam appendage) using a grasping forceps through the other trocar. He will knot the loop around the middle appendage at the provided mark. To complete the task the subject must cut the end of your loop material. A penalty is assessed if the loop is not accurately placed on the target line or if the knot is not secured on the appendage. He mustn't break or preload the ligating loop prior to beginning the task. The time starts when either the instrument or the loop material enter the field of view of the camera and it ends when the trainee have cut the end of the loop material inside the trainer box.

Task Four: Suture with Extracorporeal Knot

A penrose drain must be securely place onto the Velcro strip with the slit in vertical position as it is shown in Figure 2.1D. In this task, a long suture must be placed through the two marks in the penrose drain and then the participant has to tie three single throws of a knot, extracorporeally, using a knot pusher to secure each throw onto the penrose drain, thus,

closing the slit. Once all three knots have been secured, both the ends of the suture must be cut inside the trainer. Any deviation of the suture material from the two marks on the penrose drain is subjective to a penalty, as for not properly closing the slit in the drain, and for a knot that comes apart when tension is applied to it. The time starts when the instrument enters the field of view of the camera and it ends when both ends of your suture are cut.

Task Five: Suture with Intracorporeal Knot

The setup and the procedure are similar to the 4th task as can be seen in Figure 2.1E. On the contrary of it, the trainee must tie three throws of a knot intracorporeally, in order to close the slit in the penrose drain. The first throw must be a surgeon's one or double throw, followed by two single throws. The hand that hold the needle must be exchanged hands after each throw ensuring to tie subsequent throw with the opposite hand. Penalties and timing follow the same rules of the 4th task.

A summary of the tasks characteristics is reported in the following table (Table 2.1)

Task	Objective	Equipment	Time Limit
Peg Transfer	Six plastic objects are grasped with the tool in the non-dominant hand, transferred to the opposite hand, and placed on a pegboard. Then, the exercise is reversed starting from the dominant one.	Two Maryland dissectors, one pegboard, six rubber ring objects	300 seconds
Precision Cutting	A circle is cut from a piece of gauze on a pre-marked line	One Maryland dissector, one pair of endoscopic scissors, one jumbo clip, one 4x4 piece of gauze with a pre-marked circle, two alligator clips	300 seconds
Ligating Loop	A ligating loop is placed and secured at the base of a foam appendage on a pre-marked line.	One grasper, one pair of endoscopic scissors, one jumbo clip, one pre-tied ligating loop or endoloop, one red foam organ with appendages.	180 seconds
Suture with Extracorporeal Knot	A 2-0 silk suture with a curved needle is placed through a penrose on pre-marked dots. Three knots are tied in an extracorporeal method using a knot-pusher.	Two needle drivers, one knot pusher (either open or closed), one 2-0 silk suture of 90cm or 120cm length, one pair of endoscopic scissors, one penrose drain with marked targets, one suture block.	420 seconds
Suture with Intracorporeal Knot	Similar to task 4, except a pre-cut 15-cm 2-0 silk suture is used and the knots are tied using an intracorporeal technique.	Two needle drivers, one 2-0 silk suture of 15 cm length, one pair of endoscopic scissors, one suture block, one penrose drain with marked targets	600 seconds

Table 2.1: Schema about the objectives, the equipment and the time limits of the five FLS tasks [17]

2.2 Studies about the FLS program

Different studies have been performed in order to evaluate the FLS program, both in term of reliability of the scoring metrics and validity of the content, concluding that FLS measurements are considered to be highly reliable and valid measures of laparoscopic skill [13]. The usage of the FLS program has been also inquired to see the impact of its training on the technical competence of surgeons.

It has been assessed whether training to proficiency with the FLS simulator would result in improved performance in the operating room (OR) [19]. To verify that, a blinded clinical

trial has been conducted. A group of nineteen junior residents underwent baseline FLS testing and were assessed in the OR using a validated global rating scale (GOALS). The ones with a score ≤15 (n = 17) were randomly assigned to two different groups: a training group which had the possibility to practice with the FLS simulator in a supervised proficiency-based curriculum and a non-training group. Both groups continued their regular residency training and at the end of the study period, subjects were assessed again on the simulator and in the OR. A flowchart of the procedure is reported in the Figure 2.3. The evaluators of the performances were blinded, thus they didn't know who belonged to the training group or to the other.

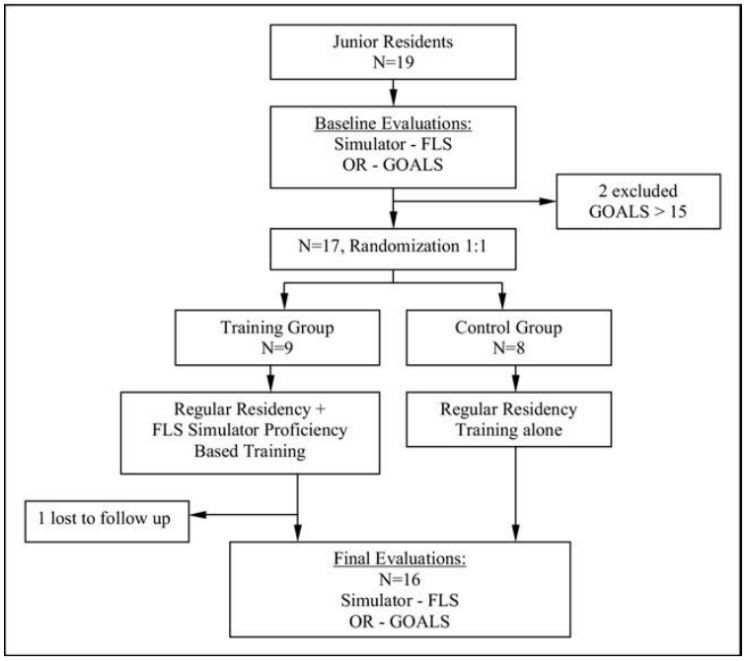

Figure 2.3: Flow of participants through the study [19]

While at baseline, no participant had a score above the level required for FLS certification, at the second valuation all trained subjects would have passed the FLS test, whereas only 3 of the 8 nontrained subjects had a passing score. Also the GOAL scores in the OR presented a bigger increase with respect to the baseline value for the trained participants. This results underline the presence of a statistically and clinically significant improvement in OR laparoscopic performance of Junior residents who underwent an FLS simulation training compared with untrained ones.

Similarly, another clinical trial has been conducted to evaluate the impact of simulator training on technical competence during a surgical procedure [20]. As shown in Figure 2.4, Residents have been divided into 3 groups: one training on a simple simulator, another

training on a virtual simulator and a control group. An initial evaluation has been made by a validated score during a laparoscopic cholecystectomy. Then, each resident has been trained for 1 month and a second evaluation has been performed. No significant difference between the two groups with a simulator has been found but both of them have shown a significant improvement.

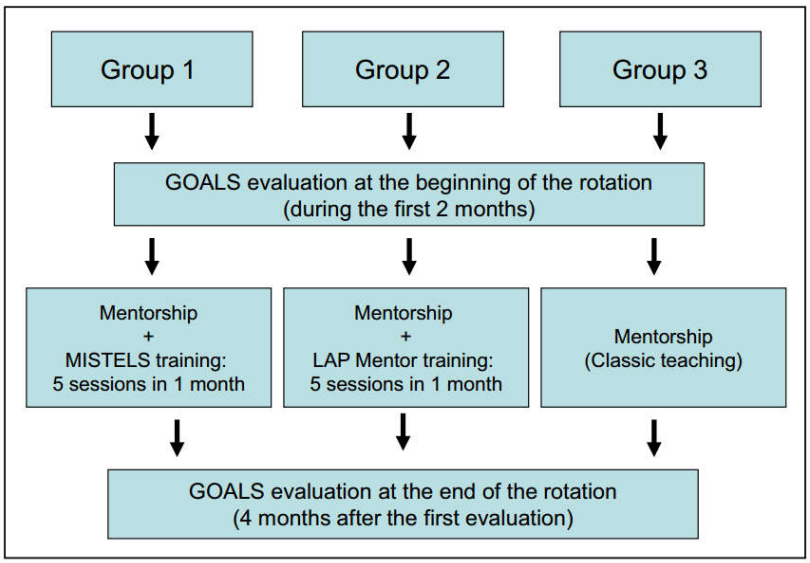

Figure 2.4: Flow of participants through the study [20]

This confirms that simulator training provides a more rapid acquisition of competence in surgical technique, especially at the beginning of training. Moreover, teaching on a simulator can help in maximizing the outcomes of mentorship teaching, which is not substitutable.

Further studies have proved as FLS training may help in minimizing the subject's skills loss over time [21] and that the delineation of proficiency targets with reporting of progress could be a way to improve interns' practice results. The latter appears to have a positive effect on their early OR performance of laparoscopic cholecystectomy [22].

The fact that the FLS program is not procedures specific, makes it not only directed to general surgeons, but also by urologists, gynaecologists, or thoracic surgeons practicing minimally invasive surgery. However, a study about the usage of this program for gynaecology residents training has shown as the practical skills test is a valuable assessment tool while the cognitive test may need further adaptation because it seems to be focused primarily on general surgical curriculum [23]. This study has been conducted on a small sample of subjects but it suggests that this kind of training could require an adaptation of the cognitive test depending on the surgical specialization.

A training in such an environment allows also studies about the estimation of the trainee's learning curve. In one of these studies [24], data from pegs exercise performed by different subjects have been analysed in order to estimate their learning curve of the task. These subjects, after viewed an instructional video demonstrating the Fundamentals of Laparoscopic Surgery (FLS) simulator peg transfer task, had 4 weekly sessions where they performed 10 repetitions of the task. Their scores have been recorded and used for the construction of a performance graph (Figure 2.5). The learning curve effect has been estimated by fitting inverse curves (Y = a - b/X) to the performance curves of 16 medical students performing 40 repetitions of the FLS peg-transfer task. An estimation of the asymptote (a) and the slope (b) for each subjects can be obtained from the curve.

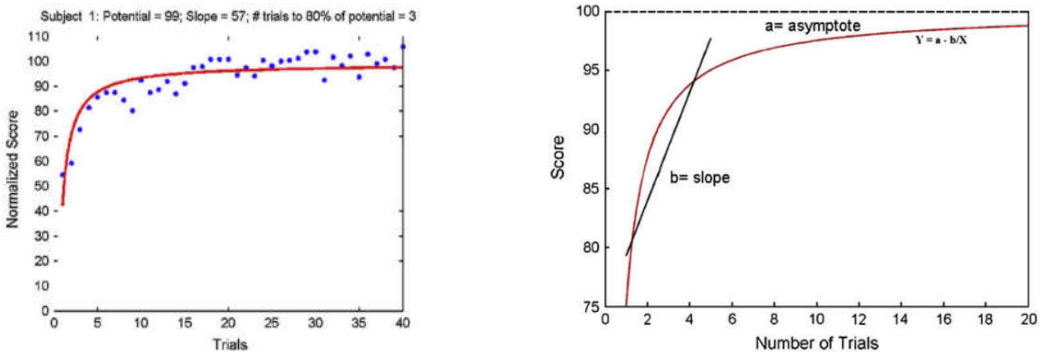

Figure 2.5: The left image represents the interpolation of the experimental data with a function Y=a – b/X. The right image represents an hypothetical learning curve, its slope b and its asymptote a.

These two values have been used to define the "learning plateau" that is the theoretical best score a subject could achieve, and the "learning rate" that is the number of trials required to achieve 90% of the learning plateau. A correlation has been found based on the parameters of the learning curve and the participant's career interests. This technique may have a role in the simulator setting when groups that comes from different educational interventions must be compared.

All these studies show and remark the valuable effect of the FLS program in the laparoscopic training.

2.3 Common stress measures

Literature suggests to describe stress as a self-reported measure (e.g. self-assessment) or observer-reported measure (e.g. human behaviour coder). These measures can support other

kind of direct measurements of stress symptoms but they are not useful to obtain instantaneous stress measure.

A survey of Sharma N. and Gedeon T. [25] gives an overview of which are the non-invasive and unobtrusive sensors for measuring stress. Firstly, under stress conditions, there is an increase of the amounts of stress hormones (e.g. cortisol or catecholamine levels) that are released inside the body. It is possible to measure these hormones via invasive methods, for example through blood, saliva or urine sample test but the duration of the required analysis makes them not suitable for real-time detection of stress.

These hormones are not the only change under stress. In fact, changes in heart rate (HR), blood pressure (BP), pupil diameter (PD), breathing pattern, galvanic skin response (GSR), emotion, voice intonation and body pose have been observed, which, unlike measuring stress hormones, can be acquired through non-invasive methods.

All this features can help in modelling stress objectively and they can be subdivided into what can be called "Physiological and Physical" features:

- Physiological feature: it requires the use of tools attached to individual′s body to detect general fluctuations. Heart rate and skin conductivity are examples of this category.
- Physical feature: it is defined as a property that humans can see change without the need for equipment and tools. Facial movements, voice intonation, body poses, and gestures are examples of this category.

Figure 2.6 summarises the physical and physiological signals that can be investigated to detect stress. These signals can be obtained from common techniques which include analysing physiological signals, electroencephalography (EEG), blood volume pulse (BVP), heart rate variability (HRV), galvanic skin response (GSR), and electromyography (EMG). In addition, physical signals for measuring stress encompass eye gaze, pupil diameter, voice characteristic, and face movement.

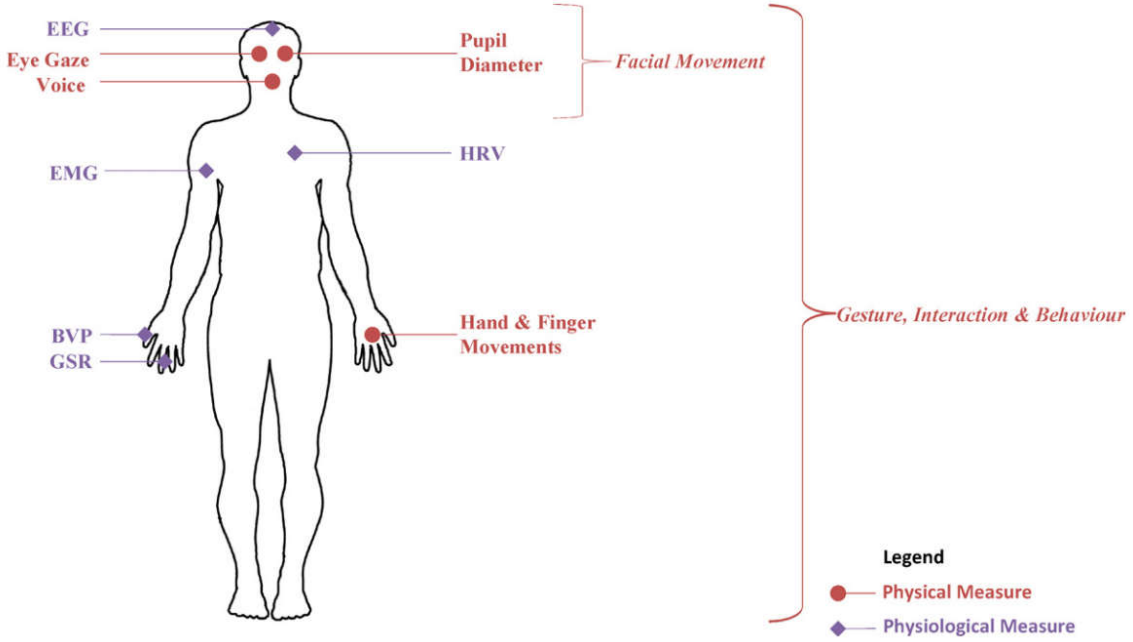

Figure 2.6: Common sources of physical and physiological signals used to detect stress [25]

It is good to underline that for all of these measure it is strongly suggested a fusion approach. It means that to base the detection of the stress only on one of them could lead to misleading conclusions. Therefore, a combination of sensors is strongly suggested.

For most of these measures a data normalization is required if the aim is to compare different people. In fact, people could present different physiological state based on a different physical activity, life-style or something else and so, their raw data cannot be directly compared. The normalization usually depends on the experimental setup but one useful and common way to normalize these data is to refer them to the rest condition.

Section 2.3.1 and 2.3.2 present respectively the most common physiological and physical measures of stress.

2.3.1 Physiological measures

Most of the physiological measures have a strong relationship with the activity of the Autonomic Nervous System (ANS). It is the part of the nervous system responsible for involuntary activity and it is made up of Sympathetic and Parasympathetic nervous systems. In stressful situations, there is a dynamic change in the ANS behaviour which consists with an increase of the Sympathetic Nervous System (SNS) activity rate and a decrease of the Parasympathetic Nervous System (PNS) one. Alternatively, the activity of the PNS dominates during resting activities.

Obviously stress is not the only cause of ANS changes. For instance, a joy feeling can elevate skin conductance like distress. The dynamic behaviour of SNS and PNS regulates the galvanic skin response, heart rate variability, and brain waves, and other physiological systems including blood pressure. A brief description of all of them will follow [25]:

- **Skin conductivity:** Galvanic skin response (GSR) is also known as skin conductance (SC) or electrodermal activity response. It consists in the measurement of electricity flow through the skin of an individual. It is considered a reliable indicator of stress because it has been observed that under that condition the skin conductance increase. This is due to an increases the flow of electricity that is caused by an increase in moisture on the surface of the skin. This changes can be measured through electrical potentials between electrodes placed on surfaces of the skin. Electrodes are typically placed on the hand, first and middle fingers.
- **Heart activity:** it encompasses lots of analysis on the ECG signal. From it, the Hearth Rate (HR) [bpm] can be determined though the detection of the number QRS complex in a certain amount of time. Acute stress condition causes an increase of the force and frequency of the hearth contraction leading to an increase of the HR and a decrease in the ECG amplitude. Various measures of the Heart Rate Variability (HRV) can be determined from an analysis on the time distance among subsequent R peaks detected in the ECG sequence. It is believed that HRV also reflects how well individuals are able to adapt to changes [26]. In general, the Heart activity has been found to have a good correlation with stress but each subject has a different baseline of heart activity depending on his cardiovascular fitness. That's why heart activity measurements cannot be directly compared across multiple people unless measurements are standardised using some baseline measurements (for example a rest condition).

  Short-term lower HRV reflects acute stress and can be caused by a decrease in the PSNS activity or an increase of SNS activity, which means that HRV can be negatively affected during stress.

  Lots of measurements of the HRV can be done based on the domain of analysis [27]:

  - The most common measurements in the time domain are RMSSD [ms] and the SDNN [ms]. The first is the square root of the mean of the sum of the squares of differences between adjacent NN intervals and the, and the second is the Standard deviation of all NN intervals.

- In the frequency domain, the spectra of human HRV can be divided into three main zones: below 0.04 Hz is very low frequency (VLF), between 0.04 and 0.15 Hz is low frequency (LF), and between 0.15 and 0.5 Hz is high frequency (HF). The VLF is related to factors like temperature and hormones, while generally, low frequency (LF) and high frequency (HF) bands of HRV are used to analyse stress and they are known to reflect SNS and PNS activities respectively. To estimate autonomic balance during short-term fluctuations in heart rate, the HF and LF spectra are commonly normalized to their total power (e.g. HF/(HF+LF)*100 in order to remove influences of VLF [28]. Stress levels are expected to increase with increase in LF/HF ratio. For a short-term analysis, recordings of at least 2 minutes are required, better if they are of 5 minutes because very short acquisitions can be affected by ectopic beats and noise.
- There are also Geometrical methods which consist into present RR intervals in geometric patterns in order to derive measures of HRV from them.
  An example is given by the HRV triangular index which is estimated from the histogram of the RR intervals as function of their duration (Figure 2.7A). From it, a correlation with the standard deviation of the RR intervals can be found but it is highly insensitive to artifacts and ectopic beats, because they are left outside the triangle. In practice, this methods are not appropriate to assess short-term changes in HRV. In fact, recordings of at least 20 min should be used to ensure their correct performance.
- Poincarè Plot: in this kind of representation each RR interval is plotted as a function of the previous RR interval (Figure 2.7B). It is a technique that portrays the nature of RR interval fluctuations. As can be observe in the figure, this plot may be analysed quantitatively by calculating the standard deviations of the distances of the R−R(i) to the lines y = x and y = −x + 2R−Rm, where R−Rm is the mean of all R−R(i). The inquired standard deviations are respectively SD1 and SD2. The first is related to the fast beat-to-beat variability in the data, while the second describes the longer-term variability [26]. From this two SD, the ratio SD1/SD2 may also be computed. It describes the relationship between the two components. Variation of the ratio from the normal value or in the data dispersion could be linked to pathological status.

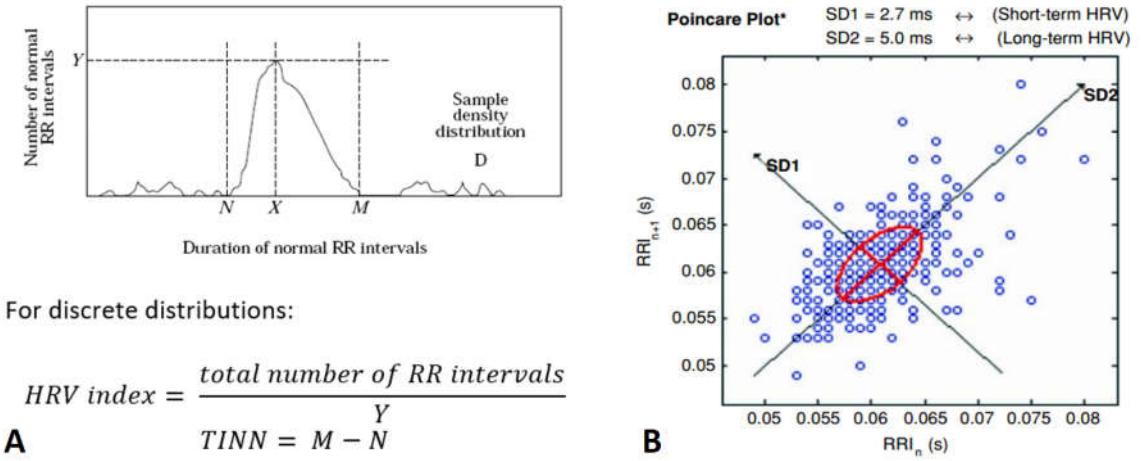

Figure 2.7: (A) example of representation the RR (or NN) intervals histogram. It is used to compute the HRV index and the triangular interpolation of NN interval histogram (TINN). (B) example of Poincare Plot for a normal subject. It is used to visually describe the nature of short-term and long-term RR interval fluctuations.

- **Brain activity:** The brain activity can be analysed with functional magnetic resonance imaging (fMRI), positron emission tomography (PET) and electroencephalography (EEG). Among these methods, EEG is the most commonly used due to its high temporal resolution and low intrusive equipment. It is able to record electrical waveforms at the scalp formed by action electrical potentials during synaptic excitations and inhibitions of dendrites. The waveforms are characterised by frequency, amplitude, shape and sites of the scalp but they are affected also by age and state of alertness.

  EEG signals can be categorized by frequency in four main wavebands as shown in Table 2.2: Beta wave in 13-30Hz range, Alpha in 8-13Hz, Theta in 4-8Hz and Delta in 0.5-4Hz. Beta and alpha waves represent conscious states whereas theta and delta waves signify unconscious states. Rapid beta wave frequencies (from decrease in alpha wave frequencies) are the main characteristics indicating stress. Through the use of bandpass filters, the part of the noise content can be removed (e.g. bandpass among 4-30Hz) and the characteristics of waves in specific frequency ranges can be extracted (e.g. bandpass among 8-13Hz for alpha waves).

  In [29] during the analysis of the mental calculation it has been noticed an active left frontal lobe. This confirms the theory of increased brain activity in the left frontal lobe during mental mathematical processing.

Wave band	Frequency range (Hz)	Individual characteristic(s)
Beta	13–30	Alertness or anxiety
Alpha	8–13	Relaxation
Theta	4–8	Dream sleep or phase between consciousness and drowsiness
Delta	0.5–4	Coma or deep sleep

Table 2.2: EEG wave band categories [25]

- **Blood pressure (BP):** it is the pressure exerted on the walls of blood vessels and it can vary between the systolic (max) and the diastolic (min) pressure. It has been observed an increase of BP in stress conditions.
- **Electromyogram:** the Electromyography (EMG) is used to record the electric activity produced by active muscles. Some trials about stress detection have been made placing the EMG electrodes on the trapezius muscle but it has been found to not be a very good source of information.
- **Skin Temperature (ST):** it has been shown has ST increases when stress level decrease and it decreases when stress increases.
- **Respiration:** The breathing rate and the inspired volume of air can be used to monitor stress. However, if their measurements imply the use of specific belts that can limit the movement of the subject, they are not so reliable.

These physiological methods are seldom used alone because there are other body triggers that can affect these signals making difficult the stress detection. So, usually they are used in combination.

2.3.2 Physical measures

A physical feature or characteristic is defined as a property whose changes can be seen without the need for equipment and tools. Physical signals that are sensitive to stress are behaviour, gesture, body movement, facial expression, eye gaze, blinks, pupil dilation, and voice. A brief description will follow [25]:

- **Behaviour, gesture and interaction:** the recognition of body language requires complex techniques that consider degrees of freedom for body configurations and vast

variations in motion. Body behaviour can be analysed by examining body language but it has been generally evaluated by the judgement of hand the human experts.

- **Facial expressions:** Increase in head and mouth movements have been found to indicate increase in the stress level.
- **Eye gaze:** It provides information on an individual's attention source, and allows to deduct the subject's intentions. The most common measures obtained from an analysis of the eye gaze are the gaze spatial distribution and percentage of saccadic eye movement.
- **Blinks:** Eye blinks have been found to be sensitive to stress but there is not a complete agreement on which should be the change in the blink rate in stress conditions. These conflicting conclusions could be due to the different experiment environment conditions in which the tests have been conducted. Results from the literature suggest a correlation between higher frequency of blinks and stress when acquired from real driving experiments whereas the results analysed from solving mathematical tasks on a computer suggest the opposite.
- **Pupil dilation:** It is not well defined if the increase of an individual's pupil diameter can be associated to a stress state. It seems that both negative and positive stimuli can cause pupil diameters to increase. However, when it has been used for this purpose in combination with other signals, it has shown an increase of the mean values for pupil diameters over time. Interpolation techniques have been used to determine pupil diameters during blinks, but simple techniques including replacing the blink with the last valid pupil diameter value are sufficient.
- **Voice:** The components of the voice that have been thought to be related to stress are the nonverbal ones. One of the features claimed to indicate increases in stress are increases in range and rapid fluctuations in fundamental frequency and increases in energy for high frequency voice components.

  Voice features for stress models include loudness, fundamental frequency, zero-crossing rate, jitter and energy frequency ratios. Stress related emotions have been estimated in speech by extracting features including voice quality, pitch, duration, intensity, formants, vocal tract cross-section areas, frequency, glottal characteristics, duration of silence, and speech rate.

2.4 Stress impact on the performance

The stress assessment during work performance is not widely used in the surgical training field even if a growing number of studies are reporting as a stressful condition can affect the subject performance. The main concern regards the difference among the training and the real practice in the OR. This could lead to have novel surgeons that could not be able to deal with intraoperative stressful situation in an easy manner.

Nowadays, different surgical training have started to include programs that allow the trainee to perform under the judgement of a supervisor and that give importance to nontechnical skills as communication, clinical judgment and teamwork. There are training programs, as the FLS one, which include the use of a physical simulator for practice in specific tasks and scenarios and other simulators which allow more complex virtual scenarios. It must be recognized, however, that simulators are not real patients and simulated operating rooms are not real operating rooms. Therefore, the reaction to stressful situation in the OR may lead to a different response with respect to the one on a simulator.

Section 2.4.1 and 2.4.2 treats respectively the impact of stress in surgical field and in others fields.

2.4.1 Stress in surgical field

There are different studies which have tried to investigate the impact of stress in the surgical performance. Thanks to review of the literature like the one of Sonal Arora et. [14], a better and easier overview of what has been discovered is possible. It has been assessed as surgeons are exposed to a large number of stressors. Among them, the most common include technical complications, time pressure, distractions, interruptions and increased workload.

There is not a specific best tool for measuring stress directly. Consequently, the best way to compute an approximation on its level is by measuring its effects based on subjects' perceptions (subjective measurements) or on their physiological state (objective measures). Among objective measures, the Heart Rate (HR) has been used in different studies, in particular the mean HR has been found to increase during a stressful procedure but less for senior residents than for junior ones. Studies which encompasses the use of stress self-assessment questionnaires, ambulatory monitoring system [30] or electrooculogram [31] have shown as Laparoscopy is a more stressful procedure with respect to open and robotic surgery requiring a bigger amount of mental resources. The one including the ambulatory monitoring system is about the analysis of the performance of three tasks executed in a pelvic

trainer in random order using both standard laparoscopic instruments and the da Vinci robot-assisted surgical system [30]. The participants wore the monitoring system beneath the clothing, allowing the subject complete freedom of movement. It has been used for the recording of three parameters: the mean square of successive differences between consecutive heartbeats (MSSD) which reflects the beat-to-beat variability of the heart rate, the PEP (time of isovolumetric contraction) which is the interval between the onset of ventricular depolarization and the opening of the semilunar valves and the average heart rate (HRA). Data of each task were divided into 30 seconds periods and the averages were compared. Bigger values of HR and lower values of PEP and MSSD that are linked to a more stressful condition have been found in the laparoscopic group.

Instead, the use of an electrooculogram allows the detection of the number of eye blinks [31]; it has been shown a decrease in the Blinking Rate from rest to open surgery task that was consistent with the subjects' reported increase in level of mental concentration. However, it has been reported an further increase from open to laparoscopic task as would be expected given the greater demands of the second task. Other methods for the blink detection are related to the use of an Eye Tracking or EEG apparatus. In fact, the blink is simultaneously visible on the EEG amplitude signal of Fp1 and Fp2 which are the electrodes located on the front [29], [32]. Moreover, the same study asserts as the power associated to the blink is way higher than the one related to the normal brain activity.

The pupil size is another indicator that has been found to change in response to both positive and negative stimuli. For its analysis, blinks must be removed and must be refer to a baseline. A way to do it could be to use interpolation technique or simply substituting the each blink with the last pupil available value [33].

The concept of stress is often associated to the concept of Mental Workload (MWL), that is commonly defined as the cognitive demand required to a subject to perform a task. Excessive mental workload can eventually lead to development of a stress condition into the subject but must be take into account that an higher task demand is not necessarily associated to an higher mental workload. The most widespread method to assess stress and MWL is through self-assessments. They typically involve interviews or questionnaires as the NASA-TLX Tool. The NASA Task Load Index is widely used in different fields like Aviation or Healthcare in order to obtain a subjective measure of the workload associated to a task but as all the subjective measurements its reliability is strongly dependent on the honest

collaboration of the subject. In the original version, the total workload score is divided into six subscales belonging to different domains that must be answered with a predefined scale range. Its use in studies regarding the evaluation of the laparoscopic performance has reported as an higher mental workload is associated with poorer performance [34].

MWL is also studied through the use of objective measures. For example, pupil diameter has been found to be a good estimator of the Mental Workload (MWL). However, it is not a practical parameter in scenarios characterized by light changes, as vehicle driving, because it is overly sensitive to brightness changes. In such conditions, the study of Saccadic Intrusions (SI) could be useful. They are specific type of eye-gaze deviations in which the gaze deviates from the original fixation point and then quickly returns. Their analysis requires a first separation among fixations and regular saccades. Then, SI are retrieved based on constraints about the displacement entity and the duration to make the round trip (from 60 to 870 ms). It has been demonstrated as SI eye movements increase for higher level of MWL with respect to low levels [35].

Another way to assess the MWL among different procedures is through the use of second tasks as proposed by Mark W. Scerbo [36]. They found out that a single incision laparoscopic procedure (SILS) requires an higher MWL than a traditional laparoscopic procedure. They investigated three primary tasks from the FLS curriculum: the peg transfer, the precision cutting, and the intracorporeal knot. The visual spatial ball-and-tunnel detection task was added as a secondary task. The video of the secondary task, in which four balls are located in a representation of a 3D tunnel, was over imposed to the primary one with a transparency of 50%. Participants were asked to respond each time a change in one of the ball position was detected. Both the subjective NASA-TLX for MWL and the performance score reflect a decrease in the performance and an increase of the MWL in the SILS. In particular, the incremental difficulty of the SILS tasks was mirrored in the secondary task scores with a decrease of the percentage of correct detections. This pattern of results shows that the increased mental workload associated with performing the SILS procedures demands most of the participants' attention, leaving few resources available to respond to targets appearing the same visual field.

As can be evinced from the previous examples, a combination of subjective and objective measures can help in determine the stress and mental workload levels. Another system is the Imperial Stress Assessment Tool (ISAT) which encompasses the measurement of salivary

cortisol and continuous heart rate monitoring (objective components) and self-reported stress levels (subjective component). It has been tested in the evaluation of real surgical interventions showing a good reliability [37].

Disregarding stress, a technical performance is generally evaluated in terms of accuracy and time required for the completion of the exercise. In case of laparoscopic procedures, the common performance scores may include the number of knots tied and the economy of motion. Another interesting aspect is the effect of distractions and the ability of the subject to focus on the exercise. It has been verified as an increasing in the distraction level may be correlated with increasing of the time, number of errors and poorer economy of motion especially during difficult exercises. This suggests that more difficult exercises are potentially more stressful.

Moreover, it has been observed as experience may help surgeons to adapt and deal with stressful situation. In this context, useful experience can derive both from lots of years of practise, or simply from the fact the surgeon has already dealt with a similar situation.

Summarizing all the information provided until now, it can be notices as there is not a specific right tool or method to assess stress. The better way to proceed is to include more than one source of information in the analysis and more important thing, the stress evaluation cannot disregard an evaluation of the subject performance.

2.4.2 Stress in other fields

Despite the relevance of stress for safety and quality of the procedure, a lack of direct relationship between a possible stressful experience and an erroneous surgical outcome in the OR prevents the inclusion of the stress factor in common surgical training programs. Anyway, it is clear as an excessive level of stress can affect the performance adversely, especially for novice surgeons.

In contrast, the impact of stress is strongly faced in field such as aviation and military. Within those fields, evidence suggests that stress may have an effect on decision making of the subject decreasing the ability to collect information by distracting attention from the primary task.

Excessive mental workload can eventually lead to the phenomenon called cognitive or attentional tunnelling. This concept is widely diffuse in fields like civil aviation and it is defined as "the allocation of attention to a particular channel of information, diagnostic hypothesis or task goal, for a duration that is longer than optimal, given the expected cost of

neglecting events on other channels, failing to consider other hypotheses, or failing to perform other tasks" [38]. In a simpler way, it is seen as the inability of the operator to reallocate his/her attention from one task to another due to the high demand of the primary task. In aviation, this concept may be linked to the inability of the subject in detecting crucial events like alarms when the demand of the primary task is to high. It is important to remind that an higher task demand is not necessarily associated with a higher mental workload. A possible approach is to merge knowledge and methods from cognitive psychology, system engineering and neurosciences which is a field known as neuro-ergonomics aimed at design systems for safer and more efficient operations through the understanding of human brain functioning in the workplace. Two neuro-ergonomics concepts concern the adaptive automation and the cognitive counter-measures that are well suited to solve the problem of resource allocation.

In this context, metrics for the detection of the Attentional Tunneling and possible countermeasures have been investigated. An example is given by a study aimed at the development of machine-learning algorithm to detect Attentional Tunneling from the analysis of psycho-physiological and oculomotor responses that are collected during an experiment in an ambient in which the attentional tunnelling has been provoked [38]. The experiment was about the manual control of a robot in a target identification task. The participants sat in front of an graphic interface and they controlled the robot using a joystick; they were instructed about how to face and recognize on the interface the occurrence of four incidents, even if only the low battery event would have been provided during the most cognitively demanding phase of the experiment. This was the provoked Attentional Tunnelling trigger in which the safety procedure was to release the joystick for an automatic return of the robot to the base.

The participants were separated in two groups: a control group which did not receive any countermeasures to help the members notice the battery failure, and a countermeasure group which received the assistance of a cognitive countermeasure. The countermeasure consisted in directly displaying a message on the panoramic video window for target identification. During the experiment the HR, the number of Area Of Interest (AOI) scanned on the user interface, and the switching rate (SWR) were acquired and processed offline. Results showed as all the members of the countermeasures group noticed the alarm and acted properly while most of the members from the control group experienced the attentional tunnelling. The

acquired data reflect this behaviour with an increase of the HR and a decrease of NBAOI and SWR in the control group during the inquired task phase. Knowing the results, part of the subjects were used to train a machine-learning algorithm to detect subject who experienced the attentional tunnelling and another part of them were used for testing. The system was pretty reliable but it presented several limitations as the limited domains of application and the use of a single probe to infer the occurrence of the attentional tunnelling. Other studies about the assessment of the mental load imply the use of task accuracy, fNIRS, Electrocardiogram (ECG) measurements, and self-report scales. It has been found as both fNIRS and HRV are sensitive to different levels of mental workload. In particular, a lower prefrontal activation as well as a lower LF/HF ratio at the highest level of difficulty was noticed [39] during the performance of computer-based tasks, suggesting that these measures are suitable for mental overload detection.

Apparently concepts such as the Attentional or Cognitive Tunnelling fit perfectly to the aviation or military fields but it could be interest to bring them in the medical field, especially in the Operating Room where lots of monitoring devices are present. In fact, the occurrence of an adverse event or specific sounds can be seen as the alarm in the pre-proposed study [38] and an excessive stress could lead to the inability of the surgeon to deal with them.

2.5 Aim of the Work

This project of thesis has been conducted at the Center for Computational Surgery (Department of Surgery, Houston Methodist, Houston, TX) during an internship of six months.

Laparoscopy has brought, together with lots of benefits for the patients, new challenges for the surgeons themselves which have to undergo specific training to learn the basis of the procedure. The ‘Fundamental of Laparoscopic Surgery’ (FLS) program diffused in US and Canada is part of some Residency programs host by Houston Methodist Hospital where the candidate is evaluated based on time and accuracy measures. However, subjects with a different level of expertise could perform the tasks with a different proficiency requiring more or less concentration, showing more or less confidence and facing stressful situation or errors in different ways. This study proposes to think at a different way of conducting training in which is assessed not only the ability to perform or not the task but also the mental condition, behaviour and physiological demand required to do it. This could lead to a new

way of conducting training with the aim of decreasing the gap among a trainee and an expert. Moreover, it could change the way in which the institution monitors the progress of its residents over the years. In fact, it is in the interest of the hospital to provide better and better training in order to improve the proficiency of its personnel.

The main aim of the work has been the development of a multisensory acquisition system for an evaluation of the FLS performance. In particular, the purpose is to realize a system which encompasses different devices and algorithms that allow to extract information of different nature describing the status and the behaviours of the subject during the performance.

A large gamma of sensors has been introduced in this preliminary study because it was not known a-priori which were the signals of interest. The study consists in the integration of an FLS trainer box with devices such as an Eye Tracker, smart cloth, EEG, Smart Trocars and different cameras. This includes the design of the experimental setup and procedure, the development of a GUI for the data acquisition and algorithms for the offline extraction and synchronization of the data.

Another purpose of the work has been the development of an algorithm for the detection of the blinking based on a multimodal analysis on ET and EEG data and of an algorithm for the reconstruction of the 2D movement of the tool through the use of the Smart Trocar.

The strict connection between the Department of Computational Surgery and the hospital environment has allowed to test the platform on some residents and experts from the Methodist Hospital.

This gave the possibility to execute a preliminary analysis on a subgroup of acquired data aimed at finding particular pattern in the signals, correlations with events and differences among categories.

Moreover, it allowed to receive feedbacks from the surgeons about the training setup, understand what could be improved and obtain a first idea of which are the signals of interest for future studies.

2.6 Work structure

This work has been divided into 5 Chapters. The entire structure has been summarized in Figure 2.8.

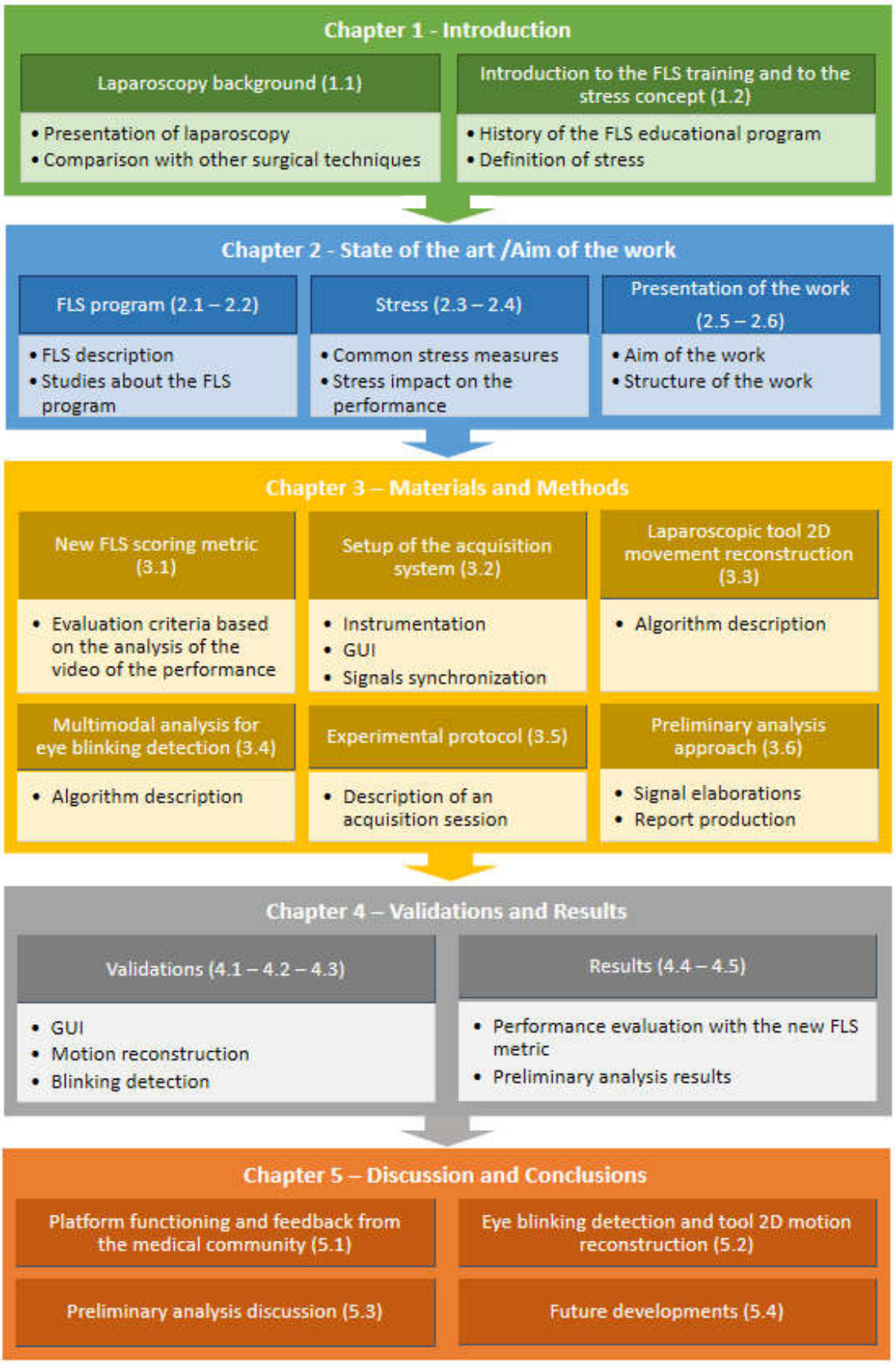

Figure 2.8 Structure of the presented work

Chapter 1 describes the field in which the work has been conducted giving a background about laparoscopy, introducing the FLS training and defining the stress.
The current Chapter (Chapter 2) presents the state of the art of the FLS educational program and the most common indicators of stress and mental load measurable with non-invasive methods. Moreover, it explains the impact of stress on the performance in different fields, the aim of the work and its structure.
Chapter 3 treats in detail the materials and methods used in this work. It starts with the creation of a new FLS metric to overcome the limitation of the standard one based on just the observation of the video of the performance. Then, it explains the development of the acquisition system, from the integration of all the devices in a standard FLS trainer box and the implementation of an acquisition GUI to the offline extraction and synchronization of all the signals. It describes the creation of algorithms for the reconstruction of the 2D motion of the laparoscopic tool and the eye blinking detection. Finally, it presents the experimental protocol followed during acquisition session and it explains in what consists the preliminary analysis approach.
Chapter 4 presents an evaluation of the GUI performance and the validation of the algorithms for the reconstruction of the 2D motion of the tool and for the eye blinking detection. Furthermore, it reports the results of participants performance using the new FLS scoring metric and all the observations extracted from the preliminary analysis.
Chapter 5 draws the conclusions and it discusses the results and the issues as well as positive aspects and future development.

Chapter 3 Materials and Methods

The following Chapter explains the materials and methods used in this work to achieve the aim of developing the multisensory acquisition system for FLS training and to conduct a preliminary analysis on a subset of data. The study has been focused on the FLS tasks of Peg Transfer, Circle Cut and Intracorporeal Knot. Figure 3.1 summarises the main steps from the data acquisition to the preliminary analysis reporting the Section in which they have been described.

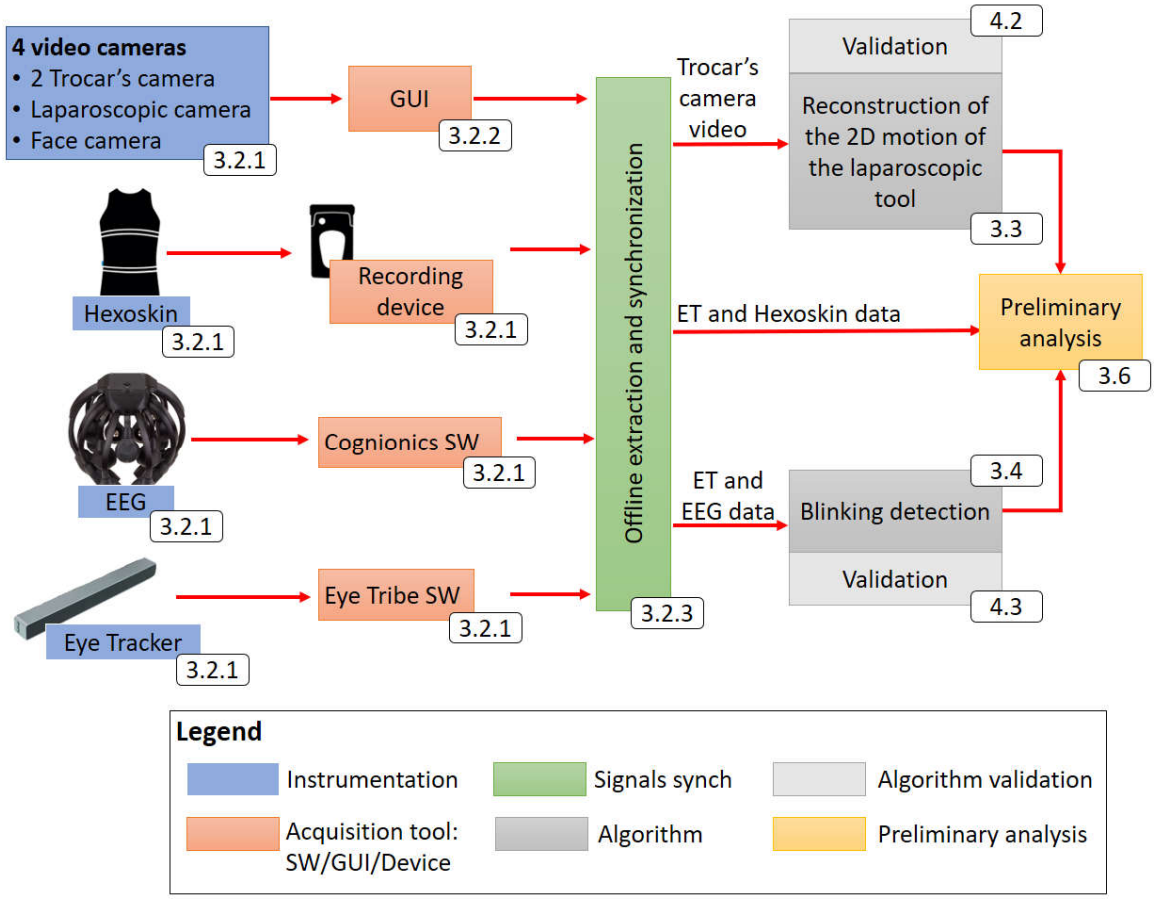

Figure 3.1: From the acquisition to the preliminary analysis. For each element, it is indicated the Section of the work in which it has been described.

Section 3.1 concerns the creation of a new FLS scoring metric suitable to evaluate subjects with very different expertise levels based on the video of their performance.

Section 3.2 presents the entire Setup developed to obtain other sources of information from the participant during the tasks. It encompasses a description of all the devices, how signals have been acquired and how they have been synchronized.

Section 3.3 and Section 3.4 regard respectively the implementation of an algorithm for the

reconstruction of the 2D motion of the laparoscopic tool and an algorithm for the eye blinking detection.

Section 3.5 explains the experimental protocol adopted for the data collection during an acquisition session.

Finally, Section 3.6 describes the preliminary analysis approach that has been adopted on the acquired data.

3.1 New FLS scoring metric

The standard FLS scoring metric has not been applied in this study because it is not suitable to evaluate the performance of subjects who could not be able to complete the tasks.

In fact, it assigns a task's score equal to 0 for a not completion of the exercise or for the occurrence of specific erroneous behaviours or events. In order to understand the differences among subjects of different expertise level a more comprehensive metric is required. For this reason, a new FLS scoring metrics has been developed to include Beginners in the evaluation. It takes into account the amount of time required to perform the task, the phases that have not been completed and the number and kind of errors that have been made.

All the most important parameters have been summarized in Table 3.1.

Global Parameters	Values
Max points for percentage of Completition Time (Tc%)	200
Max points for Phase Not Completed	400
weight for small errors	10
weight for big errors	50
weight for very big errors (things that are not allowed in a normal performance)	200
Max exercise score (starting score)	700

Task 1: Peg Trasfert parameters	Values
Max Time Limit (s)	300
Phases: max number of missing transfer of obj for the end of the exercise	12

Task 2: Circle Cut parameters	Values
Max Time Limit (s)	300
Phases: quarters of circle to cut	4

Task 3: Intracorporeal Knot parameters	Values
Max Time Limit (s)	600
Phases: needle insertion through markers, 1st knot, 2nd knot, 3rd knot, cut both strands of suture after knot	5

Table 3.1: Parameters of the new FLS metric required to score the performance

The metric works as follow:

- Each task has been assigned to starting score of 700pts.
- The time required for the completion of the task has been taken into account (Completion Time Tc). Because of the different maximum time duration among the tasks (respectively 300, 300 and 600 sec), it has not been possible to directly subtract Tc (seconds) from the starting score, otherwise this penalty would have had a different impact on the score depending on the exercise. So, the percentage of time required for the completion of the task has been used instead of Tc. This means that Tc has been normalized to the maximum time limit of the exercise. This percentage has been assigned to a maximum penalty of 200 pts (100% of Tc). It has been computed as follows:

$$penalty\ (Tc\%) = \frac{completion\ time\ (\text{sec})}{\max time\ limit\ of\ the\ task\ (\text{sec})} \cdot 200pts$$

  The more time has been required to complete the task, the bigger will be the penalty.
- The number of not completed task's phases has been taken into account. A maximum penalty of 400 pts has been given to a subject who has not been able to complete even 1 phase. The phases have been identified as follows:
  - Pegs Transfer: a complete transfer of an object from one peg to the other is a phase for a total of 12 phases.
  - Circle Cut: each quarter of circle cut is a phase for a total of 4 phases
  - Intracorporeal Knot: insertion of the needle, 1st, 2nd and 3rd throws and the cutting of the strands of the suture for a total of 5 phases.

  The penalty is computed as follows:

$$penalty\ (phases) = \frac{number\ of\ completed\ phases}{\max number\ of\ task's\ phases} \cdot 400pts$$

  The more phases have not been completed, the bigger is the penalty.
- A different weight has been applied to errors of different importance:
  - Small error weight: 10 pts. They are errors in the procedure that are not event penalized in the FLS scoring metric such as the drop of an obj in the peg transfer that the participant has been able to retrieve.
  - Big errors weight: 50 pts. They are considered penalties even in the FLS metric. An example is if the subject drops an object during the peg transfer but he/she is not able to retrieve it.

- Very big errors weight: 200 pts. They are related to errors for which the FLS program assigns a task score equal to 0 pts. For example, the detachment of the Penrose drain from the velcro strip in the Intracorporeal Knot.

The final score of each exercise has been computed as the result of:

$$Task's\ score = starting\ score - p(Tc\%) - p(phases) - p\left(\sum_{i=1}^{3} n_i w_i\right)$$

where 'p' means penalty, 'i' respectively small, big and very big errors, 'n' the number of errors and "w" the correspondent weight.

This implies that:

- Participants with a similar performances can be discriminated mainly through on Tc%.
- Participants who complete the task can be discriminated mainly through the kind of errors.
- Participants who don't complete the task can be discriminated mainly through the number of not completed phases.

The gravity of the errors have been decided in collaboration with Resident from the Computational Surgery Department. The simplicity of the rules and the objectivity of this metric allows whoever to correctly grade a performance simply by looking at its video.

The main limit of this kind of metric is that it allows to describe the performance for what concern how the exercise has been performed and its final output but it doesn't provide information about the subject behaviour and the physiological and mental demands during the task.

For these reasons, a standard FLS trainer platform has been integrated with different devices in order to extract those kind of information from the subject. The Setup of this acquisition system will be described in the following Section.

3.2 Setup of the acquisition system

The following Section presents the Setup of the acquisition system. As it can be evinced from Chapter 2, there is not an a-priori specific sensor that can be used to detect the stress and the mental load. Therefore, it has been decided to include in this first version of the platform a large gamma of sensors providing different kind of information. They encompass the use of video-cameras, Smart Trocars, Eye Tracking, physiological monitoring through

Smart Cloth and EEG.

Figure 3.2 represents the entire experimental setup. The FLS trainer box and its screen constitute the participant side while the other screen is used by the operator that run the experiment, managing the GUI and the other sensors.

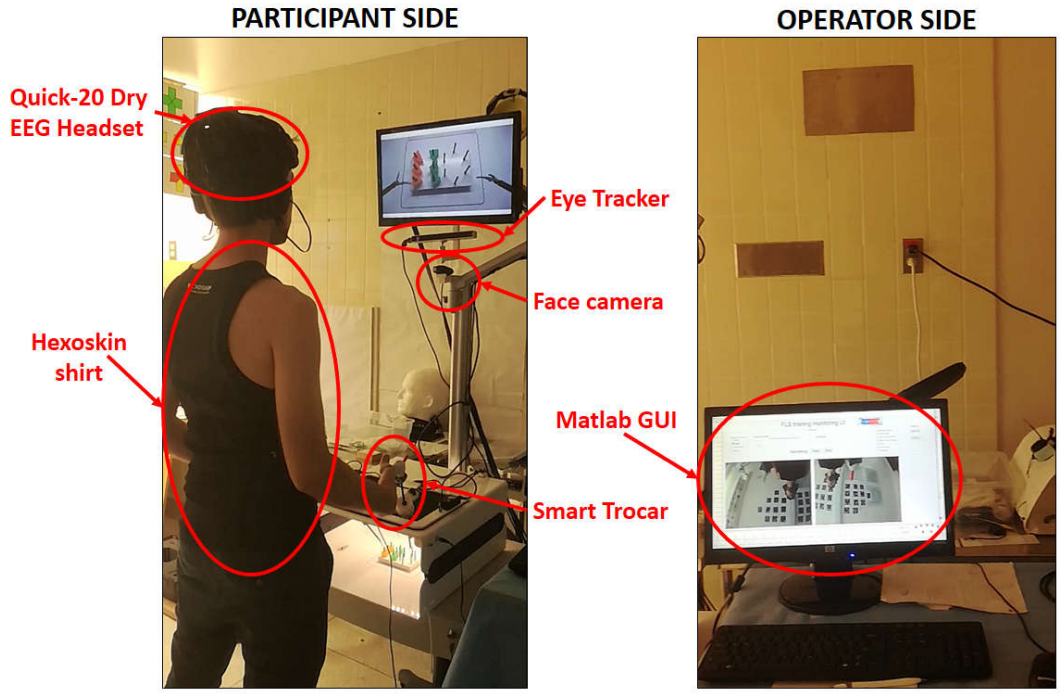

Figure 3.2: Experimental Setup

Section 3.2.1 presents the functioning of all the instrumentation which has been integrated in the platform while Section 3.2.2 describers the development of the Graphic User Interface (GUI) created with Matlab. Particular emphasis is given to the explanation of all its functionalities. Moreover, the civil aviation concepts called “Attentional Tunnelling” has been included in this UI. The idea has been to provide external events to the participant to see how they influence his/her performance. These external events will be called “Tunnel Effects” for the rest of the work.

The offline extraction and synchronization of the signals acquired from the devices has been treated in Section 3.2.3.

3.2.1 Instrumentation

The following section will describe how all the devices have been integrated with a normal FLS trainer box and their functioning (Figure 3.3).

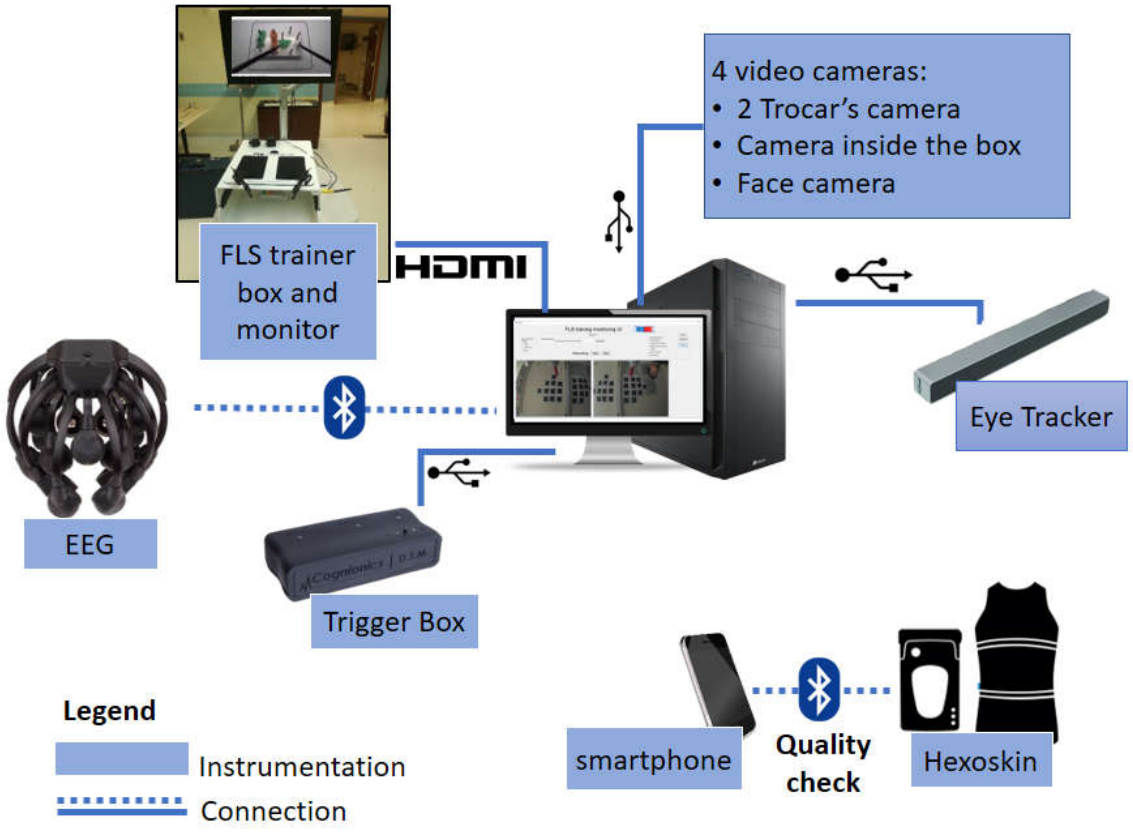

Figure 3.3: Instrumentation and connections

The instrumentation will be presented in the following order: the Smart Trocars, the trainer box and the monitor, the Eye Tracker (ET), the Smart Cloth (Hexoskin) and the EEG (Cognionics Quick-20).

Smart Trocars

The Smart Trocar consists of a standard laparoscopic trocar which has been modified to retrieve some information about the laparoscopic tool in use. The idea has been developed in the Department of Computational Surgery at HMRI [3], [40]. The modification consists in the creation of a support for the attachment of a small camera to the side of the valve head focused outward, toward the inserted laparoscopic instrument. Moreover, a perforated coloured wheel has been attached to a standard laparoscopic hand instrument near the handle (Figure 3.4). Wheels with different patterns corresponds to different instruments. When the tool is in the FOV (field of view) of the trocar's camera, the wheel will be captured in the video.

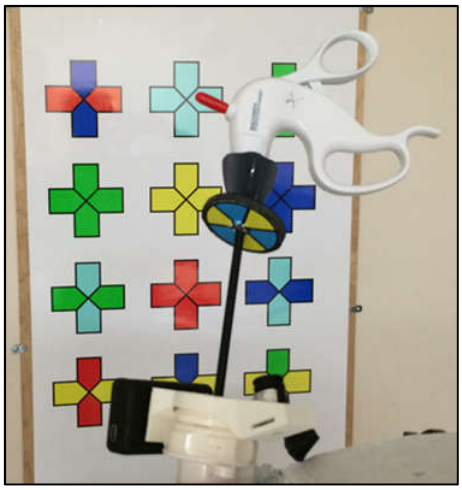

Figure 3.4: Smart Trocar: a support with a camera pointed toward the inserted tool is placed on a standard trocar. The coloured wheel is used to recognize the specific tool based on the pattern recognition algorithm. The coloured cross-shape markers on the background is normally placed on the ceiling and it is used as part of an image-based algorithm for the reconstruction of the motion of the tool.

The first kind of information consists in the recognition of the instrument in use. The video of the camera undergoes a pattern recognition algorithm which is able to extract the wheel's pattern with that, to recognize the instrument [40] (Figure 3.5 A). This information can be applied to verify the correctness of a laparoscopic procedure. In fact, information such as the type of instrument, when it has been inserted, extracted and how long it has been used, can be used to detect deviations from the standard procedure.

The other application of this technology is the reconstruction of the motion of the tip of the tool in the space. The system is based on computer vision and triangulation. It uses the reverse principle of stereoscopic vision: instead of using two different cameras separated by a well-known distance to determine the depth of the object, it uses two objects at a well-known distance and a single camera. The objects consist of specific flat shapes on the ceiling. They are normally located in different positions to allow the cameras of the trocar to capture most of them from every angulation of the instruments. Knowing some fixed features on the ceiling, the geometry of the Smart Trocar, the pose of the camera and the vertical distance from the ceiling, the position of the trocar can be estimated (Figure 3.5 B). Moreover, knowing the length of the tool and determining the size of the wheel in the video and its orientation, it is possible to find how deep the surgical tool has been inserted and its orientation. The pattern on the ceiling used in the original version of the Smart Trocar consists of coloured cross-shape markers as can be seen in the background of Figure 3.4. The system has been tested in different conditions and it provides accuracy on the rotation

angle of 0.2° and 0.4 mm along the three axes. The tolerated motion between frames is 4° of rotation and 5 mm of translation [3]. The main advantages of this technology is its portability and its easy setup in different kind of environments.

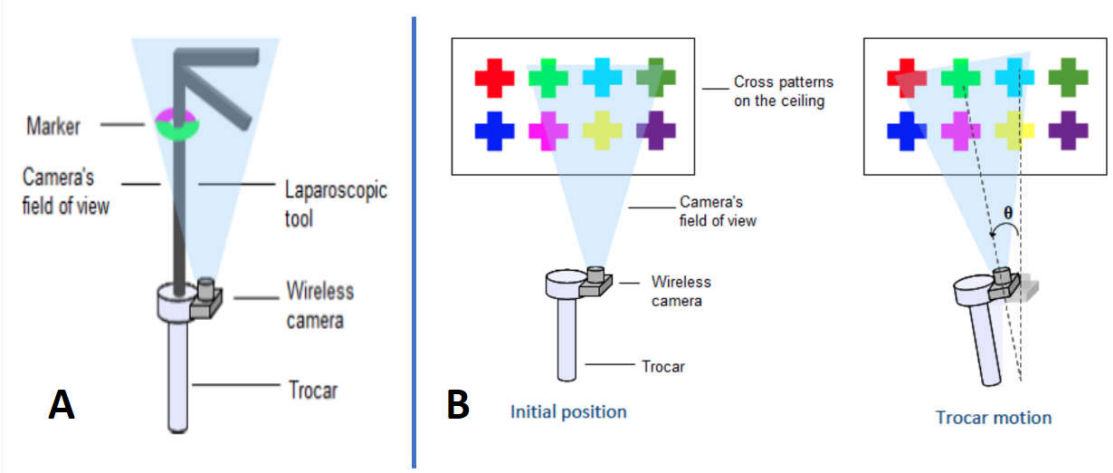

Figure 3.5: Smart Trocar information. (A) The recognition of the tool through the detection of the wheel's pattern. (B) The reconstruction of the trocar's motion based on features extracted from the pattern on the ceiling. [3]

It has been thought to include this kind of technology in this study to exploit the ability to estimate the motion of the tool. However, both the implementation of the algorithm and the design of the tool have been modified to fit the necessities of this work.

Firstly, this study regards the analysis of few task in a training environment. For this reason the recognition of the tool in use is not useful and no wheel marker has been attached to any laparoscopic tool. This decreases the number of objects/obstacles in the Field Of View (FOV) of the camera between the latter and the ceiling, increasing the possibility to detect the pattern for the entire duration of the exercise. The lack of the tool's marker limits the estimation of the motion from the 3D to the 2D space and it doesn't allow the recognition of the tool's rotations along its axis. The idea has been to use this technology to find differences among the usage of the left and right hands or to compare the tool's movement among subjects in terms of motion efficiency. For these purposes, the 2D movement of the tool is enough for a first analysis.

The cameras used in this technology are Mobius Action Cameras. As can be imagine looking at Figure 3.6, if the camera is placed in vertical position on the side of the trocar as it is, the motion of the instrument will be very limited due to its size.

Figure 3.6: Mobius Action Camera

For this reason, in the original version of the Smart Trocar, the camera has been extracted from the rest of the electronics case and connected to the latter though an electric extension. The original support was designed to put the camera alone on the side of the trocar facing up and tilt toward the inserted instrument while the case was attached on the internal part to a Velcro stripe on the other side (Figure 3.7). Once extracted, the camera itself is very small and its size makes it very suitable to be integrated on the trocar.

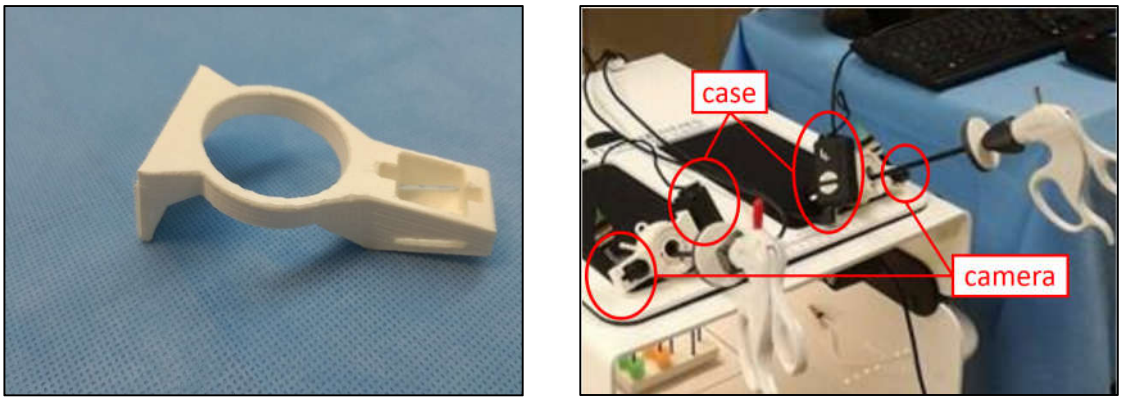

Figure 3.7: On the left the old support for the Trocar's camera. On the right its integration in the FLS platform.

After some trials it has been decided to change the support due to several reasons:

- the video was strongly affected by the presence of the subject in the middle of the image leaving the patterns on the ceiling on the side where the image is more distorted.
- For deep insertions of the instrument the view of the camera was completely obstructed by the hand of the surgeon and the handle of the tool.
- Reversing the position of the camera and its case or orienting the support in a different way would have decreased the range of motion of the tool due to impacts with the upper part of the trainer box

These problems are mostly due to the fact that the camera is placed on the side and its tilt angle is toward the tool. The new support for the camera has been designed to put the camera on the side of the trocar that is far from the user. It has been applied an inclination of about 10° not toward the instrument. This inclination has been chosen to increase the part of the FOV of the camera occupied by the ceiling and not by the tool or the subject, increasing the possibility to detect the pattern for the entire duration of the task. Moreover, this tilt allows possible future applications which require the identification of the tool because the wheel can still be seen during the insertion and the extraction when the handle of the instrument is pretty far from the camera. This study doesn't regard operations on a real body. For this reason, the case of the camera is not required to be attached to the support. Thus, a minimalistic approach has been applied on the design of the new support, according to which only the camera has been mounted on it and its case has been directly attached to the FLS trainer box increasing the manoeuvrability of the tool.

The support has been designed with Blender, an Open Source software for 3D object creation. Then, the obtained STL object has been 3D printed with a Replicator 2X obtaining the support in Figure 3.8. As can be evinced looking at these figures, the place of insertion of the camera presents a slit on the side for the wire connection and an hole on the bottom both for heat dispersion and facilitate the extraction of the camera from the support.

Figure 3.8: The new support for the Trocar's camera: the Blender's object (top-left), the 3D printed version (bottom-left) and its integration in the FLS platform (right).

Mobius Action Cameras are equipped with a micro SD. Their settings can be modified using the mSetup software of the Mobius and saved on it. Both cameras of the Smart Trocar have been integrated in the Matlab GUI presented in Section 3.2.2. To initialize and control the stream of the cameras from the interface, they have been connected to the tower of the pc via USB. This kind of connection makes them work in WebCam mode. Unfortunately, the SD card must be removed when used in this kind of modality and the only setting that can be modified with mSetup is the "WebCam Mode" option which has been set to "H.264 + audio" [41].

The impossibility to manage other settings such as Auto-focus and Auto-brightness is also extended to Matlab in which the only accessible camera's parameters are its Resolution and its Frame Rate. These limitations, together with some ambient conditions in which the experiment have been performed are the main reasons why a new algorithm for the reconstruction of the tool's 2D movement has been implemented. The autofocus modality is disabled in WebCam mode and the focus of the camera has been manually adjusted to focus on the ceiling.

As it has been already anticipated, the original method for the movement reconstruction makes used of a colour cross-shape pattern placed in different positions on the ceiling. A Matlab algorithm analyses all the frames of the video to extract specific features points from them. The knowledge of correspondent features points in subsequent frames is enough to proceed with the 2D motion estimation. The extraction of the crosses is obtained through the application of a threshold and the recognition of the specific one is made through color recognition.

The available room in which the acquisitions have been conducted was characterized by the presence of no natural light (no window) and of two very big light source on the ceiling. First, the harsh light emitted by those sources distorts colours in the room and second, without the possibility to access the Auto-brightness parameter, the cameras were strongly affected by the presence of these light sources in their field of view. Whenever they enter the FOV of the camera, the latter reacts darkening the image. The non-static position of the camera makes this process to be very dynamic alternating bright and dark frames depending on the amount of light source in the FOV. This time by time adaptation makes really challenging the segmentation and the color identification of the crosses. To overcome such limitations, a new pattern and a new algorithm for the 2D motion estimation have been

developed using the same principles in the old version (Figure 3.9). The pattern, the new algorithm and its validation will be described respectively in Section 3.3 and 4.2.

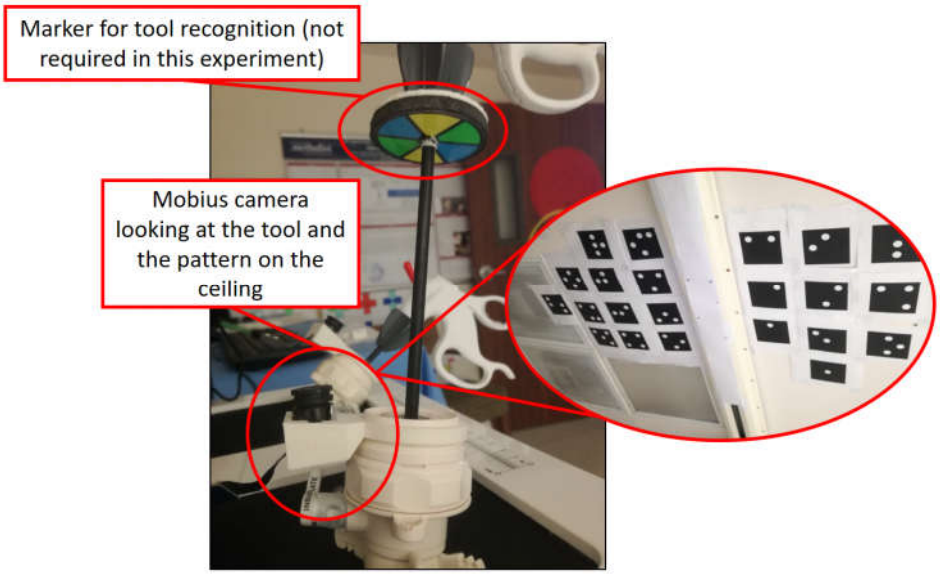

Figure 3.9: Final Smart Trocar setup. The wheel attached to the instrument has not been used in this work. The new pattern on the ceiling is shown in the circle on the right

Trainer box, TV monitor

The FLS trainer box comes with a TV Camera (RCA-NTSC), plus LED lighting to illuminate the inside. The former (Figure 3.10A) is the replacement of the laparoscopic camera used in a real procedure. On the right side of the box, there are two outlets (Figure 3.10B): one for the power supply of the LED lights and the camera and the other is for a jack video connection among the camera and the TV monitor (Insignia NS-19D220NA16) for the visualization of the video. The monitor requires its own power supply and its position with respect to the box can be regulated.

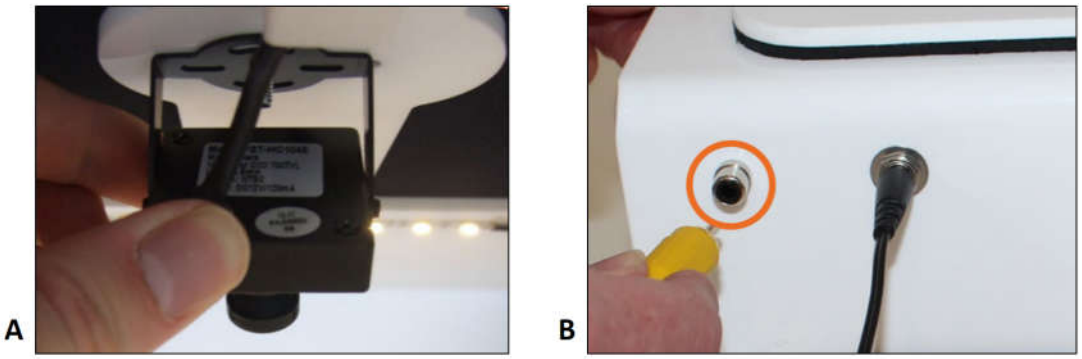

Figure 3.10: (A) TV Camera (RCA-NTSC) inside the box. (B) the two outlets on the side: the left is the jack connection for the transmission of the camera video to the monitor and the right one is for the power supply of the box.

To record and eventually interact with the video, the camera has to be connected to the PC and has to be integrated in the GUI. A Raygo USB Video Recorder adaptor has been used to create a jack-USB connection with the computer. Unfortunately, the camera is neither visible or accessible by the pc with such connection. It has been decided to unscrew the camera and replace it with another one.

The Logitech HD pro webcam C910 has been chosen. Firstly, the camera has been tested in the GUI and it has been found to have a good performance for the real-time video with an Frame Rate of 30fps. Obviously, the whole webcam was too big to fit in the box without be touched by the instruments. Thus, the case has been removed together with the microphones on the side leaving the camera connected to its electric circuit board. A support for the camera has been created with Blender, 3D printed and screwed on the top of the box (Figure 3.11).

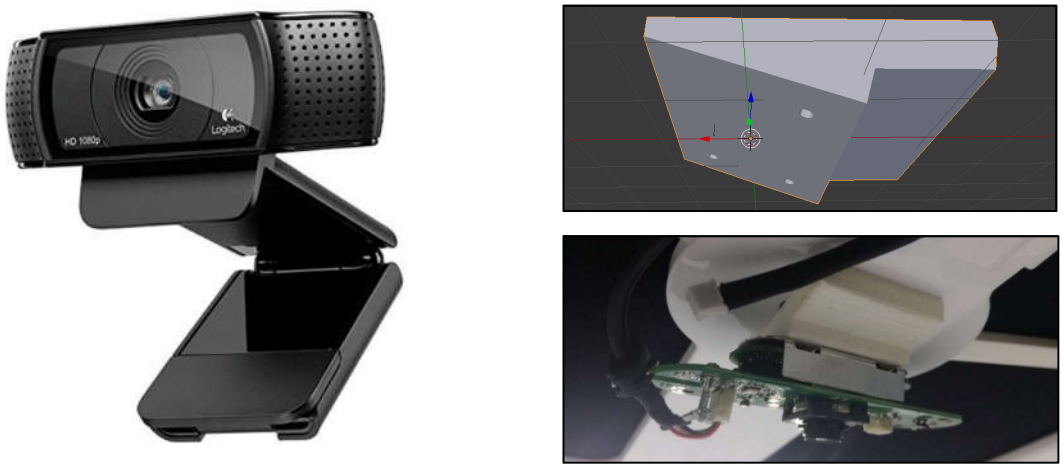

Figure 3.11: The Logitech HD pro webcam C910 (left), its support in Blender (top-right) and its integration in the box (bottom-right) once it has been removed from the case.

This camera guarantees a good real-time video management by the GUI and it doesn't interfere with any instrument because its zoom allows to place it very closely to the top of the box. Its video has been displayed on the monitor of the FLS platform through an HDMI connection with the pc.

Eye Tracker and Face Camera

The fovea of the eye is a small region of acute vision within which fine details can be discerned. Outside of it, acuity goes down rapidly. When the subject focus the attention on a movable object, his eyeball is rotated in such a way that the object of interest becomes imaged on the fovea. Since the observer pays attention to objects by foveating them, a way

to understand what the subject is focusing the attention on is through devices able to detects the observer line of gaze.

Eye tracking is the process of measuring either the point of gaze, that is where the subject is looking at, or the motion of an eye relative to the head. The device used for these purposes is called Eye Tracker (ET) and it has been used in research on the visual system, marketing or as an input device for human-computer interaction. Many eye tracking methods have been presented in the literature. In particular they can be subdivide in two categories [42]**:**

- Sensor-based Eye Tracking (EOG): It detects and analyses eye movements based on electric potentials measured with electrodes placed in the region around the eyes. These potentials changes based on the eye direction and the entity of the movement. This electric signal detected using two pairs of electrodes placed around one eye is known as electrooculogram (EOG).
- Computer Vision-based Eye Tracking: It encompasses the most common eye tracking methods. There are two main areas investigated in the field of computer vision based eye tracking. The first area regards the eye detection in the image, also known as eye localization while the second area consists in eye tracking, which is the process of eye gaze direction estimation based on the data obtained from processing and analysing the detected eye region. The most famous methods are corneal-reflection-based and shape-based. The former methods rely on external light sources such as infrared light to detect eye features. On the other hand, shape-based methods infer gaze direction from observed eye shapes, such as pupil centers and iris edges.

The use of the Eye Tracker has been embedded in this study to investigate where the subject is looking at on the FLS screen, his/her pupils' dimension and the blink rate. It has been chosen to use the Eye Tracker from "The Eye Tribe" Company which provides a good trade-off among specifics and price. This Eye Tracker is equipped with a camera and a high-resolution infrared LED that are used to retrieve information about the eye. It belongs to the family of Computer-vision based Eye Tracking and it is one of the smallest eye tracker device (20 × 1.9 × 1.9 cm). The device has been connected to the tower through the required USB 3.0 connection. Apart this connection, it doesn't require a separate power source and this makes it even more portable. The eye gaze coordinates are calculated with respect to a screen the person is looking at, and are represented by pairs of (x, y) coordinates expressed in the screen reference system whose origin is located on the top left corner (Figure 3.12A).

In order to track the user's eye movements and calculate the on-screen gaze coordinates, the Tracker must be mounted horizontally on the tripod below the monitor as shown in Figure 3.12B. It is important that the Tracker is centered relative to the monitor and the latter must be max 24". The subject have to be located within the volume in space the user can be theoretically be tracked by the system (Figure 3.12C). This volume is called trackbox and its size depends on the frame rate (30 or 60Hz); an higher frame rate corresponds to a smaller trackbox.

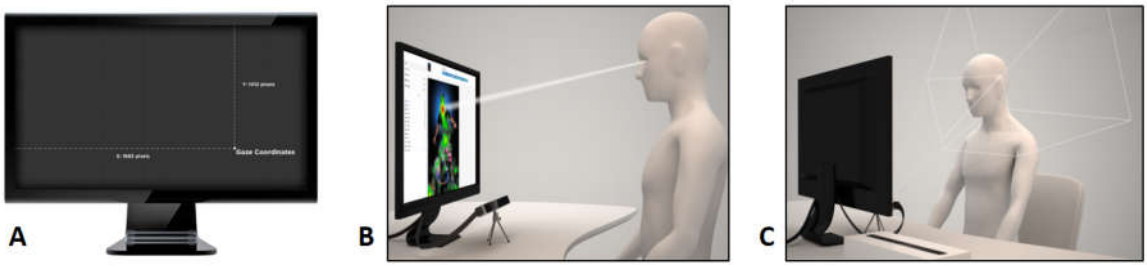

Figure 3.12: (A) Bi-dimensional screen reference frame. The origin is located in the top-left corner. (B) Standard scenario with the device placed below the center of the screen. (C) Working volume of device (Trackerbox)

The setup has been adjusted to fit the conditions in this study. A support has been 3D printed to attach the eye tracker below the movable monitor of the platform (Figure 3.13). The bottom part of the tripod has been eliminated and substituted by a screw that allows to place the ET along a guide in the support.

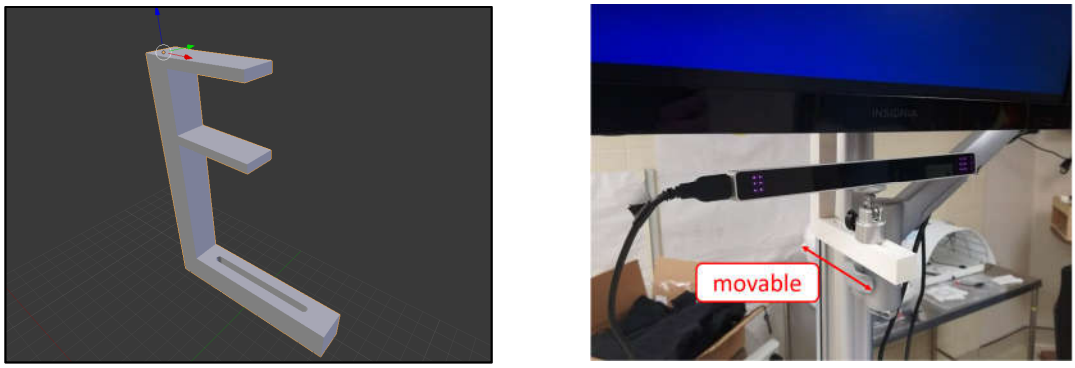

Figure 3.13: Eye Tracker support. It presents a guide on its base along which the ET can be mover (left). It is attached to the back of the monitor in order to place the ET below the center of the screen (right)

The operating range of the device is at 45-75 cm from it and the possible Frame Rates are 30 and 60Hz. In this project the subject has been located at about 60 cm from the device.
Each person has different eye characteristics that the eye tracking software needs to take into account to estimate the gaze accurately. Thus, prior to use the Eye Tracker for any

acquisition, a calibration process must be performed. The producer guaranties an average accuracy around 0.5 to 1º of visual angle and a spatial resolution of 0.1°. Assuming the user sits approximately 60 cm away from the screen/tracker, this accuracy corresponds to an on-screen average error of 0.5 to 1 cm [43].

The calibration, the management of the settings and the acquisitions have been made through the use of the Eye Tribe UI, the eye tracker's user interface. The Framerate has been set at 30Hz to maintain a larger trackbox due to the possibility to move the head during the tests. The monitor to use and its resolution have been defined in the calibration panel of the interface.

The calibration process consists in a circular target that is displayed at different locations of the screen on a blank background for a total of about 2 seconds each. During the calibration, the user has to follow the target with the eyes without moving the head. Once it finishes, a calibration's score is displayed and its quality can be checked by looking at specific circles on the display which will become red when the subject looks at them (Figure 3.14). After a successful calibration, the Tracker should not be moved otherwise a new calibration is required to update the parameters of the system with the new ones associated to the new position.

Figure 3.14: Example of calibration output where the calibration's score is displayed on the bottom part of the screen.

Once the device has been connected to the pc and the EyeTribeUI have been launched, the application opens a connection with the Tracker Server which is needed for the eye tracker to work. Then, the calibration has to be performed and the eye tracker will be ready to use. The API Console is a tool of the UI that allows to see and record the data elaborated by the

EyeTribe Server. Data are saved in a text file in which all the samples are reported row by row. Each sample encompasses lots of information. The most important are:

- Avg x: smoothed gaze x-coordinate in pix
- Avg y: smoothed gaze y-coordinate in pix
- Left x: smoothed x-coord of the left eye
- Left y: smoothed y-coord of the left eye
- Pupil center left x: pupil x-coordinate normalized of the left eye
- Pupil center left y: pupil y-coordinate normalized of the left eye
- Pupil size left: pupil size of the left eye
- Right x: smoothed x-coord of the right eye
- Right y: smoothed y-coord of the right eye
- Pupil center right x: pupil x-coordinate normalized of the right eye
- Pupil center right y: pupil y-coordinate normalized of the right eye
- Pupil size right: pupil size of the right eye
- Time and date of the acquisition of the sample

Matlab has been used to read the produced TXT and to extract from it only the useful information.

The device's accuracy guaranteed by the developer has been verified. An image of the same resolution of the screen has been created. Its background was gray with nine black squares of 4x4 pixels located in specific positions. The image has been displayed at full screen on the monitor. Due to the fact that the image and the screen have the same resolution, it has been possible to use the 2D gaze coordinates (x,y) from the eye tracker to identify which pixels of the image the subject was looking at. The device has been located at about 60 cm from the subject. The latter has been asked to look at each of the squares in the image maintaining a stable gaze for few seconds each. The x and y coordinates of the gaze have been extracted from the TXT acquisition file with Matlab and displayed directly on the image taking into account the origin of the ET reference frame (Figure 3.15). Two circles have been drown for each of the nine squares. They represent the extremities of the average error (0.5 and 1 cm) guaranteed by the developer and their dimensions have been scaled in pixels based on the horizontal and vertical pitch of the monitor's pixels. It has been found that for all the fixation points the gaze samples were inside the larger circle with a decrease in the accuracy moving from the center to the left and right side of the screen.

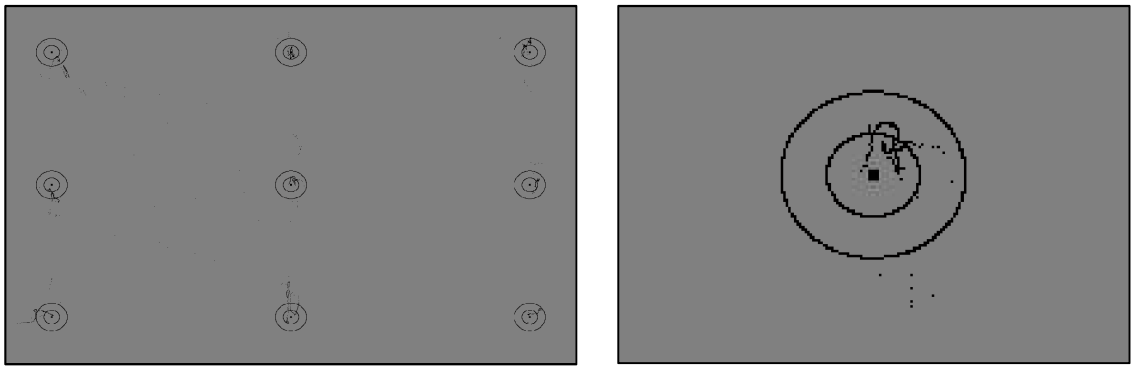

Figure 3.15: Verification of the ET specifics. The circles around each target represent the extremities of the average error (0.5 and 1 cm) guaranteed by the developer. Samples are inside each external circle (left). Focus on one of the targets (right).

A Mobius Action Camera has been mounted under the screen in order to record the face of the subject during the performance of each task (Figure 3.16). The blinks observed in the video has been used to validate the blinks detected by the algorithm. As for all the others cameras, the "Face Camera" has been connected to the PC via USB and integrated in the GUI.

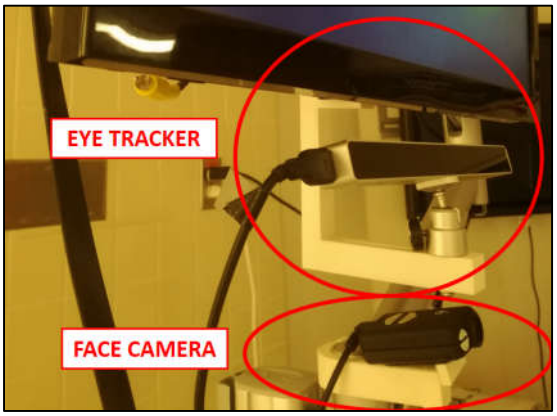

Figure 3.16: Eye Tracker and Face camera with the respective supports.

Hexoskin Smart Cloth

Heart and Respiration parameters can be a great source of information while studying the subject's physiological state during the performance. However, it is not possible to use any invasive device in this kind of study. Moreover, the sensors should not obstacle the movement of the subject or make him feel uncomfortable. For these reasons, it has been decided to use an Hexoskin Shirt which is a Smart Cloth produced by "Hexoskin" wearable body metrics company. It is a sensor-embedded smart shirt clinically validated that allows ECG cardiac monitoring with lung function and activity monitoring. It is used in sport as

well as for healthcare applications. It is made by built-in all-textile sensors that make it light and comfortable. Moreover, it is water-resistant, machine washable and easy to wear.
Talking about healthcare applications, the Hexoskin system has been designed to reduce the frequency of patient travel and allow remote communication among the patients, caregivers or researchers. During the recording, data can be seen real-time through a Bluetooth communication with the Hexoskin App that can be installed on any compatible devices.
The whole instrumentation encompasses (Figure 3.17):

1. Hexoskin shirt
2. Hexoskin device: it is where data are stored. It must be plugged in the shirt cable for the recording.
3. USB cable: is used to connect the device to the pc and upload the recorded data from the Hexoskin recording device on the Hexoskin dashboard from where they can be downloaded.
4. Elastic bands: they are used to stuck the sensors to the body ensuring a better signal quality. One of the bands must be placed at the thorax level (only for men) and the other at the abdomen level (both for men and women).

Figure 3.17: Hexoskin instrumentation

The sensors are localized in two bands of the shirt, one at the thorax level and one at the abdomen level. The specifics about the cardiac and breathing sensors have been summarized in Figure 3.18.

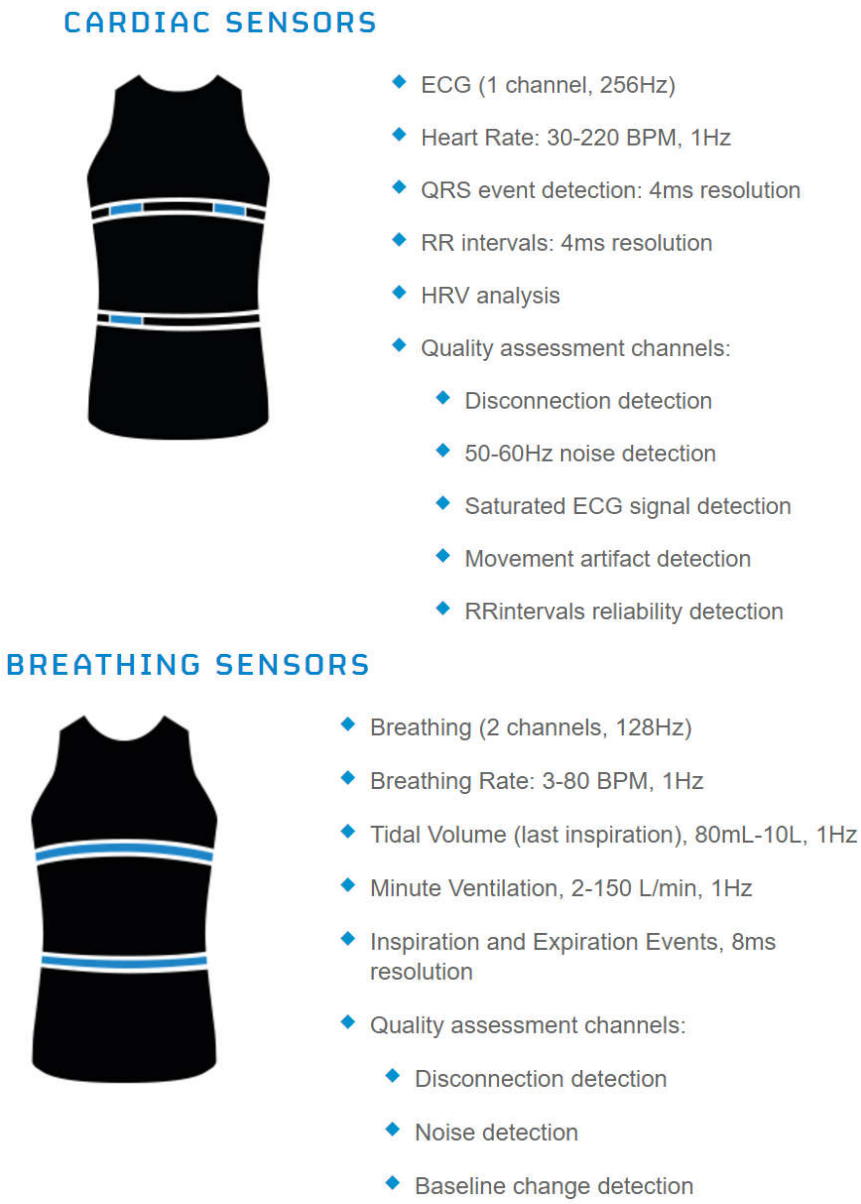

Figure 3.18: Hexoskin cardiac and breathing sensors specifics [44]

The three cardiac electrodes are used to obtain the Lead I of the ECG at 256Hz. The Breathing information can be obtained through the Respiratory Inductance Plethysmography (RIP) method by measuring the movement of the chest and abdominal wall. The method is based on two channels of information made of wire coils insulated and placed at the thorax and abdomen levels. They are connected to an oscillator and subsequent frequency demodulation electronics to obtain the digital waveforms. During the respiration, both inspiration and expiration, the cross-sectional area of the rib cage and abdomen changes altering the self-inductance of the coils and the frequency of their oscillation. This change in frequency is converted by the electronics to a digital respiration waveform where the

amplitude of the waveform is proportional to the inspired breath volume and two subsequent peaks identify a respiratory cycle.

The Hexoskin is able extract and elaborate these raw data to obtain more common information such as Heart Rate, Breath Rate, Minute Ventilation, Tidal volume and so on.

A description of all the signals (raw and processed) can be found on the Hexoskin API documentation [45]. The signals of interest for this study are:

- Breathing Rate [rpm]: Calculated over the last 7 respiration cycles. Sampling freq: 1Hz.
- Breathing Rate status: Quality of breathing rate signal. Sampling freq: 1Hz.
- ECG [mV * 0.0064]: 1 lead ECG channel with a 12 bits resolution. Sampling freq: 256Hz.
- Heart Rate [bmp]: Average over the last 16 heart beats. Sampling freq: 1Hz.
- Heart Rate Status: Quality of heart rate signal.
- Minute Ventilation (raw or adjusted taking into account the user profile) [mL/min]: volume of air/minute inspired in the last 7 complete respiration cycles. Sampling freq: 1Hz.
- NN interval [s]: Time between to heart beat detections, calculated for every QRS event.
- Abdominal and Thoracic Respiration [NA]: 2 RIP (Respiratory inductance plethysmography) sampled at 128 Hz with a 16 bits resolution.
- Tidal Volume (raw or adjusted taking into account the user profile) [mL]: Volume of air inspired in the last inspiration. Sample freq: 1Hz.

To start a data acquisition, the Hexoskin device has to be plugged in the Smart Shirt and placed in its pocket on the side. As soon as the device is connected to the shirt, the data recording starts. It is possible to see the data extracted by the shirt by pairing the device via Bluetooth with any mobile device on which it is installed the Hexoskin app. This is very usegul application that has been used to check the quality of the data and to adjust the placement of the sensors based on its information.

The device must be unplugged to terminate the recording. Then, it has to be connected to the PC via USB cable to extract the data from it. The HxServices software of the Hexoskin allows to synchronize the device with the online Hexoskin server and upload the recording on it. At this point, all the data can be managed from the online dashboard acccesible from the Hexoskin account. It is possible to look at the Reports produced by the Hexoskin or to

download all the data in different file formats, mainly CSV and WAV. Raw data in .WAV format can be converted into .CSV thanks to the "HxConvertSourceFIle" application.

Cognionics EEG

The activity of the brain is another useful parameter to assess the performance of the participant in terms of mental load and stress. It can be measured in many ways, differing from each other in terms of technology, invasiveness, and nature of the recorded signals. In particular, it can be measured from the electrical, magnetic and metabolic point of view [46]. As done in different studies proposed in Chapter 2, it has been decided to monitor the electric activity of the brain which can be potentially used for a wider range of future analysis. The non-invasive device used in this study is the Quick-20 Dry EEG from the Cognionics [47]. The entire apparatus (Figure 3.19) is composed by:

- A 20 Dry EEG headset (10-20 system)
- A Beacon: for Bluetooth connection
- A Trigger box: to send triggers

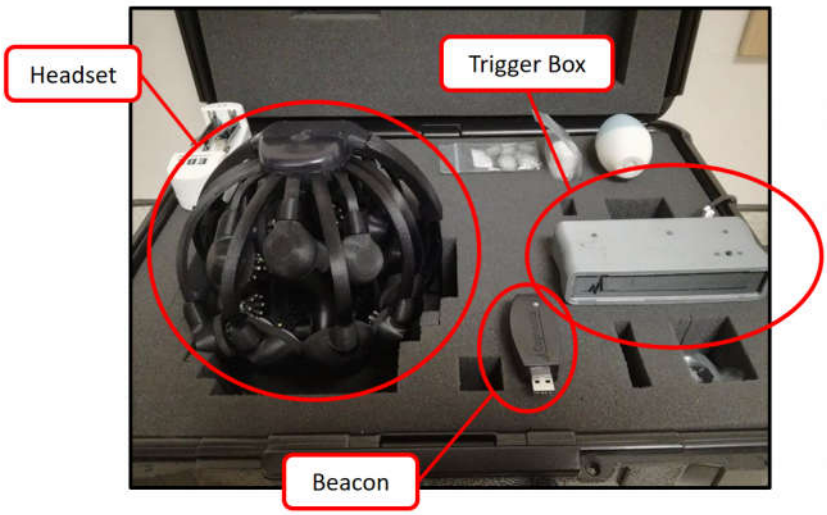

Figure 3.19: Quick-20 Dry EEG instrumentation

The Quick-20 is a complete portable EEG system that can easily adapt to scalps of different size. It is a "Dry" EEG, so it doesn't require the application of electrolytic gel on the head. This, in addition to the wireless Bluetooth communication make it really easy and fast to wear. The headset supports a 10-20 system configuration represented in Figure 3.20A. The 10-20 system is an international method to describe how to place the electrodes on the scalp. The '10' and '20' refer to the fact that the distances between adjacent electrodes are either

10% or 20% of the total nasion-onion or right–left preaurical distance of the skull (Figure 3.20B).

The electrode are of two types:

- Flex electrode: designed to work through hair (Figure 3.20C)
- Draypad electrode: designed for bare skin. It is made of ionically conductive polymer (Figure 3.20D).

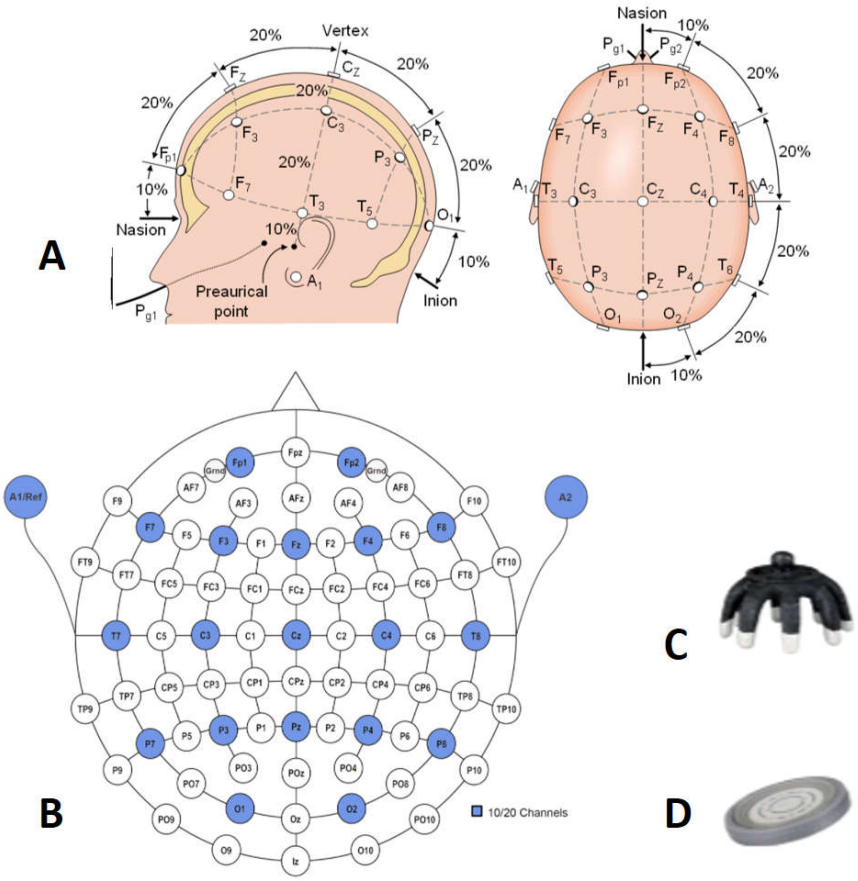

Figure 3.20: (A) Lateral and top view of a 10-20 system. (B) top view of the 10-20 system of the Quick-20. (C) Flex and (D) Draypad electrodes

A summary of all the device's specifics is reported in Table 3.2.

Channel Count	Full 10-20 EEG array (20-channels plus reference and ground), plus 2 optional referential lead wires
Extension Channels	8 optional analog inputs with add-on module for ECG/EMG/respiration/GSR, etc.
Sensor Type	Active dry electrodes with local active shielding
Impedance Monitoring	Real-time with EEG acquisition
Bandwidth	0-131 Hz at 500 samples/sec, 0-262 Hz at 1,000 samples/sec
Sampling Rate	500 or 1000 samples/sec
Resolution	24 bits per sample
Noise	0.7 µV RMS from 1-50 Hz, shorted inputs
Wireless	Bluetooth, optimized for high speed
Storage	microSD and microSDHC
Motion Sensing	3-axis Accelerometer, each axis an additional channel
Power Supply	Dual hot-swappable lithium ion batteries, 8-hours wireless, 16-hours microSD
Triggering	Compatible with Cognionics wireless trigger

Table 3.2: EEG acquisition system specifics [47]

Both the TriggerBox and the Beacon have to be connected to the pc via USB. The former can be used to send trigger (used as temporal markers) to the EEG and the second allows the Bluetooth communication.

The headset, powered by a lithium ion battery, must be turned on and paired with the Beacon. The Cognionics software allows to configure the device and visualize the real time output. The device has been configured with a pre-compiled protocol. The Sampling Rate has been set to 500Hz.

Once the headset has been configured, the signal from every channel will be visible in real-time on the interface. As it is shown in Figure 3.21 there are some additional channels respectively three from the 3-axis accelerometer embedded in the headset and the Trigger signal. Whenever the button on the Trigger Box is pressed, a trigger is sent to the EEG and a red spike will appear on the Trigger signal. In study, this function has been used to create temporal markers to be used as references in the overall EEG tracks. However, it has not been used manually; its functioning has been control through a serial communication implemented in the GUI through which also the amplitude of the trigger can be manipulated.

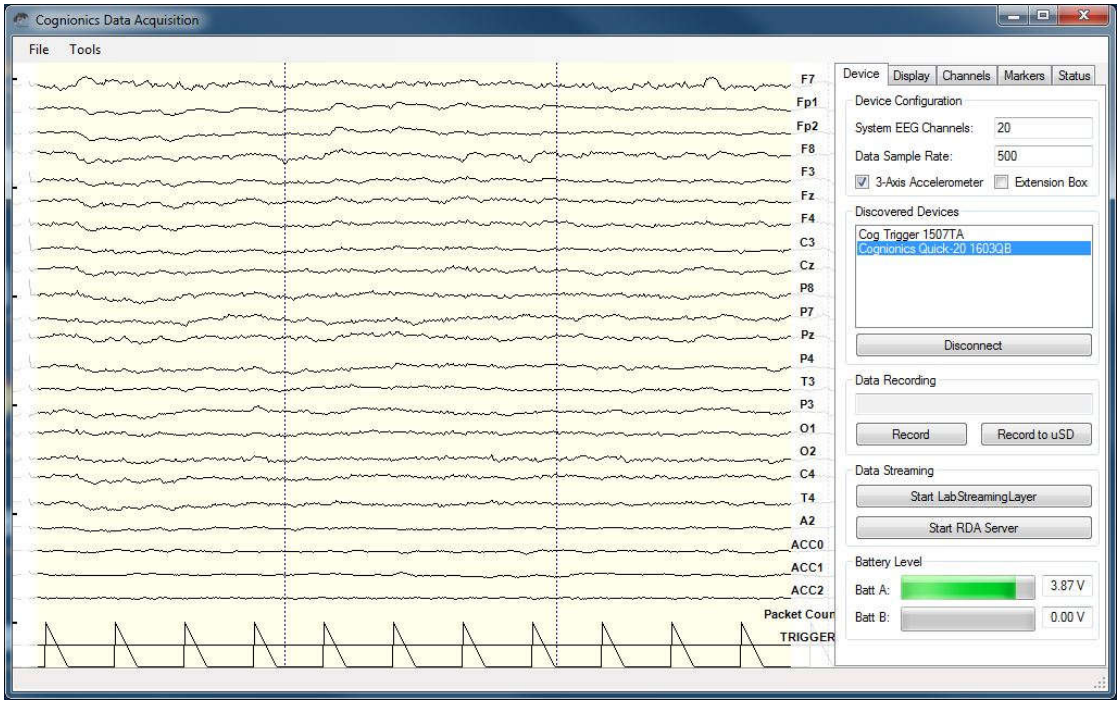

Figure 3.21: Signals visualization with the Cognionics Software. They encompass the signals from the channels on the scalp, other three from the 3-axis accelerometer and the Trigger signal.

From the software, it is possible to check the level of the battery, to change some basic parameters such as the Sampling Rate, to modify the display settings and to check the Real-time measurement of sensors impedance. The latter is a very important information to ensure a good quality signal. Therefore, the position of the electrodes must be checked prior the start of the recording. Bad impedances are identified with a red color electrodes while good ones with a green color.

The device comes with a micro SD card to store the data but is has not been used in this study. Data have been saved locally in the pc launching the recording directly from the interface. The recorded data comprise:

- Signals from each of the 20 channels of the headset (with reference on A1) [μV].
- Signals from the 3-axis accelerometer (one for each axis).
- Trigger signal.

Each recording produces three different files respectively with extensions .eeg, .vhdr and .vmrk. This output has been read and managed with the EEGLAB toolbox of Matlab.

3.2.2 Graphic User Interface (GUI)

A Graphic User Interface (GUI) has been created with Matlab to control the functioning of some devices and allow the operator to manage the acquisitions.

For this purpose, the GUI development environment of Matlab called GUIDE has been used. Summarizing its functionalities, the GUI has been created to:

- Initialize, synchronize and save the videos from the four cameras: two from the trocars, one face camera and the one inside the box that from now on will be called laparoscopic camera for the sake of semplicity.
- Create a serial communication with the trigger box to send trigger to the EEG.
- Generate the Tunnel Effect to test the Attentional Tunnelling concept from Civil Aviation (Section 2.4.2).
- Insert and manage participant information.
- Control the start and the stop of the acquisition of each task.

From these points, it is clear that the GUI has not been used to control the start and termination of the recordings of Eye Tracker, EEG and Hexoskin signals whose acquisition has been done by means of their SWs. On the other hand, different camera videos will be produced for each task thanks to the GUI control of the start and end times of the exercise.
Two main problems have been experienced during the development of the GUI:

1. Ensure the real-time video from the camera inside the box (Logitech HD pro webcam C910 described in Section 3.2.1).
2. Choose the kind of Tunnel Effect (i.e. specific event aimed at testing the Attentional Tunnelling concept described in Chapter 2) to be provided to the subject during the performance. The idea has been to see if the occurrence of external events has an impact on the subject performance, for example by distracting him/her from the main task.

For what concern the first, it has been found useful to display the laparoscopic view with the preview function optimized to fit the screen and stop the preview of the other videos (i.e. the 2 trocars' cameras and the face camera) during the performance of the tasks. Moreover, the videos from the four cameras have been directly written into video-files with a Frame Rate of 5Hz decreasing the impact on the RAM of the PC. This helps in maintaining the same performance of the acquisition system for the entire duration of the experiment.
For what concern the second problem, in a first moment it has been tried to manipulate the image of the laparoscopic video generating rotations of the view or simulating the appearance of smoke during the performance. However with those Tunnel Effects, each frame must be read, manipulated and displayed on the screen introducing delays in the video. For these reasons, the sound has been chosen as Tunnel Effect due to its low impact on the

time require to process all the other operations. During the exercises of Peg Transfer and the Circle Cut, it has been decided to provide beep sounds generated with Matlab at specific moments. The first beep has been provided after about 40 seconds from the beginning of the task to let the subject focus on the main task "forgetting" about the rest.

On the suggestion of Residents of the Department of Computational Surgery, an heart beat audio track has been played during the Intracorporeal Knot task. The reason behind this is that surgeons are used to hear this kind of sounds, especially in the OR. That sound is associated to the status of the patient and a change in the sound corresponds to an improvement or a deterioration of the patient's conditions. This concept has been used to test if a sound related to specific patient condition affects the performance of the participant. The audio track encompasses a sequence of different rhythms: pseudonormal beat, ventricular tachycardia, ventricular fibrillation and no sound. Its duration has been thought in order to allow also the fastest subject to listen the whole track. Both the occurrences of the beeps and the start of each part of the audio track is managed within the Matlab GUI.

Launching the Matlab script of the GUI the interface will open. It consists of two panels: one for the insertion of the participant basic information and one to initialize the devices and start the acquisitions. The first has been represented in Figure 3.22.

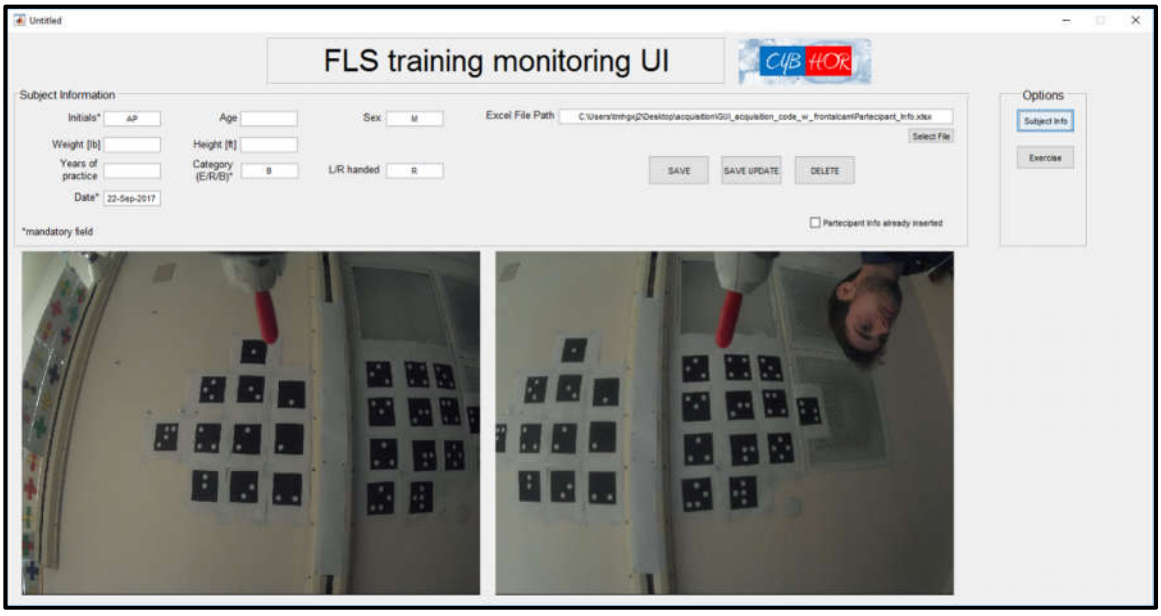

Figure 3.22: Subject Information panel of the GUI

In this panel, the operator has to fill the blank boxes with the participant's information. Only his/her initials, the category of membership (Beginner, Resident or Expert) and the date of the acquisition are mandatory. The interface allows:

- To save, update or delete the information of the current subject into an excel file appositely created for this purpose. It consists of a big excel table filled with participants information row by row.
- To avoid errors during the completion of the blank boxes. In fact, it comprises controls to check consistency of the data and an appropriate notification will be sent to the operator in case of errors.

It is also possible to bypass the insertion of the information by clicking on a specific checkbox in the right part of the panel. In this case, the only required box to fill prior the start of the acquisitions is the subject "Initials" because it is used to save the data with an appropriate name.

Figure 3.23 represents the second panel which is dedicated to the acquisition.

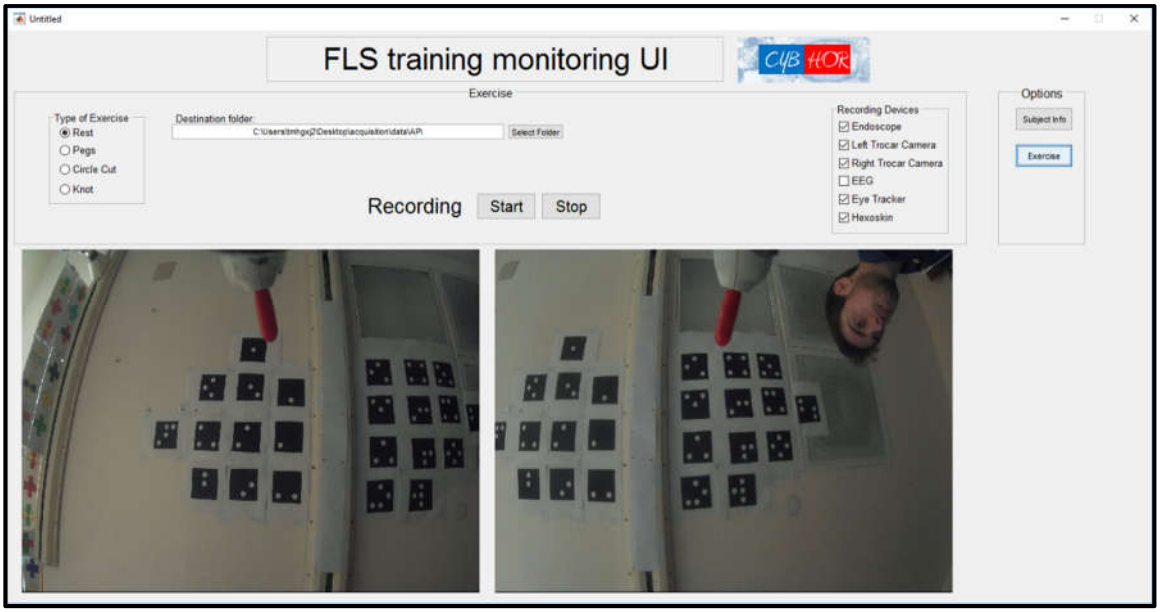

Figure 3.23: Acquisition panel of the GUI

From this panel it is possible:

- To select the kind of task that have to be performed by selecting the correspondent radiobutton on the top-left side. Variables relating to the kind of task, its maximum time limit and the associated tunnel effect will be updated accordingly. They are respectively:
  - Rest: no tunnel effect and max time limit of 120 sec.
  - Pegs: beep sound and max time limit of 300 sec.
  - Circle cut: beep sound and max time limit of 300 sec.
  - Knot: heartbeat audio track and max time limit of 600 sec.

At the end of the acquisition of a task, the selected radiobutton will automatically change to the one corresponding to the following task updating all the parameters.

- To initialize the different devices by clicking on the checkboxes on the top-right:
    - Laparoscope, Left and Right Trocar Cameras checkboxes: they set and open the previews of the cameras with the resolutions defined in the GUI.
    - EEG checkbox: it initializes the serial communication with the Trigger Box.
    - Eye tracker and Hexoskin checkboxes: they are only used to keep track in the excel file of the use of these device in the acquisition.
- To select the destination folder in which the data will be saved
- To start and stop the acquisition pressing respectively the START and STOP button.

To manage the cameras with Matlab, the "OS Generic Video Interface" *Matlab Support Package* has been installed. It provides Image Acquisition Toolbox Adaptors such as "winvideo" on Windows for the acquisition from any generic video interface. They have been initialized with a Frame Rate = 30Hz but their videos have been recorded at 5Hz during the tasks.

The Trocars cameras have been set with a resolution of 1024x768 (4:3) as a trade-off among quality and time required to process the video with the algorithm in Section 3.3.2.

The face camera, used only for validation purposes, has been assigned at a low resolution of 640x480 (4:3).

The resolution of the laparoscopic camera (1280x720) has been chosen together with the resolution of the FLS monitor (1280x800) to maximize the laparoscopic view in the middle of the screen (Figure 3.24).

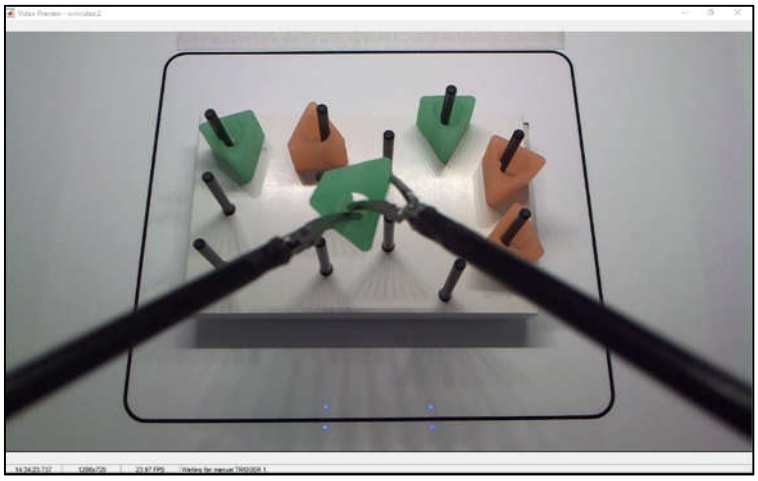

Figure 3.24: FLS monitor display during the Peg Transfer.

The absence of any magnification and the knowledge of the position occupied by the camera view on the screen allow to reconstruct where the subject is looking at on the video using the 2D gaze coordinates (x,y) detected by the Eye Tracker.

For what concern the serial communication, it has been initialized with a BaudRate of 57600bps as specified in the Cognionics Datasheet.

In conclusion, the algorithm produces four video files and a matrix with all the time reference for each task.

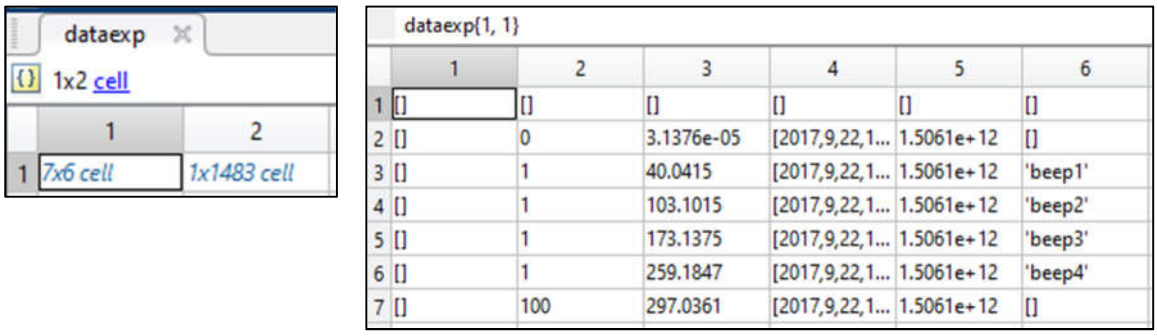

	1	2	3	4	5	6
1	[]	[]	[]	[]	[]	[]
2	[]	0	3.1376e-05	[2017,9,22,1...	1.5061e+12	[]
3	[]	1	40.0415	[2017,9,22,1...	1.5061e+12	'beep1'
4	[]	1	103.1015	[2017,9,22,1...	1.5061e+12	'beep2'
5	[]	1	173.1375	[2017,9,22,1...	1.5061e+12	'beep3'
6	[]	1	259.1847	[2017,9,22,1...	1.5061e+12	'beep4'
7	[]	100	297.0361	[2017,9,22,1...	1.5061e+12	[]

Figure 3.25: Example of matrix produced by the GUI at the end of a task (left) and a focus on its first cell (right)

Observing the example in Figure 3.25 , the time matrix “dataexp” has been structured as follows:

- Cell {1,1}: triggers information
    - The second column can be:
        - 0: beginning of the recording
        - 1: occurrence of the tunnel effect during the recording
        - 100: end of the recording
    - The third is the elapsed time from the beginning of the recording in correspondence of the specific event. It has been obtained with “toc” function (seconds)
    - The forth is the correspondent time in the “clock” (current data&hour) format
    - The fifth is the correspondent time in the posixtime (also called Unix) scale. It is obtained using java.lang.System.currentTimeMillis which returns the elapsed time in milliseconds since January 1, 1970 00:00:00 UTC.
    - The sixth (not always present) contains strings to describe the specific tunnel effect

- Cell {1,2}: time vector [ms] with the posixtime references in which each frame of the videos has been sampled.

The Trigger information have been used for the offline synchronization of the signals of the different device as will be described in the following Section.

3.2.3 Signals extraction and synchronization

This section describes how the data have been extracted from the different files and synchronized over time.

At the end of the acquisition, a participant folder contains the following files:

- 4 videos (laparoscopic, trocars and face cameras) for each task.
- A Matrices for each task with the time references.
- EEG files: eeg.eeg, eeg.vhdr, eeg.vmrk. They are the output of the Cognionics SW and they contain the whole acquisition (with all the tasks and the pauses phases)
- Eye Tracker file: eye.txt. It is the output of the EyeTribe SW and they contain the whole acquisition (with all the tasks and the pauses phases).
- Hexoskin files: .CSV and .WAV files downloaded from the online dashboard. They contain the whole acquisition (with all the tasks and the pauses phases). Each file contains the samples of one specific signal with the related time vector. The HxConvertSourceFile application has been used to convert all the file to the CSV format, to add a third quality column (with the quality status of each sample) for the Heart Rate and Breathing Rate files, and to convert all the time references of all the samples of all the signals to the Unix (posixtime) timescale.

A Matlab algorithm has been created to extract and synchronize the signals stored in the different files. This pre-treatment process has been based on the following concept:

- Signals have to be referred to the same time line in order to be synchronized. Unfortunately, each device starts the recording in different moments. So, samples captured in the same time are associated to different time reference depending on the sensor time line. As can be seen in the “case 1” of Figure 3.26 , it is not possible to identify correspondent samples unless the delay in the sensors timelines is known. Taking track of the time delay among the start of each recording is not very practical. A solution is to choose a specific time reference in the past and express all the sensors timelines with respect to it. It has been chosen to use the POSIXTIME scale. It is also known as Unix time or epoch time. It is a system for describing a point in time, defined

as the number of seconds that have elapsed since 00:00:00 Coordinated Universal Time (UTC), Thursday, 1 January 1970. There are specific functions such as the "java.lang.System.currentTimeMillis" function included in Matlab which allow to retrieve the current time expressed in Unix scale in milliseconds. As can be evinced in the "case 2" of Figure 3.26 , the advantage of such a scale is that the time is always expressed with respect to a fixed reference in the past and it is not related to the moment in which the operator starts the recording of the specific device. Once all the time references of each sample has been expresses in posixtime scale, samples of different devices that occur in the same moment can be identified.

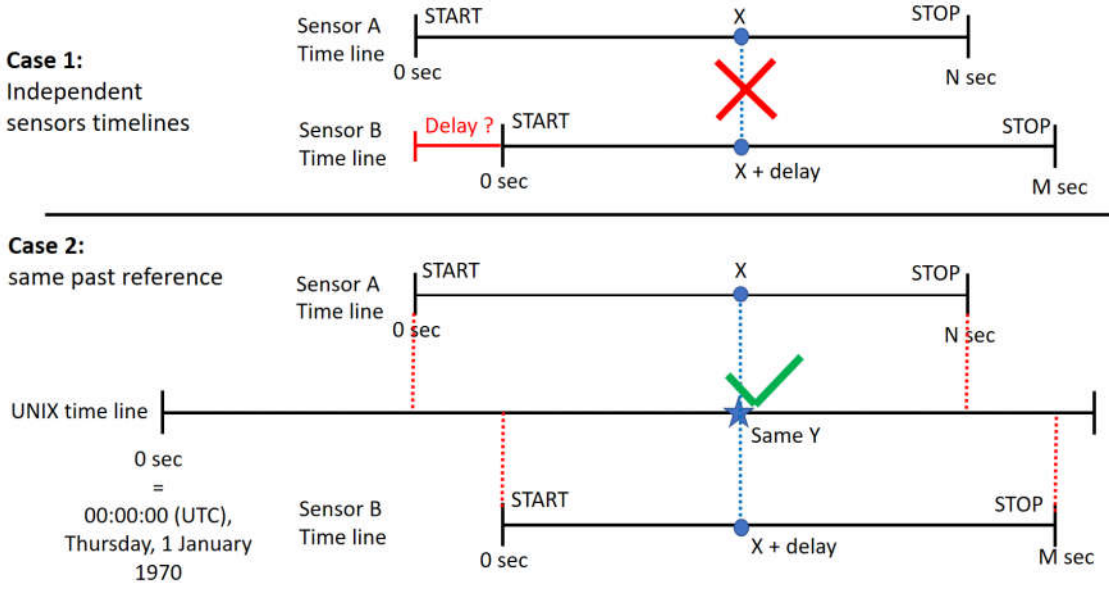

Figure 3.26 Representation of two methods to identify correspondent samples captured with different sensors. Case 1: the identification is possible only if the time delay among the start of the acquisitions is known (the complexity increases with the number of sensors). Case 2: the UNIX scale allows to express all the time with respect to the same past event; thus correspondent samples can be easily identified whatever is the number of sensors.

All the files' names of each subject have been saved and all the subject's data folders have been arranged in a standardized way. For example, the text file produced by the Eye Tracker has been always named eye.txt or the video of the left trocar's camera during the circle cut has been always saved as: "circle_1_trocar_(INITIALS)".

This has been done to allow the algorithm to find and access the required data simply reading from the excel file which subject has to be analysed.

The whole algorithm for the data extraction and synchronization has been made of two steps. The final output is a Matlab matrix in which all the signals from the different devices are collected with their time references subdivided by exercise and by device (Figure 3.27).

- Step1: It has been used to extract the subject's information from the excel file, the synchronization times (e.g. start and stop reference times of the acquisition of each task) from the matrices produced with the GUI and the 2D trajectory of the Smart Trocars from an elaboration of the videos. At the end of this step, the first four columns of the matrix in Figure 3.27 will be completed.
- Step2: the synchronization data extracted in the previous step have been used to identify and extract the data during the four tasks (Rest, Pegs, Circle, Knot) from the ET, Hexoskin and EEG files.

all_data

5x7 cell

	1	2	3	4	5	6	7
1	'info'	'exercise'	'synch'	'smart traj'	'eye tracker'	'hexoskin'	'eeg'
2	2x13 cell	0	3x5 cell	[]	2x14 cell	2x23 cell	2x29 cell
3	2x13 cell	1	5x6 cell	2x11 cell	2x14 cell	2x23 cell	2x29 cell
4	2x13 cell	2	7x6 cell	2x11 cell	2x14 cell	2x23 cell	2x29 cell
5	2x13 cell	3	[]	[]	[]	[]	[]

Figure 3.27: Example of Beginner's output matrix with all the signals subdivided by task and device

A brief explanation on how the data have been extracted from each device and synchronized will follow:

- Eye Tracker: in the TXT file, all the samples are organized row by row. Each samples contains a date&time reference. A code for the extraction of all the useful information from this text file has been made. Then, the vector with the data&time references of all the samples has been converted to the posixtime scale using the "posixtime" and "datetime" functions of Matlab. At this point, the start and stop posixtimes for each task (from the synchronization matrices) have been used to extract from the overall acquisition only the data regarding the tasks.
- Hexoskin: after the conversion with the HxConvertSourceFile application, all the signals files contain the time reference of each sample in posixtime scale. Once all the data have been retrieved from those files, the intervals of samples related to the different tasks have been extracted as previously explained for the ET. Moreover, a statistical analysis about the quality of Heart Rate and Breathing Rate data has been made using the Quality Status information added during the data conversion.

- EEG: the EEGLAB toolbox has been required to read the files produced by the Cognionics software. In this case, there is no date&time reference of the acquisition, thus it has not been possible to use the same approach of the previous devices. Here, it has been used the serial communication with the Trigger Box of the EEG during the acquisitions. In correspondence to the start and the end of each task a trigger has been sent by the GUI to the Trigger Box which generates spikes in the Trigger signal of the EEG. Triggers for different tasks have been sent with a different amplitude and they have been used as temporal markers to identify the interval of values related to the specific task. A vector timeline for the EEG has been constructed knowing the sampling rate of the device and the time references associated to each start.
  The EEGLAB allows to process EEG data with predefined functions only if the data are organized in a specific Struct format. For this reason, objects have been created for each task with the selected data to allow further elaborations.
- Trajectory or 2D movement of the tools: the algorithm created for its extraction will be described in the next Chapter. No adjustment for the time associated to each frame has been required because it had been already produced in posixtime by the GUI.

From the pre-treatment phase a Matlab cell matrix as the one in Figure 3.27 has been produced for each subject. It contains all the recorded signals subdivided by task and by device and it has been used as input for a first analysis approach.
For a complete description of the content of each cell of the output matrix refer to the Appendix A.

3.3 Laparoscopic tool 2D movement reconstruction

The 2D reconstruction of the movement of the tool is one of the information that can be retrieved though the use of the Smart Trocars. As explained in Section 3.2.1, it has been necessary to change both the pattern on the ceiling and the algorithm due to the room's light conditions and the impossibility to access some specific parameters of the cameras (e.g. Auto-Brightness).
The difficulties in the cross detection using the old algorithm have been summarised in Figure 3.28. From left to right are represented respectively: the input frame, its grayscale conversion with contrast enhancement and the mask obtained with a specific threshold. As can be observed, only dark color crosses can be easily extracted. The result will be even

worst in case of a light source in the FOV because the camera reacts to it by darkening the image. This is due to the exposure parameters of the camera that unfortunately cannot be access when it is used in WebCam mode.

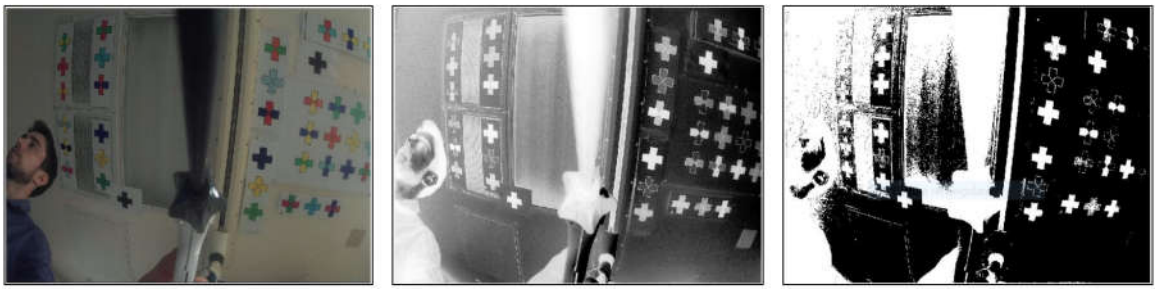

Figure 3.28: example of cross segmentations in a poor light environment. From left to right: an RGB frame, its grayscale conversion and contrast enhancement and the mask obtained applying a specific threshold. Only dark color cross have been easily extracted. The result will be even worst in case of a light source in the FOV because the camera reacts to it by darkening the image (change in the exposure).

Section 3.3.1 treats the ideation and creation of the new pattern placed on the ceiling while Section 3.3.2 describes the functioning of the new Matlab algorithm for the 2D movement reconstruction of the tool.

3.3.1 Pattern for the feature points extraction from the ceiling

A new flat pattern has been developed due to the difficulties in extracting the coloured crosses from the ceiling in the video frame's. To decrease impact of the ambient light conditions in the color crosses detection, the idea has been to use black objects in the pattern to maximize the contrast with the background (ceiling). However, the usage of black crosses is not sufficient. In fact, in order to correctly compute the roto-translational matrix among subsequent frames, it would be better to use clouds of correspondent in the two frames. This can be done only if it is possible to know to which object the features points belong. So, the new pattern has to be something that can be "easily" segmented from the frame and can allow to label each object in it. The first idea has been to the use of pre-existing codes such as QR or ArUco codes (Figure 3.29) which fulfil these requirements.

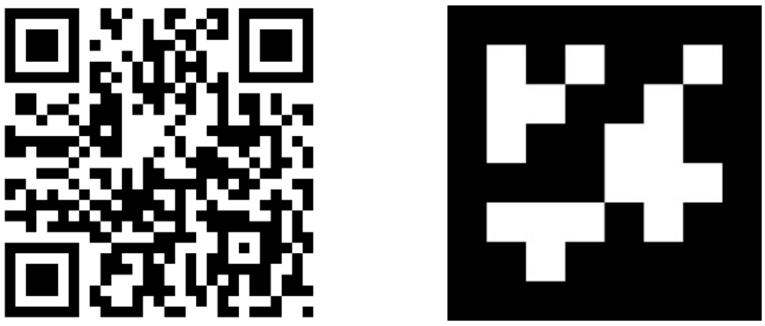

Figure 3.29: Example of QR code (left) and ArUco code (right)

Both can be easily detected using OpenCV library analysing their binary pattern codification. The main problem of the first (QR) code is given by its complexity that requires a very accurate acquisition from a close position. The second (ArUco) is a simpler version of the QR code but due to the binary codification of the information requires high resolution images due to the distance of the camera from the ceiling. Moreover there is no reliable function implemented in Matlab for their detection. Since Matlab has been used for the old algorithm and the whole infrastructure has been made in that language, it has been decide to find another solution to maintain the same environment.

It has been decided to create a new code similar to the ArUco but less dependent from the resolution required to decode the inner binary patter.

This new code has been based on black squares with an inner geometric white pattern (Figure 3.30). Each square has a side of 14 cm and each white circle has a diameter of 2.4 cm. The black background of the square facilitates its detection in the image due to the high contrast with the ceiling while the white pattern allow the identification of the specific square.

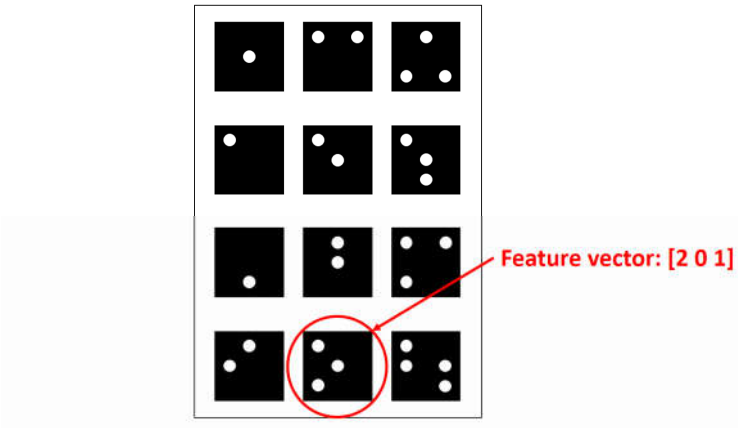

Figure 3.30: Example of new pattern: 12 different squares in a poster. The feature vector (ID) of the square inside the red circle is [2 0 1] which means: 2 white circles near 1 vertex of the square, 0 white circle near 2 vertexes of the square and presence of the one in the center of the square.

The geometric discrimination criteria concerns the possible positions of the white circles inside the black square. Each square is characterized by a specific feature vector (ID) consisting of three numbers:

1. Number of circles whose centroids are close to only one vertex of the square;
2. Number of circles whose centroids are close to two vertexes of the square;
3. Presence (=1) or not (=0) of a circle in the center of the square.

For instance, the feature vector (ID) of the square inside the red circle in Figure 3.30 is [2 0 1] which means: 2 white circles near 1 vertex of the square, 0 white circles near 2 vertexes and presence of the one in the center.

The relative size of the white object with respect to the size of the black square has been used in the algorithm to discriminate among noise/artefacts and real circle.

Table 3.3 shows an example of database containing all the feature vectors of the squares using a maximum of 2 white circles in the internal pattern.

ID	n° circles near 1 vertex	n° circles near 2 vertexes	Presence of the middle circle
1	1	0	0
2	0	1	0
3	0	0	1
4	2	0	0
5	0	2	0
6	1	1	0
7	1	0	1
8	0	1	1

Table 3.3: Database of the possible inside patterns combination using a maximum of 2 white circles in a square

The database will be used in the algorithm to label the squares detected in a frame with the relative ID.

3.3.2 Algorithm for the 2D movement reconstruction of the tool

The reconstruction of the 2D movement of the tool consists in a computer-based analysis of the video of the camera mounted on the trocar. The algorithm can be briefly summarized in the 3 steps reported in Figure 3.31.

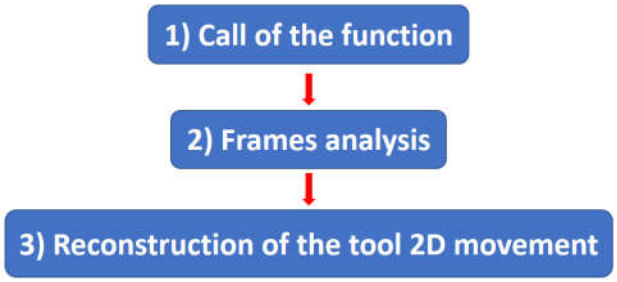

Figure 3.31 The three main steps of the flowchart of the algorithm for the reconstruction of the 2D movement of the tool.

The final version of the algorithm encompasses the possibility to include or not the correction of the radial distortion in the frame. The operations related to this correction have been reported in red (optional path) in the next flowcharts.

A description of these steps follows:

1. "Call of the function". A flowchart of this step has been represented in Figure 3.32. The algorithm requires in input a cells vector with all the frames in the video and the vector with the times [ms] expressed in Unix scale related to each frame.

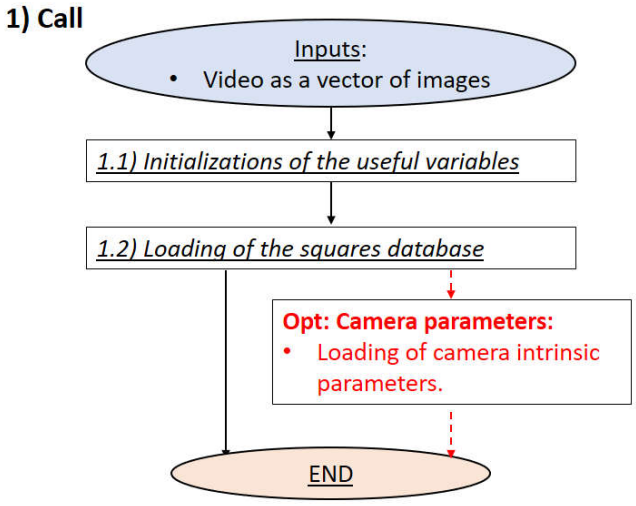

Figure 3.32: description of the flow in the "Call of the function" step of the Algorithm for the reconstruction of the 2D movement of the tool. The red dashed line represents an alternative pathway that imply the correction of the radial distortions of the frame.

It initializes all the useful variables such as the List in which all the feature points will be saved and it loads the database of features vectors of all the squares on the ceiling.

The algorithm has been tested both with and without frame distortion correction. For the first, the Mobius Action Camera intrinsic parameters (i.e., focal length, principal point, distortions vector) have been estimated. It has been used the Camera Calibrator which is an image processing and computer vision app of Matlab. It is based on Zhang's camera

calibration method [47] and it implies the use of a planar rigid calibration pattern (chessboard) made of a square grid. A number among 10 and 20 images of the calibration pattern taken from different angles is usually required for a good estimation of the camera intrinsic parameters.

2. "Frames analysis". The algorithm analyses all the frames of the video in order to extract the feature points (corners and centroid) of the squares recognized in each image. The main operations have been reported in Figure 3.33.

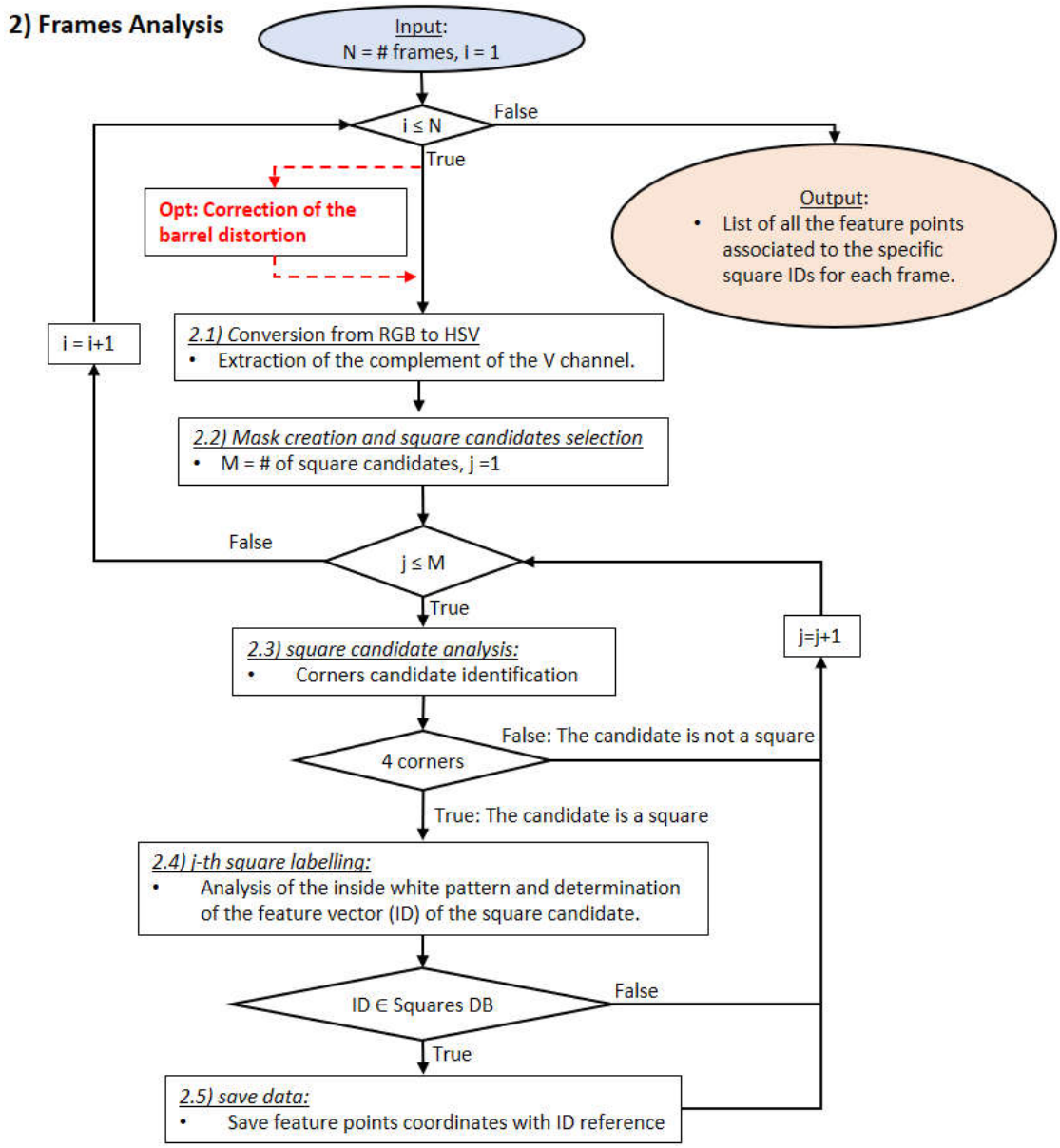

Figure 3.33: description of the flow in the "Frames analysis" step of the Algorithm for the reconstruction of the 2D movement of the tool.

Following the flowchart (Figure 3.33), each frame goes through:

- Block 2.1: conversion from RGB to HSV of the input frame. The algorithm extracts only the Value (V) channel and it computes its complement.

  Figure 3.34 report an example of this elaboration. The upper line (Figure 3.34 a,b) represents respectively: the input RGB frame and the complement of the Value channel of its HSV conversion. The bottom line (Figure 3.34 c,d) represents the same elaboration on an RGB frame where the radial distortion has been corrected. From now on, all the image examples for the algorithm description will be related only to frames without correction of the radial distortion and elaborated from HSV scale conversion.

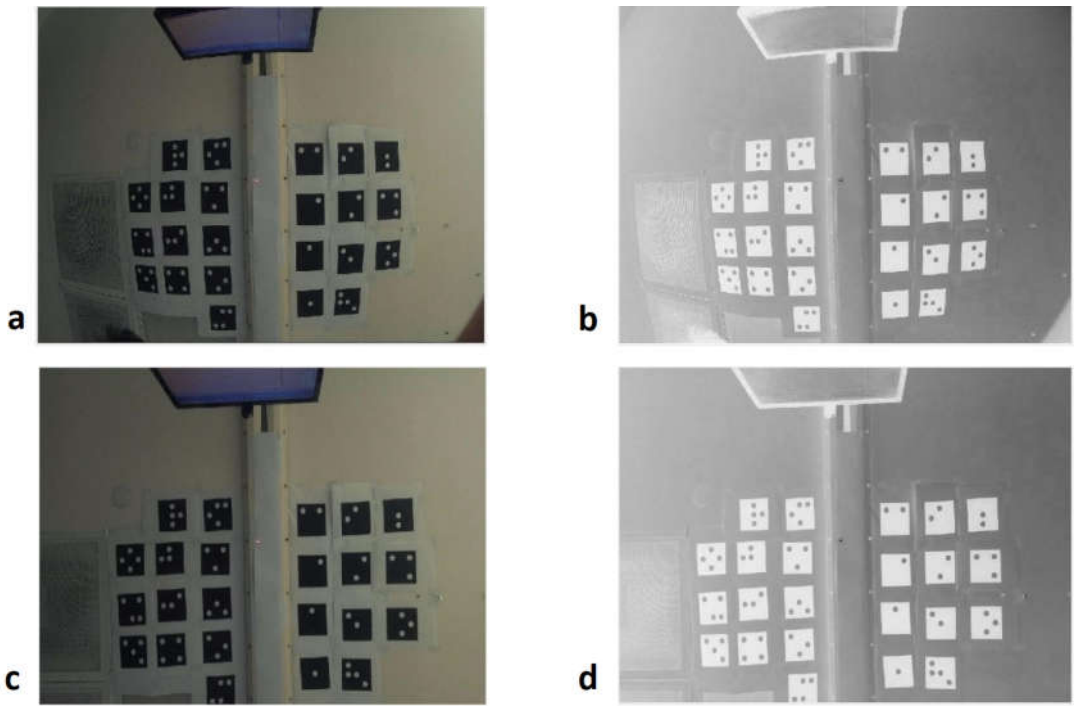

Figure 3.34: Example of block 2.1 in Figure 3.33. Upper row from left to right: input RGB frame without correction of the distortion (a) and the complement of the Value channel of its HSV conversion (b). Bottom row (c, d): same conditions of the upper row but with the correction of the distortion.

- Block 2.2: Mask creation and square candidates selection. The process has been described in Figure 3.35 where the output of Block 2.1 undergoes:
  (a) Thresholding: the threshold has been determined dynamically analysing the histogram of the frame. The output is a binary image (mask).
  (b) 'imfill' function: it has been used to fill the region of each segmented white object to obtain white full-filled squares.

(c) Square candidates selection: all the white closed regions in the mask have been clustered. Then, properties of each region (e.g. area, perimeter, centroid..) have been determined with the 'regionprops' function. The possible squares have been identified based on area and perimeter constraints. These criteria are useful to discriminate among squares and the other white objects in the mask. They have been manually defined in the code depending on the resolution of the image and the distance of the camera from the ceiling.

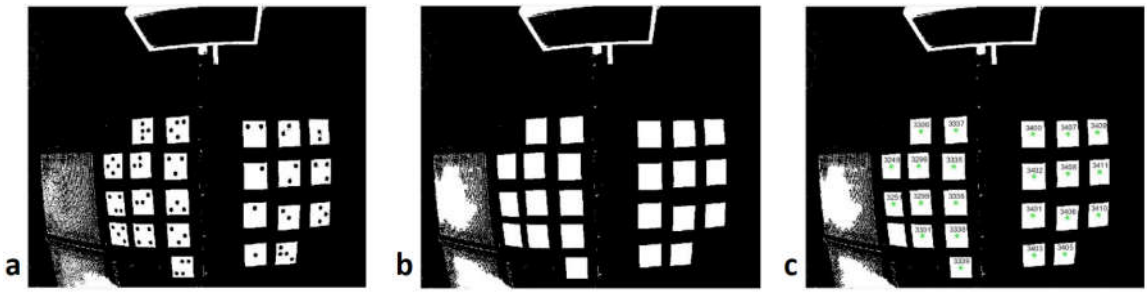

Figure 3.35: Example of blocks 2.2 in Figure 3.33. Respectively: (a) mask obtained through the application of the dynamic threshold on the output frame of block 2.1, (b) the result of the imfill function, (c) white object clustering and labelling based on area and perimeter criteria (first square candidates selection).

- Block 2.3: square candidate analysis to understand if the white object is a real square or something else. The algorithm computes a convolution with a gaussian smoothing kernel with the candidate mask in order to reduce the noise on the edge. Then, it computes the corners of the white region with the 'corner' function. It could produce additional false detections due to the not perfect square edge. These false corners have been eliminated applying the following constraints:
    - The algorithm computes the distance among each identified 'corner' and the centroid of the white region and finds the maximum value. All the 'corners' whose distances are lower than 80% of that value are eliminated.
    - If the distance among two identified 'corners' is lower than perimeter/8, the algorithm eliminates the one with the lower distance from the centroid.

  If the remaining corners are four, the candidate is recognized as square. An example of the corners detection has been represented in Figure 3.36.

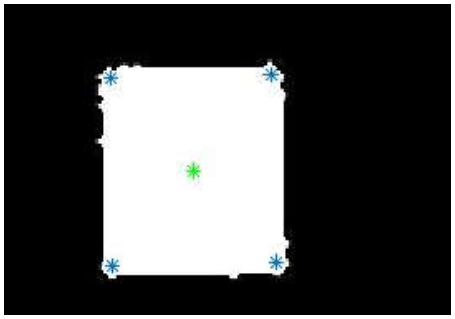

Figure 3.36: Examples of corners determination. The blue asterisks represent the corners while the green one identifies the centroid of the j-th square.

- Block 2.4: square labelling. If the candidate analysed in Block 2.3 has been recognized as square, the algorithm extracts its internal pattern. An example has been proposed in Figure 3.37.

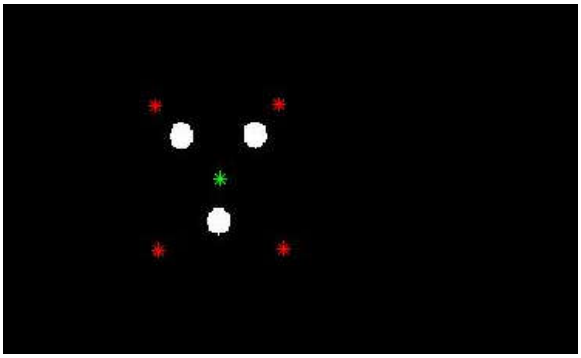

Figure 3.37: Examples inner pattern extraction. In this case, three white circles have been identified. In red and in green respectively the corners and the centroid of the square.

  True internal white circles have been identified based on area constraints with respect to the square dimension. Based on their position, the features vector (ID) of the square is computed as it has been explained in Section 3.3.1. The obtained ID will be compared with the ones in the squares database; if it doesn't match with anyone, the square candidate is discarded.

- Block 2.5: save data. If the ID of the candidate matches one of the squares in the DB, the algorithm saves its feature points 2D coordinates (i.e. corners and centroid) in a matrices (feature points list) in the columns assigned to the current frame keeping track of the ID.

The process is repeated for all the square candidates in the mask. If two squares have been classified as the same square (same ID) in a frame, they will be both eliminated from the feature points list in order to decrease the probability of errors due to misclassification.

Figure 3.38 represents the output of the analysis of one frame where for each recognized square have been displayed its feature points (centroid and corners) and its ID.

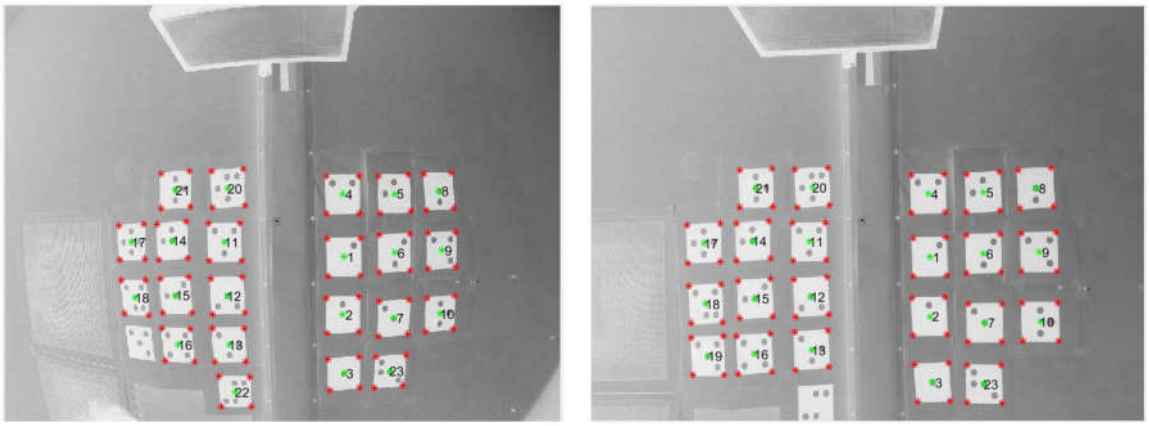

Figure 3.38: Example of outputs from the step in Figure 3.33 in uncorrected (left) and corrected (right) images. Each identified square has been labelled with the ID in the database and all its feature points (centroid and corners) have been identified.

The algorithm repeats the process for all the frames. The output consists in a matrix (feature points list) containing all the feature points detected frame by frame associated to the correspondent square ID.

3. "Reconstruction of the 2D movement of the tool". This phase aims at computing the roto-translational transform [R,T] among each couple of subsequent frames. A flowchart with the main operations has been represented in Figure 3.39. It has been based on the analysis of the list of feature points obtained in the previous step. What it has been called list consists in reality in a (100)x(#frames x 3) matrix. Each 3 columns refer to a frame; they contain all the features points of the identified squares in it. A feature point has been described by x and y coordinates in the frame and the ID of the square to which it belongs.

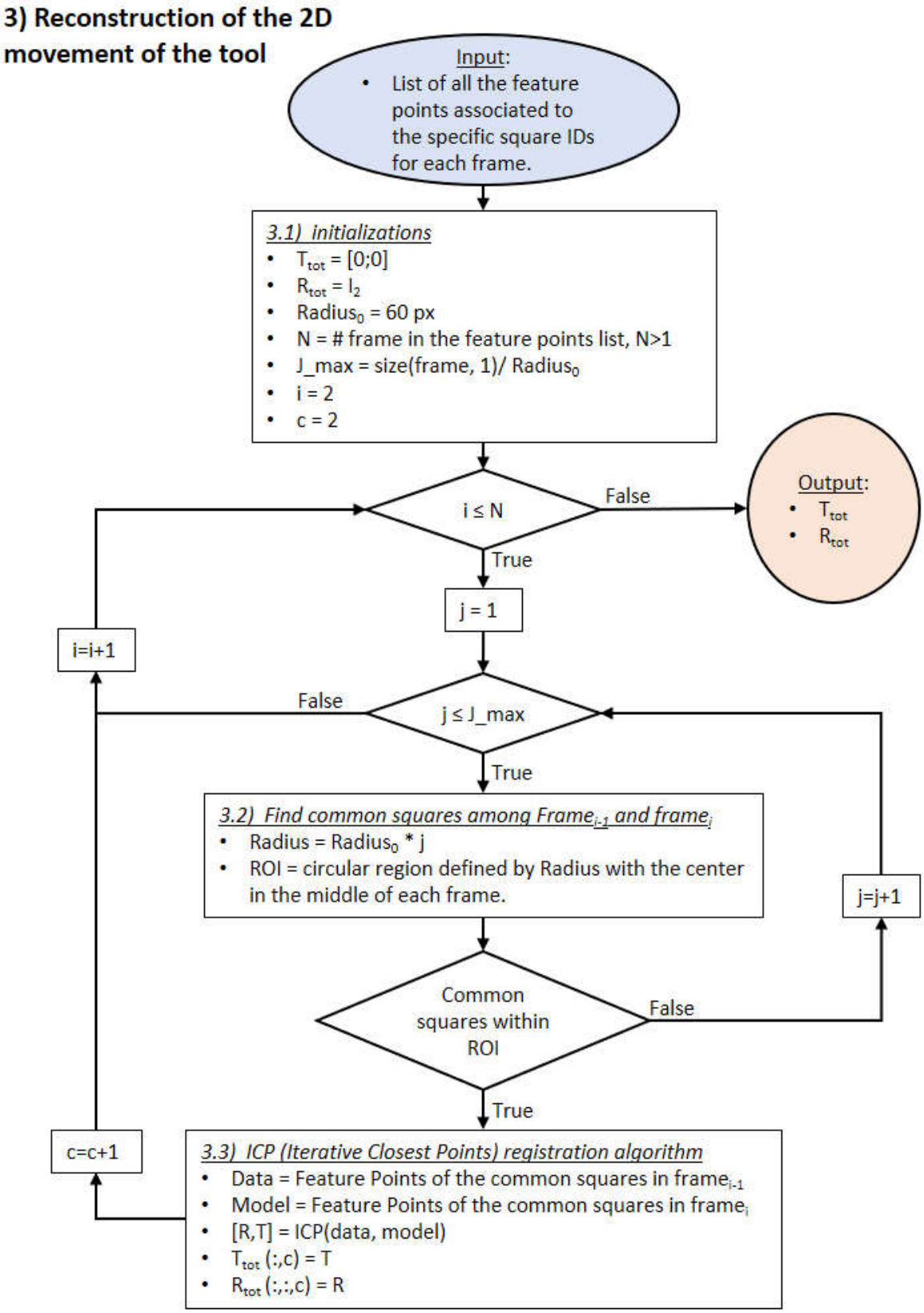

Figure 3.39: description of the flow in the "Reconstruction of the 2D movement of the tool" step of the Algorithm for the reconstruction of the 2D movement of the tool.

Following the flowchart in Figure 3.39, the algorithm goes through:

- Block 3.1: Initializations. Useful variable are initialized. In particular, the first element of the vector which will contain all the translational vectors of the roto-translational matrix among each couple of subsequent frames is initialized at [0;0] and the one of the matrix which will contain the relative rotational matrices is initialized at I_2.
- Block 3.2: Find common squares among $frame_{i-1}$ and $frame_i$. Features points belonging to correspondent squares in subsequent frames have been used to reconstruct the 2D motion. Not all of the them have been used for this purpose. Common squares have been seeked inside a circular region of interest (ROI) in the two frames. This region is centred in the middle of each frame and it has been enlarged until at least a centroid with the same square ID is found in both ROIs.

  Figure 3.40 represents an example of common squares in subsequent frames whose centroids are inside the ROI (yellow line).

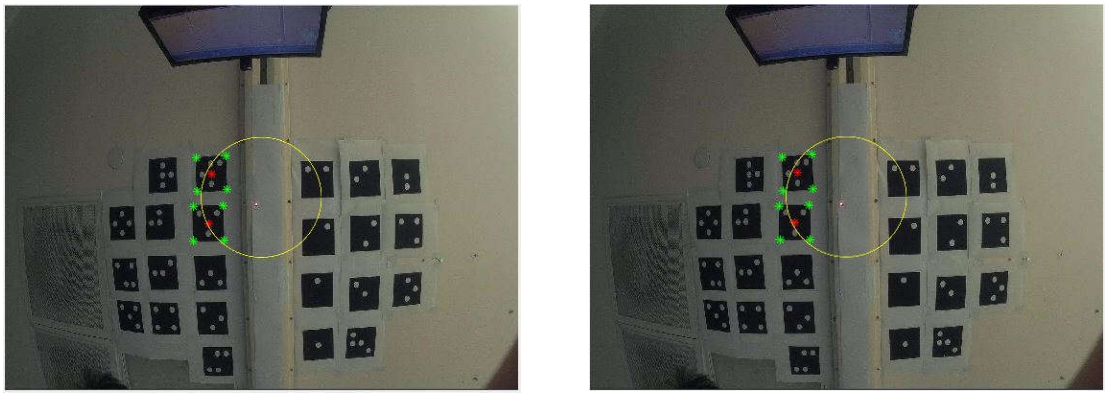

Figure 3.40: Example of common squares identification in subsequent frames within a specified ROI. It refers at block 3.2 of Figure 3.39

  Once the condition has been satisfied, all the features points (corners and centroids) of the common squares in the ROI have been used as in input to the ICP function which computes the roto-translational transform among the two frames described in Block 3.3. This has been done because the highest accuracy in the feature points detection is obtained for the squares that are close to the center of the image.

  The algorithm takes also track of the radius of the ROI required to satisfy the conditions for each couple of frames giving an idea about the quality of the estimated movement.
- Block 3.3: ICP (Iterative Closest Points) registration algorithm. The 2D coordinates of all the feature points in $frame_{i-1}$ which satisfy the criteria in Block 3.2 constitute a cloud of points called 'data'. The correspondent points in $frame_i$ are assigned to a cloud of point

called 'model'. The ICP algorithm is used to compute the roto-translational transform among the two clouds of points. The obtained [R,T] allows to pass from data to model as follows:

$$model = R * data + T$$

where R and T are respectively the Rotational matrix and the translational vector of the roto-translational transform. R and T are added respectively to R_{tot} and T_{tot}.

Each roto-translational transform has been assigned to the time reference of the 'model' frame expressed in Unix time scale.

It is important to highlight that only the frames from which at least one square has been extracted contributes to the reconstruction. For this reason, the input frames vector and the output translation vector can have significantly different dimensions.

Some observations about the algorithm:

- The movement among two subsequent frames which has no squares in common will be lost. A counter variable takes track also of this kind of problems providing another estimation of the quality of the reconstructed movement.
- The algorithm is not sensitive to rotation of the tool along its axis.
- The algorithm has been found to provide good results for both good quality and little blurred images (Figure 3.41)

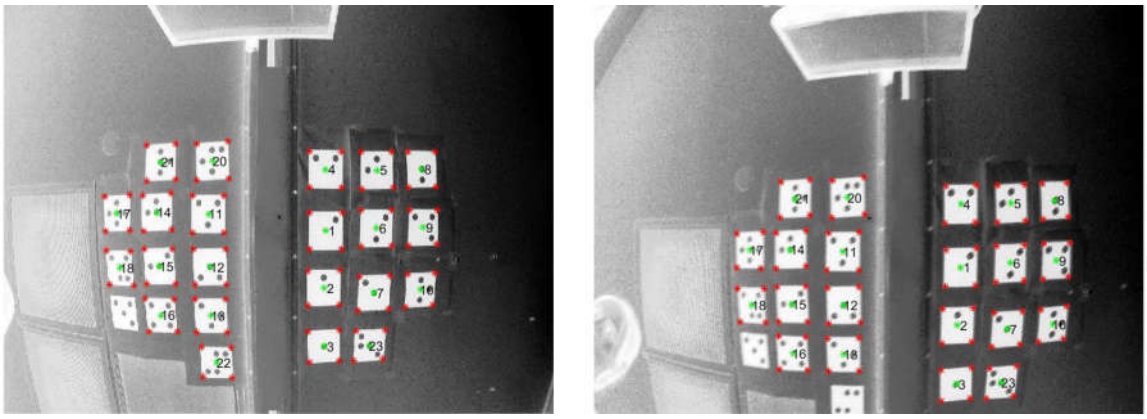

Figure 3.41: Squares labelling and feature identification in a good quality (left) and in a slightly blurred (right) image

The output of the algorithm consists of:

- The vector of all the translational vectors (T_{tot}) and the matrix of all the rotational matrices (R_{tot}) to pass from the disposition in one frame to the following one.
- The correspondent time references

- Some statistics: percentage of video that has been converted in motion and quality vector that counts the possible gaps in the reconstruction.

The output can be used to study the kind of movements frame by frame. If the quality of the conversion is quite high, it could be used also to give a nice representation of the movement for the entire duration of the task by applying the chain of roto-translational matrices to a starting point.

3.4 Multimodal analysis for eye blinking detection

Blinking is a semi-autonomic, reflexive, rapid closing of the eye and it is an essential function that helps in keeping clean (removing irritants) and hydrate the surface of the cornea and conjunctiva. It is a movement that occur on both the eyes at the same time and it has been found to variate depending on what the subject is doing or on his/her emotional state.

Data from the Eye Tracker (ET) and the EEG have been used to detect the eye blinking. The conduction of this multimodal analysis has been possible thanks to the signal synchronization described in Section 3.2.3. Thus, the signal were subdivided into the three different tasks (i.e. Peg Transfer, Circle Cut and Intracorporeal Knot) and synchronized in time.

The algorithm has been developed in Matlab and it consists of a first separated analysis of Eye Tracker (ET) and EEG signals and a subsequent comparison of the obtained blink candidates (Figure 3.42).

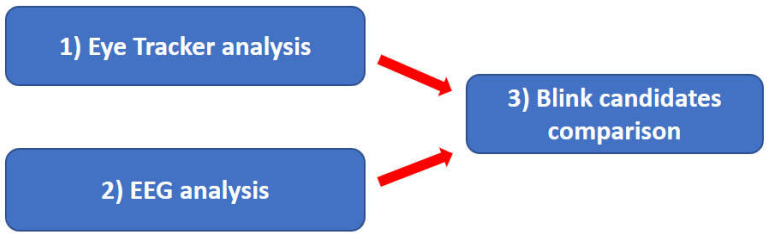

Figure 3.42: The three main phases of the flowchart of the algorithm for the eye blinking detection.

Details about this three main phases will follow:

1. "Eye Tracker analysis". The main operations have been reported in Figure 3.43. The analysis of ET data has been focused on the average gaze coordinates signal. It represents the 2D gaze coordinates (x,y) on the screen.

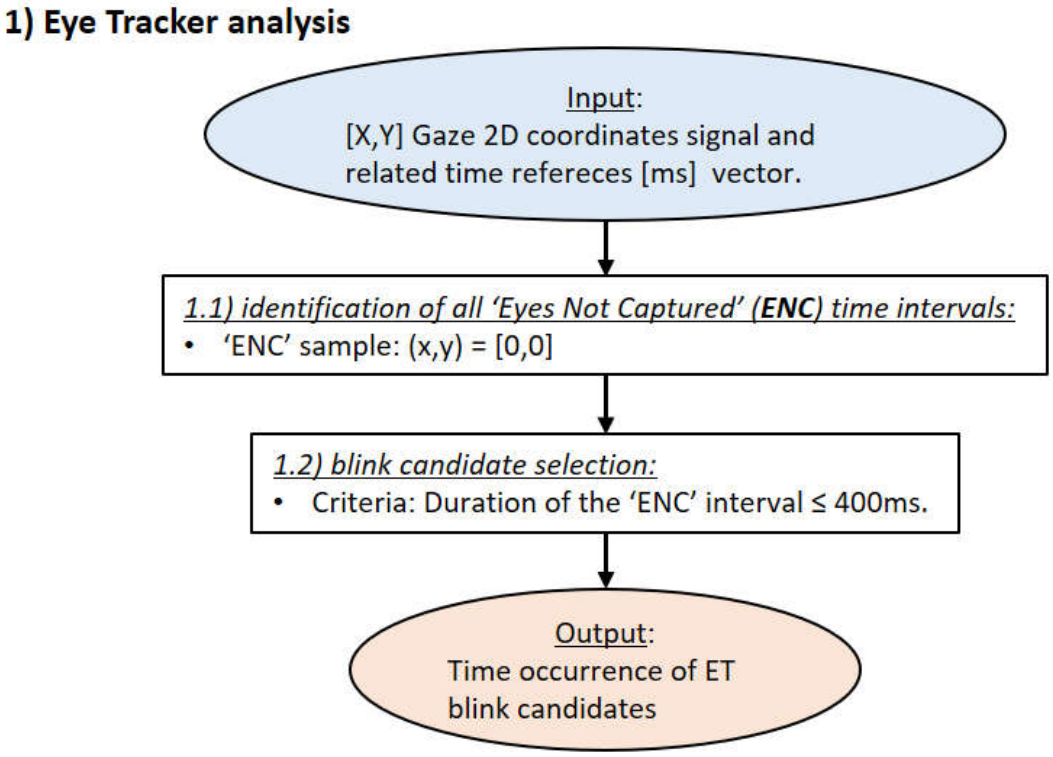

Figure 3.43: description of the flow in the "Eye Tracker analysis" step of the Algorithm for the blinking detection.

When both the eyes are not captured by the ET, the device is not able to compute the gaze of the participant. These samples can be easily identified because their gaze 2D coordinates are equal to [0, 0]. Subsequent samples of **Eyes Not Captured (ENC)** constitute an 'interval of ENC'. Knowing the time occurrence of each sample [ms] that the ET sampling frequency is 30Hz, it is possible to estimate for how long the device has not been able to track the eyes (**ENC time interval**). A representation of how an 'ENC' time interval is identified has been reported in Figure 3.44.

There is no complete agreement about the average blinking duration in literature. For example, it can vary between 100-150ms according to UCL (University College of London) researcher or between 100-400ms [48] according to Harvard Database of Useful Biological Numbers.

In this algorithm, it has been decided to consider eye blinking candidates all the 'ENC' time intervals ≤400ms.

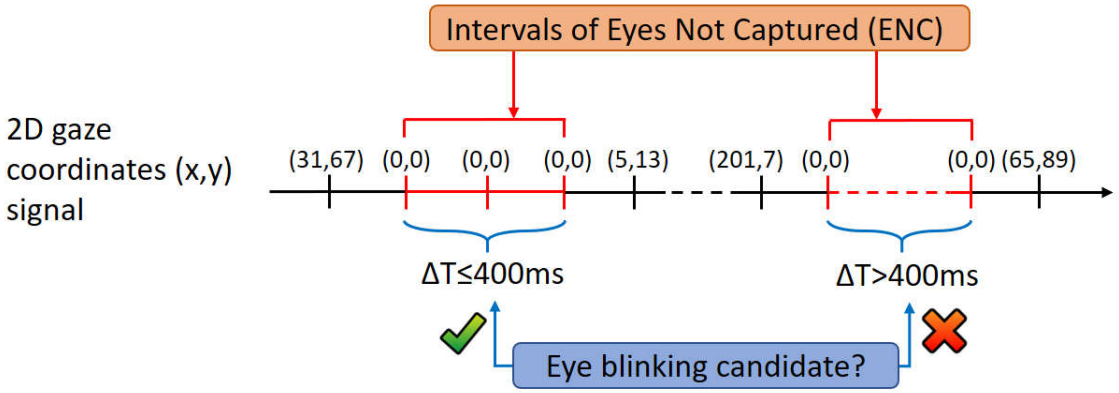

Figure 3.44: Identification of Eyes Not Captured (ENC) interval over the gaze (x,y) signal. Intervals with a time duration below or equal at 400 ms are considered blinking candidates.

Figure 3.45 represents a practical example of the identification of the interval of 'ENC' in the gaze (x,y) signals. The acquisition comprises 4 blinks within 23 seconds of recording. The start and end of each interval has been identified with respectively green and a black vertical lines. These intervals have been all identified as blink candidates because their duration is below 400 ms.

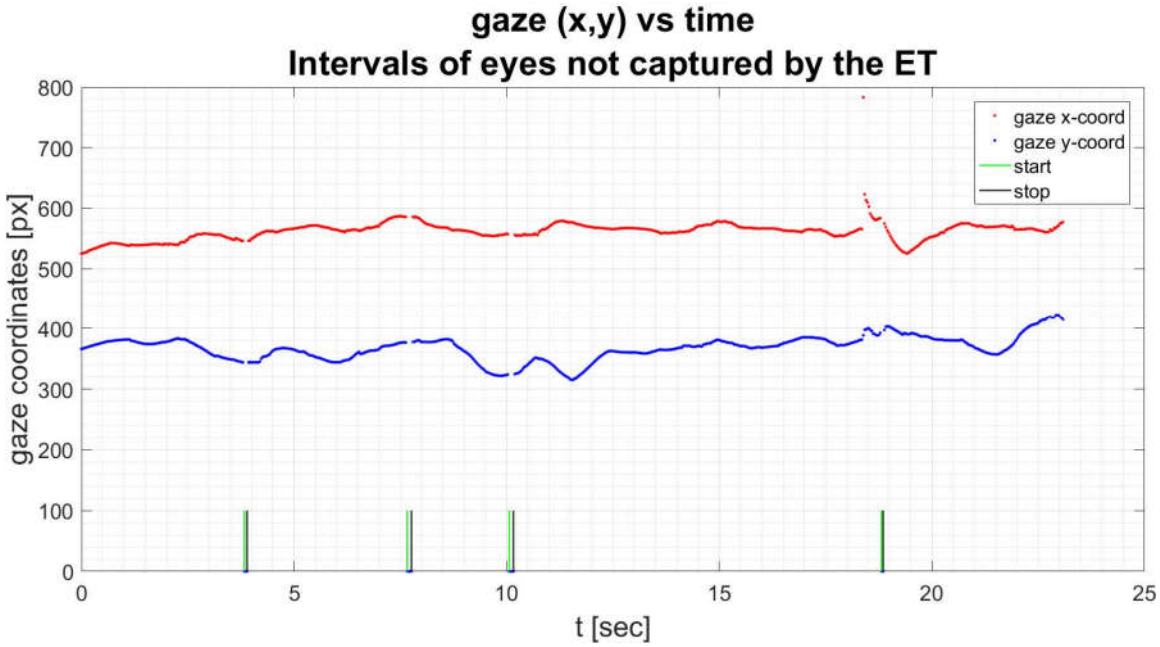

Figure 3.45: Avg gaze (x,y) vs time. The samples with both (x,y) gaze coordinates equal to zero correspond to samples of eyes not captured by the ET. The start and end of each time interval of eyes not captured are identified with respectively green and a black vertical lines

The output consists in the time occurrences of each ET blink candidate.

2. "EEG analysis". A diagram representing the main phases of this step has been reported in Figure 3.46. The analysis of EEG data have been based on Fp1 and Fp2 signals. These two electrodes are located on the frontal lobe (precisely on the forehead), over the eyes and for this reason, they are the most affected by the skin artifacts (noise) introduced by the blinking.

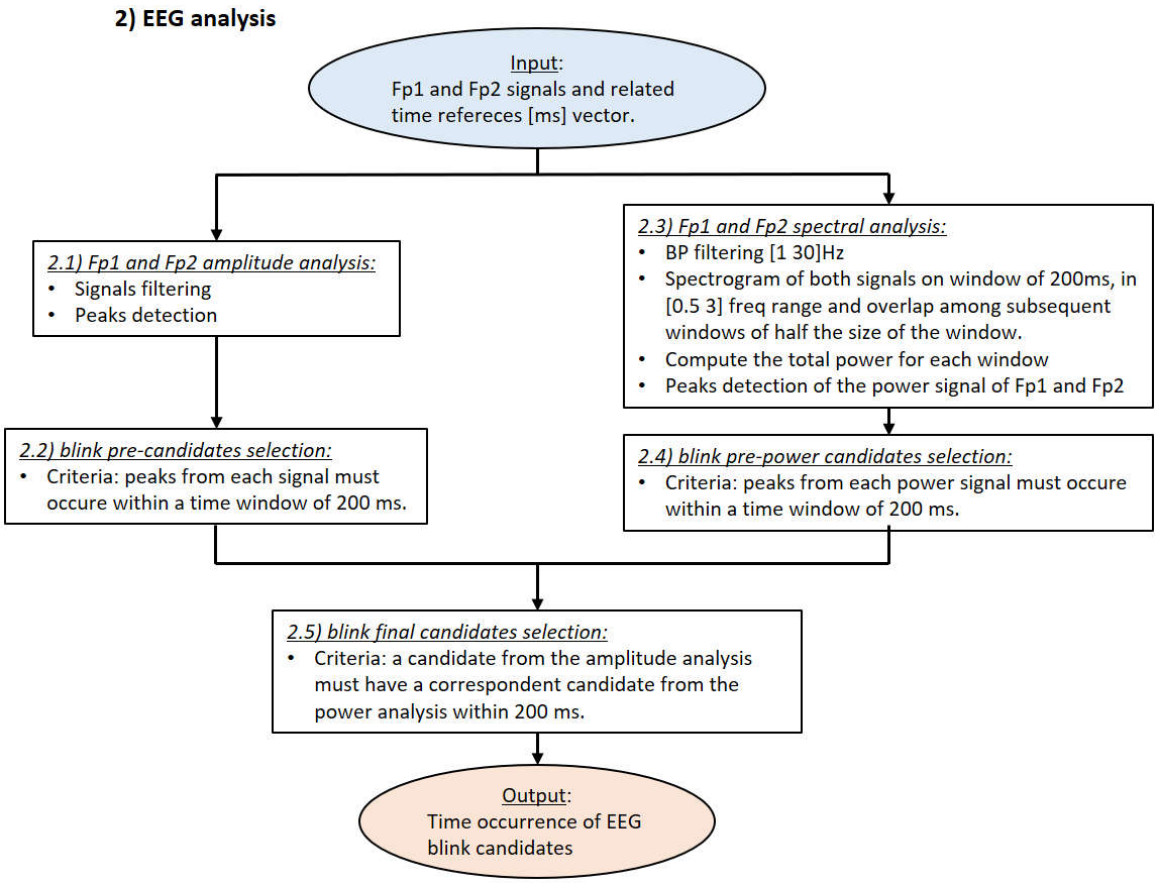

Figure 3.46: description of the flow in the "EEG analysis" step of the Algorithm for the blinking detection.

These signals undergo two analysis:

- Block 2.1: Fp1 and Fp2 amplitude analysis. The normal activity of the brain recorded by Fp1 and Fp2 presents a lower amplitude than the rest of the electrodes. This make them usable for an automatic blink detection by simply controlling their EEG amplitude in the time domain. The occurrence of a blink can be easily observed on these signals as a clear peak over the normal activity [29]. This is due to the noise introduced by the skin moments of the blink that are summed to the electric activity of the brain.

  The 'findpeaks' function of Matlab has been used to detect the peaks in the signals. Within the function it has been found useful to set parameters such as the minimum prominence, which allow measure how much the peak stands out due to its intrinsic

height and its location relative to other peaks (peaks over the signal pseudorandom baseline activity can be easily identified) , and the minimum distance among subsequent peaks. Figure 3.47 represents an example of peak detection over the amplitude signals.

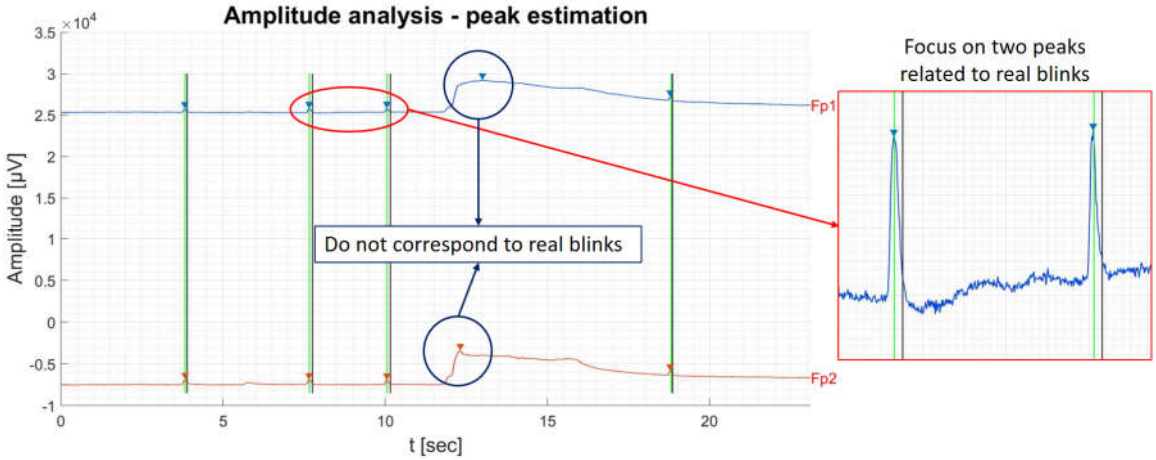

Figure 3.47: Example of peak detections in the amplitude analysis of Fp1 and Fp2 (left) and a focus on two blink peaks (right). On the left it is possible to observe one wrong detection for both signals (blue circles) due to a movement artifact (knit the brow). The vertical lines identify the intervals of the blinks detected by ET.

One wrong peak on both signals can be observed in the figure. They are due to the artifact introduced by knit the brow.

- Block 2.2: blink pre-candidates selection. The eye blinking occurs on both the eyes at the same moment. Therefore, EEG blink pre-candidates have been identified each time a peak on Fp1 and a peak on Fp2 are contained in a same time window of maximum 200 ms.

  In this way, detected peaks which don't correspond to blinking can be eliminated. For example, the erroneous peaks in Figure 3.47 are distant in time more than 200 ms, therefore they will be discarded from the EEG blink candidates as can be observed in Figure 3.48.

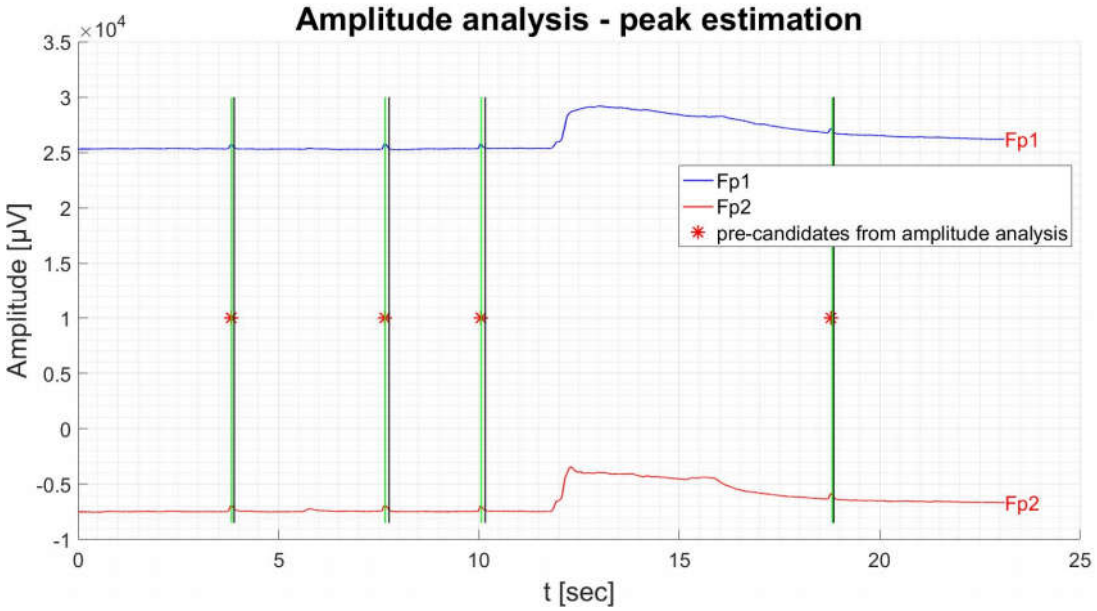

Figure 3.48: EEG candidates (red asterisks) from the amplitude analysis of Fp1 and Fp2 (block 2.2 of Figure 3.46). The vertical lines identify the intervals of the blinks detected by ET.

- Block 2.3: Fp1 and Fp2 spectral analysis. Due to the pseudorandom nature of the EEG signal, it has been decided to apply a second kind of analysis on Fp1 and Fp2. The blinking occur mostly in the 0.5-3 Hz range of the power spectrum. In this range, the powers associated to the EEG with a blink and to the EEG normal activity are really different. It has been found as the first is way more higher than the blinks-free one [29], [32]. This different behaviour has been used to identify the eye blinking in different way. Firstly, the signal has been filtered with a Butterworth PB filter in [1 30] Hz. Then, the spectrograms of the signals have been computed for the range [0.5 3] Hz subdividing the signal in temporal window of 200 ms with an overlap of half-window among subsequent intervals.

  Figure 3.49 reports the spectrograms of the filtered Fp1 and Fp2 of the acquisition with four blinks used in the previous figures. The maximum power peaks (toward orange and yellow in the spectrograms) occur in correspondence of the four blinks and of the artifact generated by the knit of the brow at 12 sec.

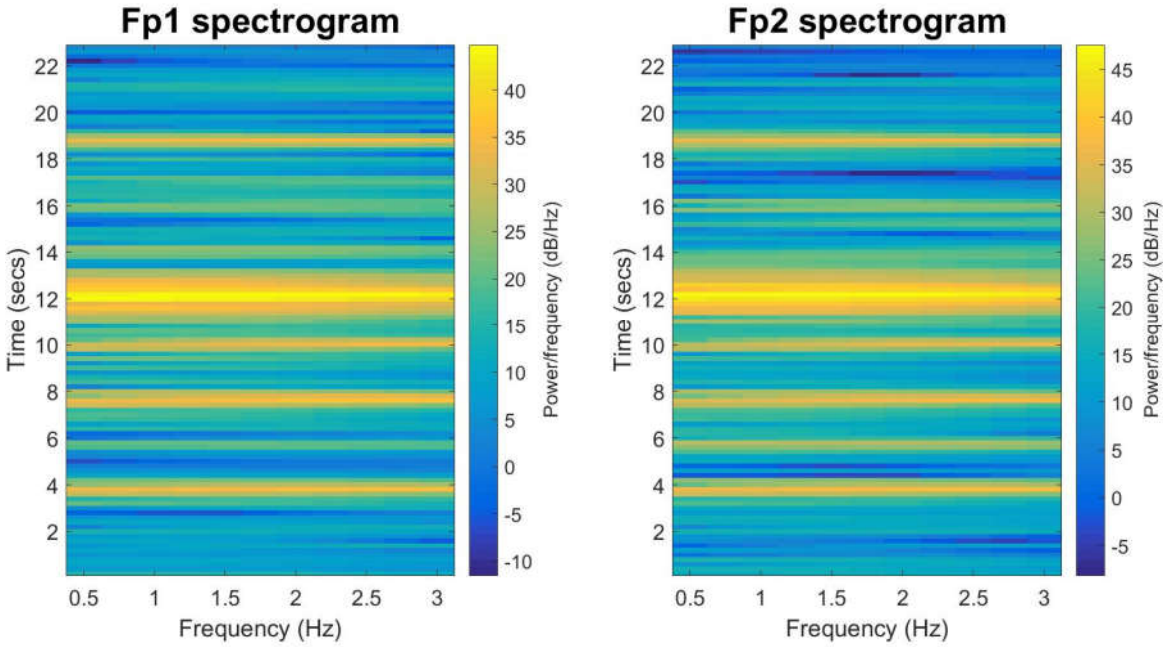

Figure 3.49: example of spectrograms computed in block 2.3 of Figure 3.46. They respectively the spectrogram of the filtered Fp1 (left) and Fp2 (right) . The big yellow band cantered around 12 sec in both the graph represent the artefacts of knit the forehead. The blinks are clearly identified as the orange bands with a limited duration that occur simultaneously in both the graphs.

The sum of the power contribute of all the frequencies ([0.5 3]Hz) has been computed for each time window (200 ms) obtaining a power signal over time for each channel (Fp1 and Fp2). A peak analysis has been conducted on these power signals with the 'findpeaks' function based on minimum prominence and minimum distance among subsequent peaks.

- Block 2.4: blink pre-power candidates selection. Blinking candidates have been identified in correspondence of simultaneous peaks on Fp1 and Fp2 power signals (max time distance = 200 ms).
- Block 2.5: blink final candidate selection. The algorithm compares the blinking candidates from the amplitude and the spectral analysis. EEG final blink should match the following criteria: a candidate from the amplitude analysis must have a correspondent candidate from the power analysis within 200 ms.

  Figure 3.50 represents the final identified blinks on the amplitude graph. The red asterisks correspond to the EEG blink candidates from only the amplitude analysis, the blue ones from the spectral analysis and the green ones the final candidates which satisfy all the criteria.

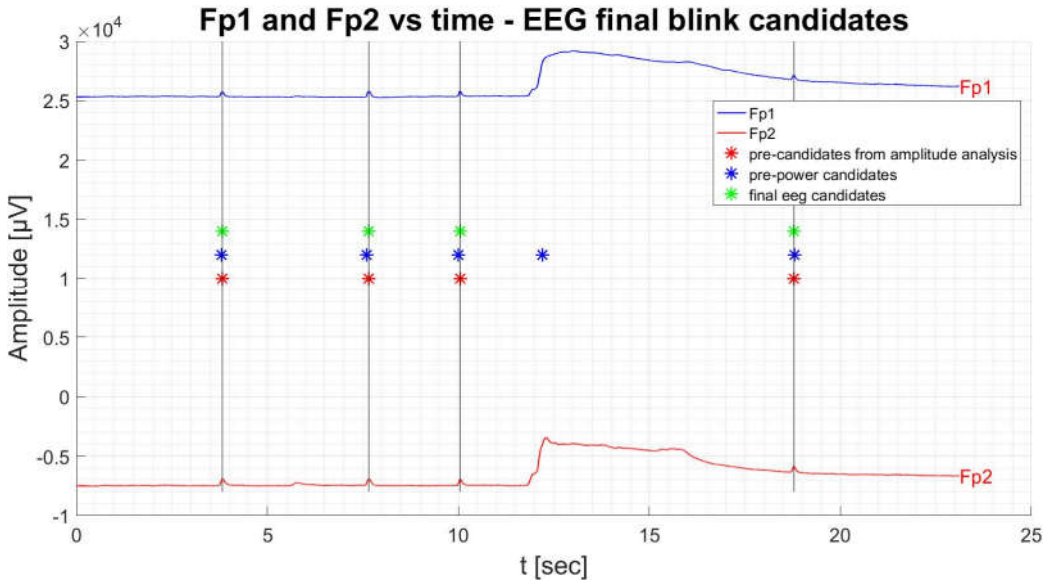

Figure 3.50: Example of output of block 2.5 Figure 3.46: EEG final candidate selection: in red the pre-candidates obtained from the amplitude analysis and in blue the pre-power candidate obtained in the spectral analysis. From their comparison the EEG blink candidate locations are estimated (in green)

3. "Candidate comparison". Figure 3.51 represents a diagram to describe this phase. The time occurrence of the blink candidates obtained from the two devices (ET and EEG) have been compared to eliminate the false positive detections.

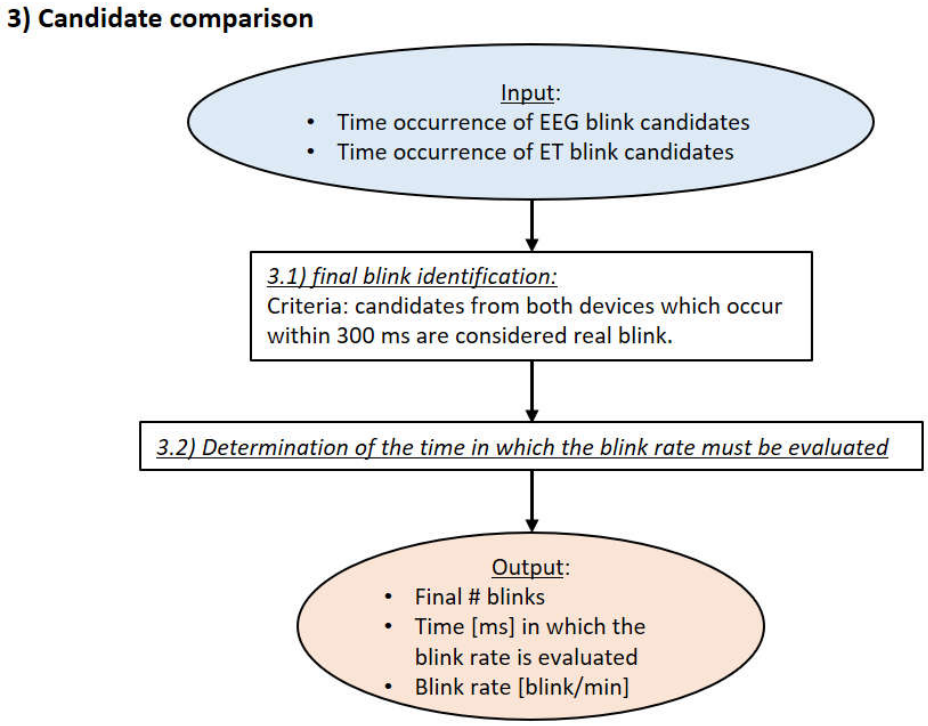

Figure 3.51: description of the flow in the "Candidates comparison" step of the Algorithm for the blinking detection.

- Block 3.1: final blinks identification. Candidates from the two devices which occur within a time window of 300 ms have been considered real blinks

  Figure 3.52 shows the Fp1 signal and gaze x-coord within the same graph. The y-axis is not representing any particular unit of measure. It has just been used to show the occurrence of the final detected blinks (common candidates = green asterisk) in correspondence of not detection of the eyes (y = 0) for the gaze and peaks for the eeg signal. The ET candidates and the EEG ones have been reported respectively in red and blue.

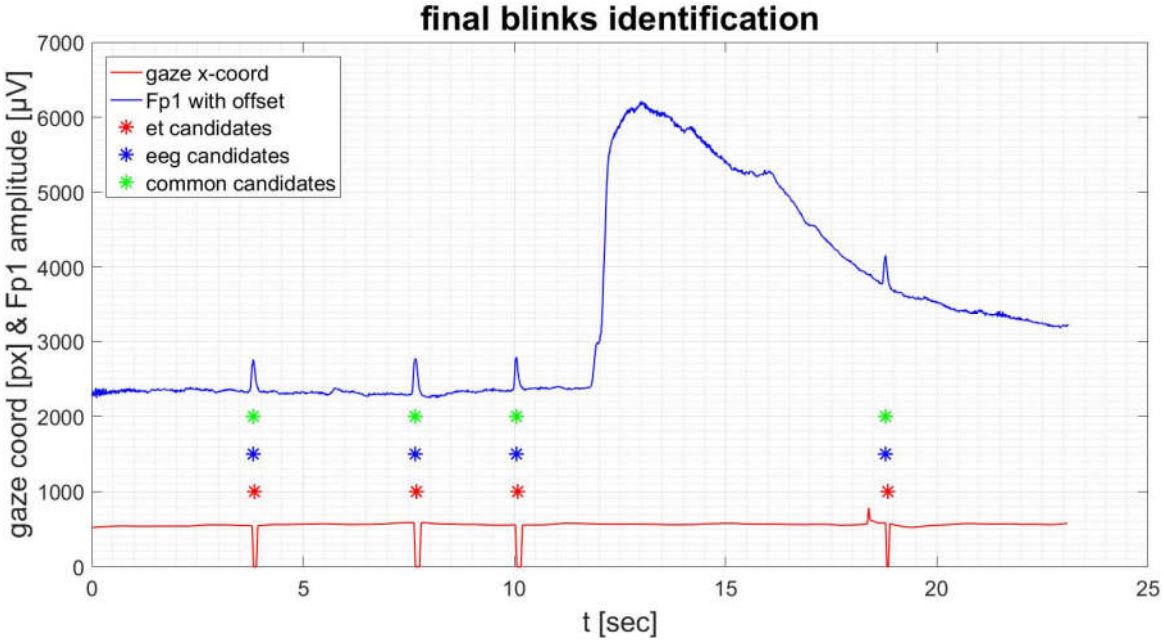

Figure 3.52: Example of the final detection of the blinks based on both ET and EEG candidates. The gaze x-coord and the Fp1 (with different offset) have been represented together to underline the simultaneous blink events on both signals. The red, blue and green asterisk are respectively: the ET candidates, the EEG candidates and the final blinks obtained by a comparison of the previous two.

This criteria allows to detect only the eye blinking which occur while the subject is looking at the screen.

To consider also the ones which occur while the subject is looking away from the monitor, also all the EEG candidates identified during long periods (>400 ms) of eyes not captured should be considered real blink.

Anyway, it has been decided to not consider them to not be conditioned by blinks occurring during for instance the exchange of the tools (i.e. while the participant is not looking at the monitor).

- Block 3.2: Determination of the time in which the blink rate must be evaluated. Knowing the number of blinks and the time interval in which they have been detected, it is possible to compute the blink rate [blink/min]. However, the eye blinking have been detected only while the subject is looking at the screen. Therefore, the time has been adjusted subtracting the durations of all the eyes not captured intervals bigger than 400 ms (blink duration) from the total time required to do the exercise.

The output of the algorithm is mainly represented by the number of blinks during the exercise, the time in which the blink rate must be evaluated and the blink rate itself. Information about the time occurrence of each blink and the time intervals of eyes not captured by the ET are also available.

A variant of the code based only on EEG candidate has been made to detect the blinking on one subject who was wearing glasses with which the ET doesn't work properly.

It has been found useful to display the graph in Figure 3.52 at the end of the algorithm to let the operator understand if the parameters used in the peak detection need to be modified or not for a better detection.

To provide a comprehensive graphic representation of what the method has been based on, a GUI has been created to display dynamically all the signals at ones together with the face video. Figure 3.53 represents the situation in correspondence of a blink (the eyes of the subject are close in the video). Analysing the image: the red asterisks that move along the time axis of the two spectrograms on the left are in correspondence of yellows horizontal lines (power peaks) while on the right, Fp1 and Fp2 present a spike and the gaze position (x,y) goes to 0 (eyes not detected).

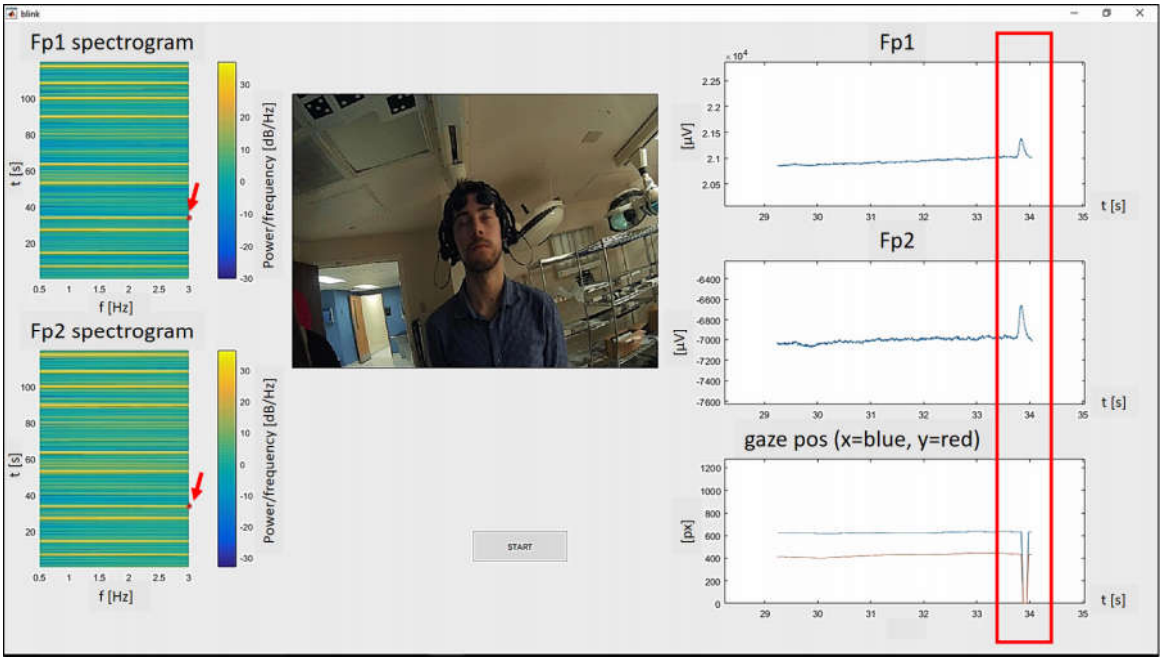

Figure 3.53: GUI created to show the behaviour of all the signals used in the algorithm for the eye blinking detection. It is possible to see that in concomitance of a blink: Fp1 and Fp2 amplitude signals present a peak (top-right), the gaze goes to zero (bottom-right) and the red asterisks that moves along the time axis of the spectrograms during the video are in correspondence of a yellow horizontal line representing a power peak (left)

3.5 Experimental Protocol

An acquisition protocol has been created to standardize the way to conduct the experiment. Firstly, it has been decided to analyse three tasks which are part of the FLS practical test and they are respectively: the Peg Transfer, the Circle Cut and the Intracorporeal Knot. The subjects that took part to the experiment belongs to three different categories: Beginners who are not from the medical field, Residents and Expert from Houston Methodist Hospital. It has been decided to not let the Beginners perform the Intracorporeal Knot because it has been considered to be too difficult and not intuitive. This has been the only difference among Beginners and the other two categories.

At the end, data have been acquired from a total of 12 participants: 4 beginners (B), 5 residents (R) and 3 experts (E). The subjects were all right handed, composed by 3 females and 9 males not homogeneously subdivided into the three categories and aged 23 to 40.

All the tasks' scenarios have been reproduced based on the information in the FLS guidance which has been explained in details in Section 2.1. To make observations about the

physiological status of the subject during each of these tasks, a reference condition is required. For this purpose, a "Rest" acquisition has been added at the beginning of the experiment. A complete experimental protocol has been structured as follows:

Preparation of the material:

- Check all the batteries: hexoskin device, eeg headset.
- Check that the laparoscopic camera, the two trocars cameras, the face camera, the EEG beacon, the ET and the Trigger Box have been connected to the tower.
- Prepare the setup for the first task: the Peg Transfer.
- Adjust the volume of the pc for the Tunnel Effect (Sound)
- Launch the Matlab GUI and test the cameras. In particular check that the cameras associated to the left and right trocars have not been reversed. In case, the correspondent IDs in the code must be modified.
- Preparation of all the laparoscopic tools required for the three exercises (Figure 3.54)

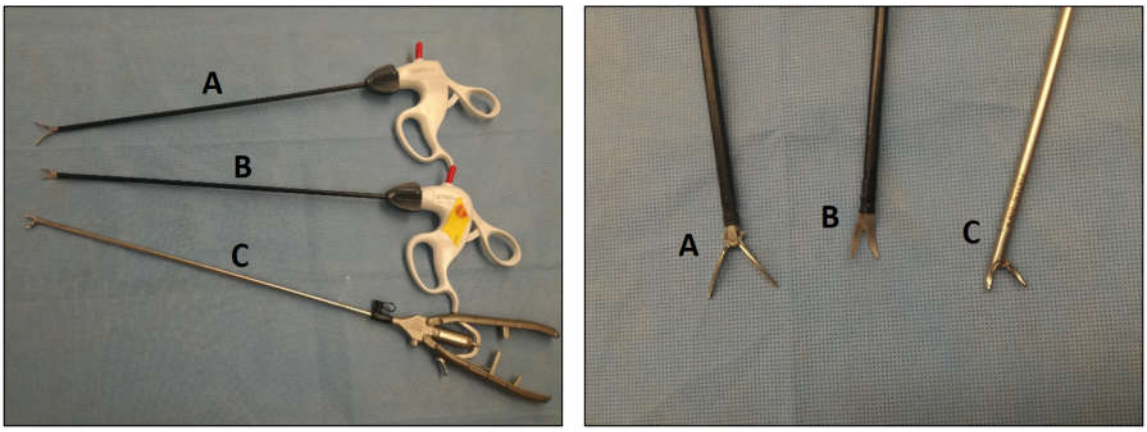

Figure 3.54: (A) Maryland dissector (grasper), (B) endoscopic scissors, (C) needle driver

Participant setup and signals checking

- The subject has to sign a form of consent and compile a paper with some basic information such as age, years of practice, right or left handed and so on.
- The subject has to wear an Hexoskin shirt of the desired size without any cloth in between the skin and the shirt. The belts must be use to guarantee the adherence of the sensors to the skin at the thorax and abdomen levels. Then, he/she has to worn the Cognionics headset.
- In the meanwhile, the operator can fill the participant information on the GUI and create the subject data folder. It must be created with the initials of the participant.

- Turn on the headset, launch the Cognionics software, configure the device and check the signal quality. As it has been explained in Section 3.2.1, the quality of the EEG signals can be checked by observing the quality of the electrode impedance with the scalp. The electrodes must be adjusted until a good impedance is reached for all of them. Another way to check the placement of the electrodes and their quality, is to ask the subject to blink; a spike will appear on all the channels in correspondence of the blink. It will be more evident for Fp1 and Fp2 which are located on the front and therefore, they are more sensitive to the skin motion induced by the blink.
- Launch the EyeTribeUI and calibrate the Eye Tracker on the subject as it has been described in Section 3.2.1.
- Pair the Hexoskin device with a smartphone, plug it on the Hexoskin shirt and check the quality of the signals on the App.
- Check that the pattern on the ceiling is visible by the trocar cameras while the subject moves the tools.

Acquisition protocol:

- Start the recording for the Hexoskin, the Eye Tracker and the EEG. They will record for the entire duration of the experiment without interruptions.
    - The Hexoskin recordings starts as soon as the Hexoskin device has been connected to the Shirt.
    - Start the recording of the Eye Tracker and set the name of the output file as eye.txt
    - Start the recording of the EEG and set the name of the output file as eeg.eeg
- The time for the exercise is controlled by the GUI. For each task, start and terminate the acquisition of the videos pressing respectively the START and STOP buttons. If the maximum time limit of the specific exercise is reached, the acquisition will stop automatically. The tasks have been executed in the following order:
        - "REST" task: the subject stands in front of the platform looking at the screen for 2 minutes. Useful to obtain a baseline for Hexoskin, EEG and Eye Tracker signals at rest.
        - "PEG TRANSFER" task: maximum time = 300 seconds.
        - "CIRCLE CUT" task: maximum time = 300 seconds.
        - "KNOT" task (only for Residents and Experts): maximum time = 600 seconds.

- Stop the recording of the Eye Tracker, the EEG and unplug the Hexoskin device from the shirt.
- Remove the Hexoskin shirt and the headset.

3.6 Preliminary analysis approach

This section explains how all the data from the different devices have been elaborated in order to conduct a preliminary analysis.

Due to the large amount of data and because it was not known which could have been the more significant signals in this kind of study, it has been decided to conduct a first analysis based on observations of the signals trend. In practice, a subgroup of signals has been selected and prepared in order to produce reports with charts and basic statistic parameters for each subject. This huge amount of information has been investigated with two purposes: to find particular trends or reaction to specific events within each subject and to compare the data among different subjects.

The signals included in the report represent data from the Eye Tracker, the Hexoskin, the Smart Trocars and the blinking information. Their elaboration, together with the report production will be treated in Section 3.6.1.

For what concern the EEG, its signals have been just prepared for a future analysis due to the extension of the brainwaves field that has not been possible to examine in depth in this work. It will be described in Section 3.6.2.

3.6.1 Signals elaboration and report production

Subgroups of signals from the Eye Tracker and the Hexoskin have been selected and elaborated to be inserted in the report.

The elaboration on the Eye Tracker data comprises an analysis on the pupil dimensions and gaze 2D coordinates [px] signal, which indicate where the subject is looking on the monitor during the task.

The first has been treated in order to determine the pupil's size during the blinks or whenever at least one of the eyes was not captured. Three different method have been tried:

- linear interpolation
- cubic interpolation
- Simple substitution with the last available value

It has been found that all the techniques provides very similar results (Figure 3.55), so the substitution with the last available value has been chosen for its simplicity.

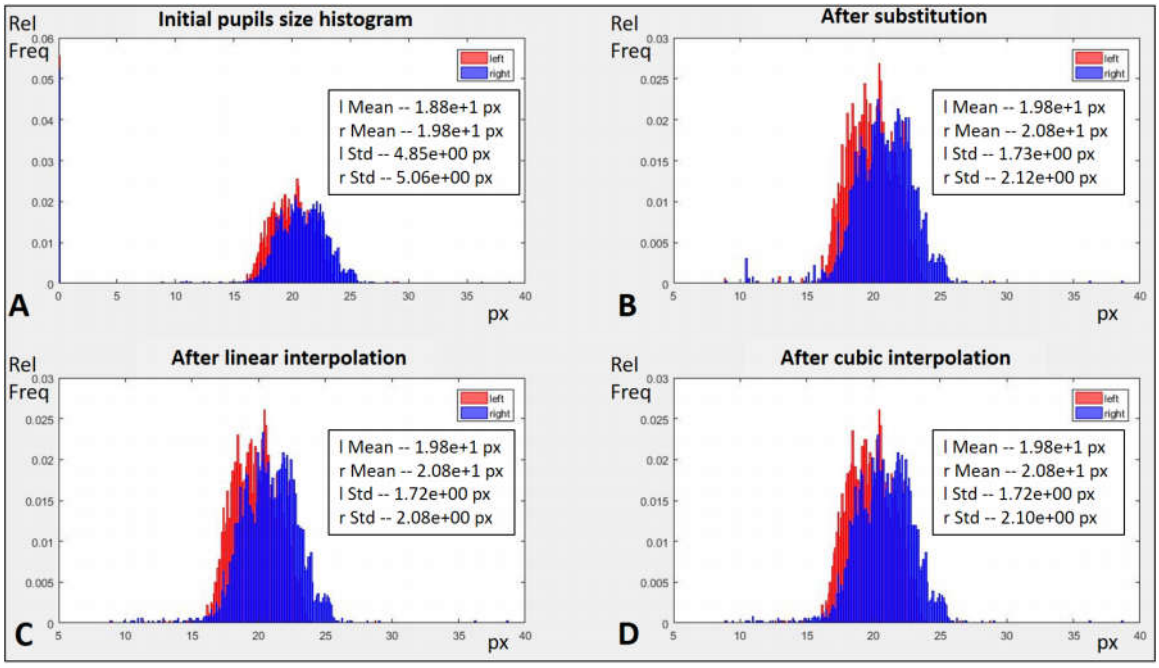

Figure 3.55: Histograms of the pupils' size of the left (red) and right (blue) eyes in a Rest acquisition. The pupils show almost the same histograms (slightly different probably due to the placement of the light in the room). (A) the raw signals which present lots of occurrences at 0 px (size when the eyes are not captured by the device). The removal of this gaps respectively with substitution of the last available value (B), linear interpolation (C) and cubic interpolation (D) show the same statistic result.

The obtained signals of the dimension of the pupils over time have been included in the report for each task. Moreover, mean and std of the size of both pupil have been computed. For what concern the gaze, the analysis has been mainly focalized on captured samples inside the laparoscopic video. For each exercise the following signals and parameters have been included in the report:

- Knowing the position of the laparoscopic video in the monitor and the ET reference frame it has been possible to compute:
    - The percentage of samples inside the laparoscopic video on the monitor
    - The percentage of samples outside the laparoscopic video on the monitor
    - The percentage of sample of both eyes not captured

  A graphic representation of the gaze movements on the screen over time has been provided. Figure 3.56 represents all the samples captured inside the laparoscopic video

on the monitor. The movement over time has been represented with a colorscale starting with blue.

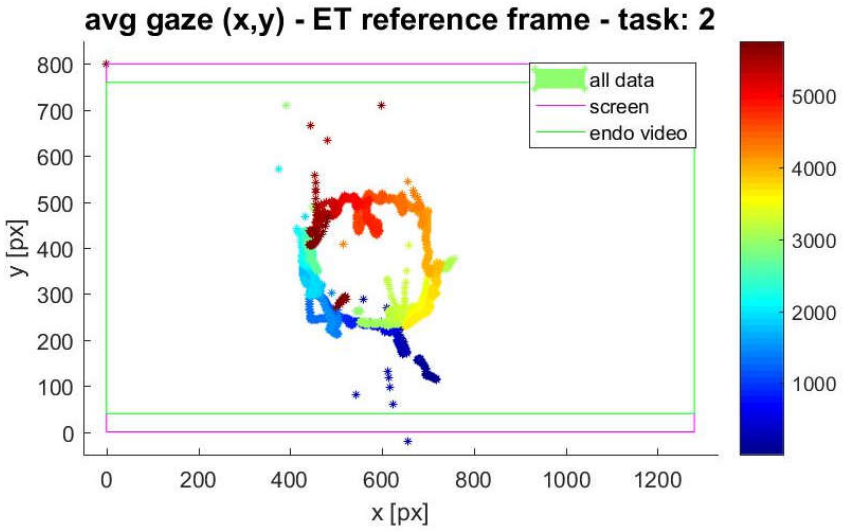

Figure 3.56: Representation of the (x,y) gaze coordinates [px] over time on the monitor during the Circle Cut task. The screen and the laparoscopic video inside are identified respectively by a violet and green rectangles. A color scale has been used to show the motion of the gaze over time starting from blue.

- Mean [px] and Std [px] of the samples inside the laparoscopic video on the monitor along x and y directions
- The displacement among subsequent gaze samples position inside the laparoscopic video. In this way, a vector with all the translations among subsequent positions of the gaze on the screen describing the entity of the eyes movements of the subject along the performance has been obtained. This vector has been used to produce histograms about the relative frequency of the entity of gaze displacements during the execution of the task. As it has been reported in the example in Figure 3.57 , the attention has been focused on the probability of big displacement which could represent the level of focus and of confidence of the subject: the less probable are the presence of big gaze shifts, the bigger is the concentration of the participant on just an area of the screen.

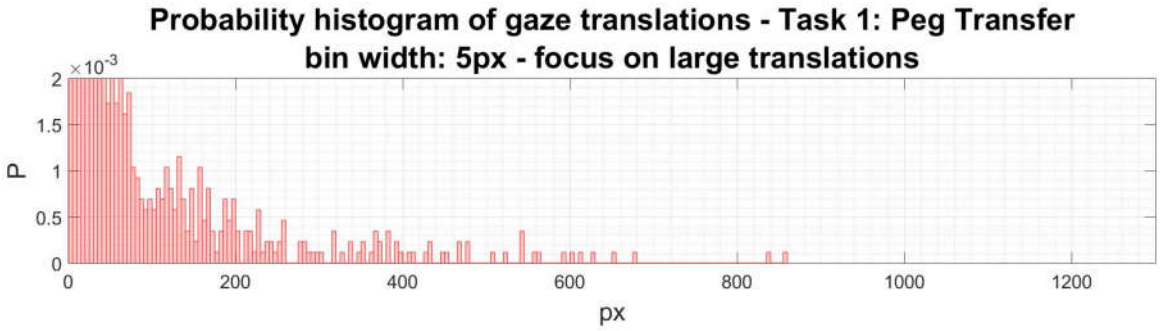

Figure 3.57: Probability histograms of the sample by sample gaze translations in a Peg Transfer task. The y axis has been limited at [0 - 2·10^{-3}] in order to focus on the big translation (lower P) which could contain information about how well the subject is able to complete the exercise remaining focus on the region of interest.

- The mean variation on the vector of gaze translation computed in the previous point. It is a parameter based on the Total Variation. The latter allows to differentiate signals of the same duration which present more or less variability along time and it is defined as:

$$Total\ Variation = \sum_{i=1}^{N-1} |Y_{i+1} - Y_i|$$

  Where N is the number of samples and Y is the signal. In this context, $|Y_{i+1}-Y_i|$ can be seen as the translational vector among subsequent gaze positions. A subject who is poor focused and moves the eyes around on the screen will present an high Total Variation. However, each participant presents a different duration of the task. For this reason, it has been decided to normalize the Total Variation value with the number of samples of the signal which varies depending on its duration. In this way it has been obtained the mean variation among subsequent samples characterizing the signal that can be compared among different tasks and different subjects.

$$mean\ Variation = \frac{Total\ Variation}{\#\ of\ samples}$$

- The velocity and the accelerations of the x and y gaze coordinates signals over time. The (x,y) gaze signals have been firstly cleaned from the gaps introduced by the blinks as for the pupil's size signal. Then, the first and the second derivative of both signals have been computed to retrieve the components of the velocity and the acceleration of the gaze in the two directions. A GUI has been created to display these information (i.e. position [px], velocity [px/s] and acceleration [px/s^2] for both gaze coordinates) dynamically together with the video of the performance (Figure 3.58). A red circle has been moved

on the video indication where the subject was looking at. Anyway, only the first graph (i.e. x and y coordinates over time) has been included in the report.

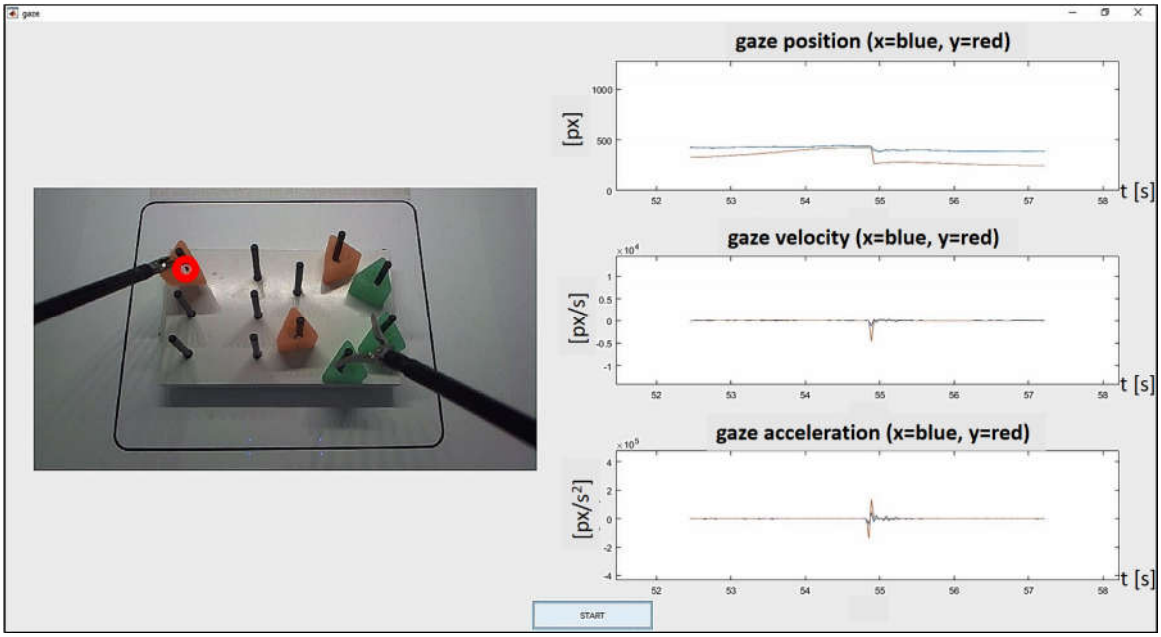

Figure 3.58: View on the GUI created to show how gaze position, velocity and accelerations change dynamically over time. A red circle is placed in correspondence of the (x,y) point of gaze on the screen.

For what concern the Hexoskin, four main signals have been selected to be part of the report:

- The Heart Rate (HR) [bpm]: Average over the last 16 heart beats. Sampling freq: 1Hz.
- The Breathing Rate (BR) [rpm]: Calculated over the last 7 respiration cycles. Sampling freq: 1Hz.
- The Tidal Volume [ml]: Volume of air inspired in the last inspiration. Sample freq: 1Hz.
- The NN intervals [sec]: Time between to heart beat detections, calculated for every QRS event. It is a clean version of the RR intervals.

The mean, std and mean variation have been computed for each of them in each task as it has been explained for the gaze.

Chats with the trend of each signals have been included in the report. Based on the Hexoskin data, it has been possible to measure:

- The percentage of HR samples considered erroneous by the device
- The percentage of BR samples considered erroneous by the device
- NN/RR %: values closed to 1 mean that most part of the RR intervals are considered true.

This small analysis allows to decide if the graphs of an acquisition contain errors or if the can be considered meaningful.

The information retrieved with the algorithms presented in Section 3.3 and Section 3.4 have been also included in the report.

For what concern the 2D movement of the tools, a graphic representation of it has been provided in the 2D space. Moreover, the movement has been subdivided into different phases for each task for a better understanding and comparison of each of them:

- Peg Transfer motion phases: 1st and 2nd half (i.e. transfer of all the obj from one side to the other and viceversa)
- Circle Cut motion phases: A separation has been done each time a tools exchange occurs because it implies the extraction of the tools from the trocars.
- Intracorporeal Knot phases: needle insertion, 1st , 2nd and third throws.

An example of the Peg Transfer can be seen in Figure 3.59. The color scale has been used to show the motion over time starting from blue. The left and right tools have been separated to not create too much confusion in the representation. This has been done applying all the roto-translational matrices to a starting point of coordinates [0,0]; then, the two motion representations have been separated in order to not touch each other.

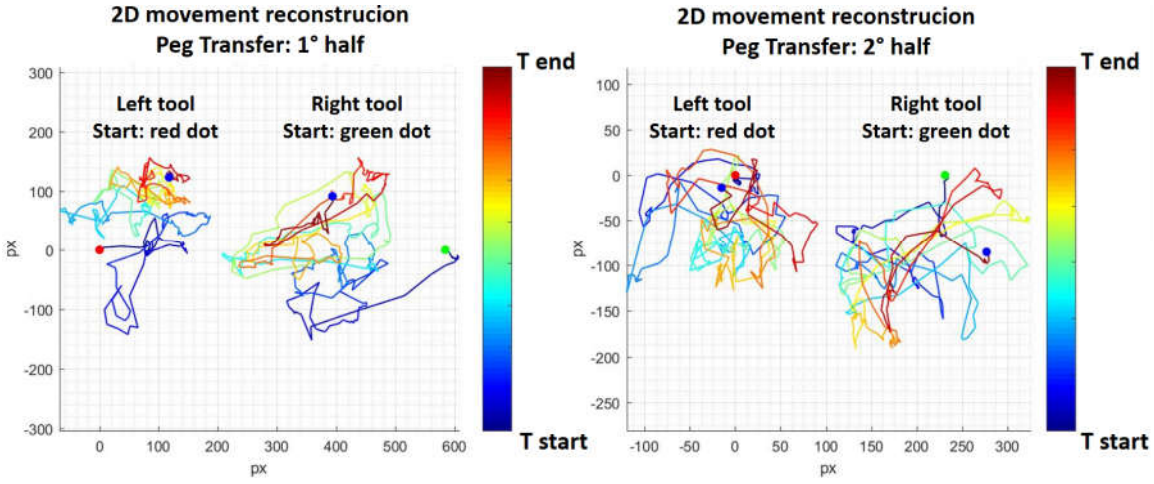

Figure 3.59: Representation of the reconstructed 2D movement of the tools during an exercise of Peg Transfer. The left image represents the first half of the exercise and the right its second half. The colorscale has been used as timeline to allow the observer to follow the movement starting from the blue. The two tools have been separated in the graphs to create less confusion.

The reconstruction algorithm provides also a vector describing the quality of the output. The latter has been always associated to the graph to understand its reliability.

On the other hand, the blink information has been used to compute the blinking rate [blink/min] for each task and for each phase of the task. In this case, the phases have been referred to the same subdivision used in the creation of the performance Scoring Metric described in Section 3.1.

Each graph representing a signal over time has been enriched with information regarding the time occurrence of specific events [sec]. They have been manually detected for each participant from its task's videos and they have been placed on two lines parallel to the time axis. A legend of the symbols associated to the different events depending on the task has been described in Table 3.4 and Table 3.5 respectively for the upper and the bottom lines.

SYMBOLS UPPER LINE	REST	PEGS	CIRCLE	KNOT
●	/	grasp the object	quarters: 1/4, 2/4, 3/4, 4/4 of circle cut	ex phases: needle insertion, 1st knot, 2nd knot, 3rd knot, cut
●	/	release the object	tools exchange	tools change
●	/	half ex	/	/
▲	/	Drop object inside the field of view (the subject is able to retrieve it)	/	Forget to change hand in the following knot, more than one attempt in inserting the needle
▲	/	Drop object (the subject is not able to retrieve it)	Cut deviation from the circle line (both inside and outside the circle)	Detachment of the needle, no double knot

Table 3.4: Legend of the events present on the upper horizontal line of the report graphs.

SYMBOLS BOTTOM LINE	REST	PEGS	CIRCLE	KNOT
✶	blink	blink	blink	blink
Red segment	Long interval of eyes not captured	Long interval of eyes not captured	Long interval of eyes not captured	Long interval of eyes not captured
◆	/	Sound (beep)	Sound (beep)	Sound change (normal, tachycardia, fibrillation, nothing)

Table 3.5: Legend of the events present on the bottom horizontal line of the report graphs.

As can be evinced looking at these tables, the upper line regards specific events which identify phases along the exercise and the occurrence of errors. On the other hand, the bottom one regards events like the blinking, the tunnel effect and the periods in which the subject is not looking at the screen.

A practical example of this kind of representation has been presented in Figure 3.60 which represents the HR signal (normalized with respect to the max value) during a Peg Transfer task.

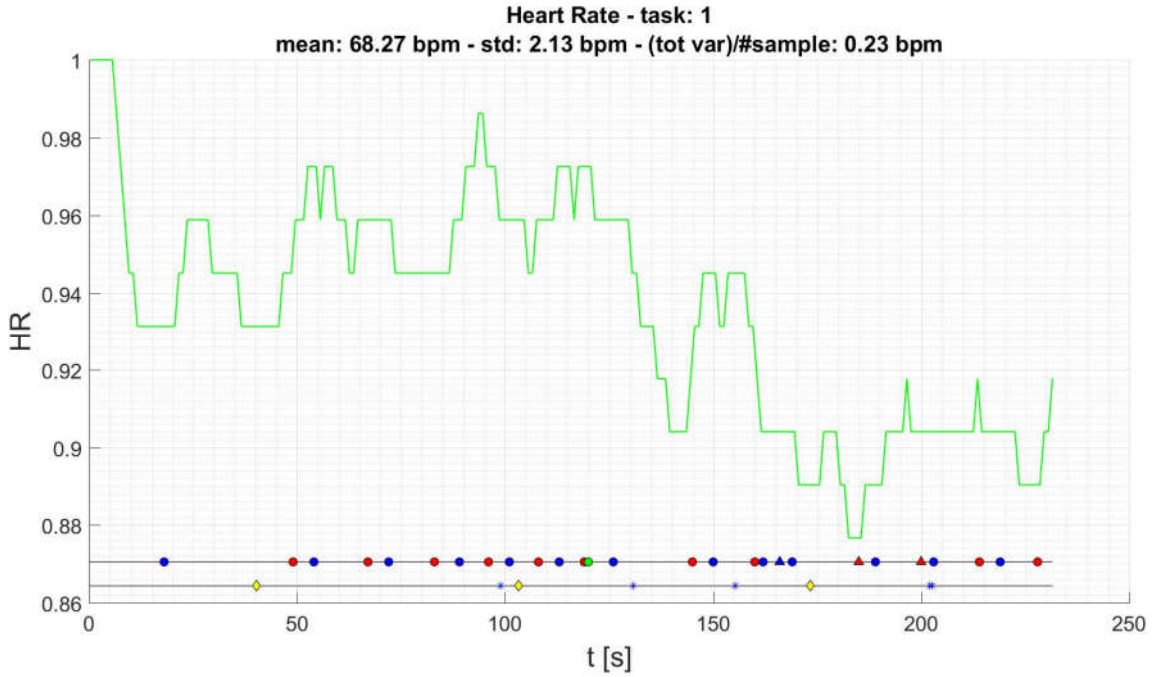

Figure 3.60: Example of HR graph of a Peg Transfer. The Heart Rate has been normalized in [0 1] with the max value. Mean, std and mean variation have been reported under the title. The two timelines parallel to the x-axis (time) contain the symbols related to the events reported in Table 3.4 and 3.5.

The tasks have been identified with their name or the following nomenclatures:

- Task 0 = Rest
- Task 1 = Peg Transfer
- Task 2 = Circle Cut
- Task 3 = Intracorporeal Knot

Once all the events have been manually detected, the report of each subject has been produced directly through a Matlab algorithm.

These reports have been subjected to investigation aimed at the identification of particular, trends, behaviours, pattern or correlation with events that can suggest hypothesis for further studies.

3.6.2 EEG preprocessing

The process consists in the removal of the artifact which affect all the channels of the EEG headset. Some artifacts can be sources of information as it has been explained in Section 3.4 for the detection of the blinking but in general they hide the information content of the signals which in this case is the brain activity. Ocular and movement artifacts affect the lower frequencies. In this study where that head is free to move in the space but it mainly remains still (looking at the screen) for large part of the procedure, the main source of artifacts are blinks. They have been found to contaminate the EEG signals up to 13Hz, especially for the electrodes that are closer to the eyes location [32].

For the cleaning of the signals some useful implemented functions of the EEGLAB toolbox of Matlab have been used. The following steps have been performed [49]:

- Filtering: firstly, signals from all the channels have been filtered with a Pass-Band Butterworth of the 3rd order in the range [1 40]Hz in order to keep only the information regarding wavebands of interest which comprise mainly: Beta wave in 13-30Hz range, Alpha waves in 8-13Hz and Theta waves in 4-8Hz and Delta in 0.5-4Hz.
- Artifacts removal: ocular and movement artifacts have been removed through the use of the Artifact Subspace Reconstruction (ASR) technique comprises in the EEGLAB toolbox. It consists in an automated artifact rejection technique which detects segments of EEG signal that contain artifacts using a sliding window principal component analysis. Each segment with a variance greater than a certain threshold is detected as an artifact and that component is removed. The threshold is computed on segments of EEG signal that are detected and considered to be clean by the algorithm itself. After performing ASR on the filtered EEG data, ocular and movement artifacts have been removed.

An example of two steps has been reported in Figure 3.61 where they have been applied on the signal of Fp1 channel during a Rest acquisition.

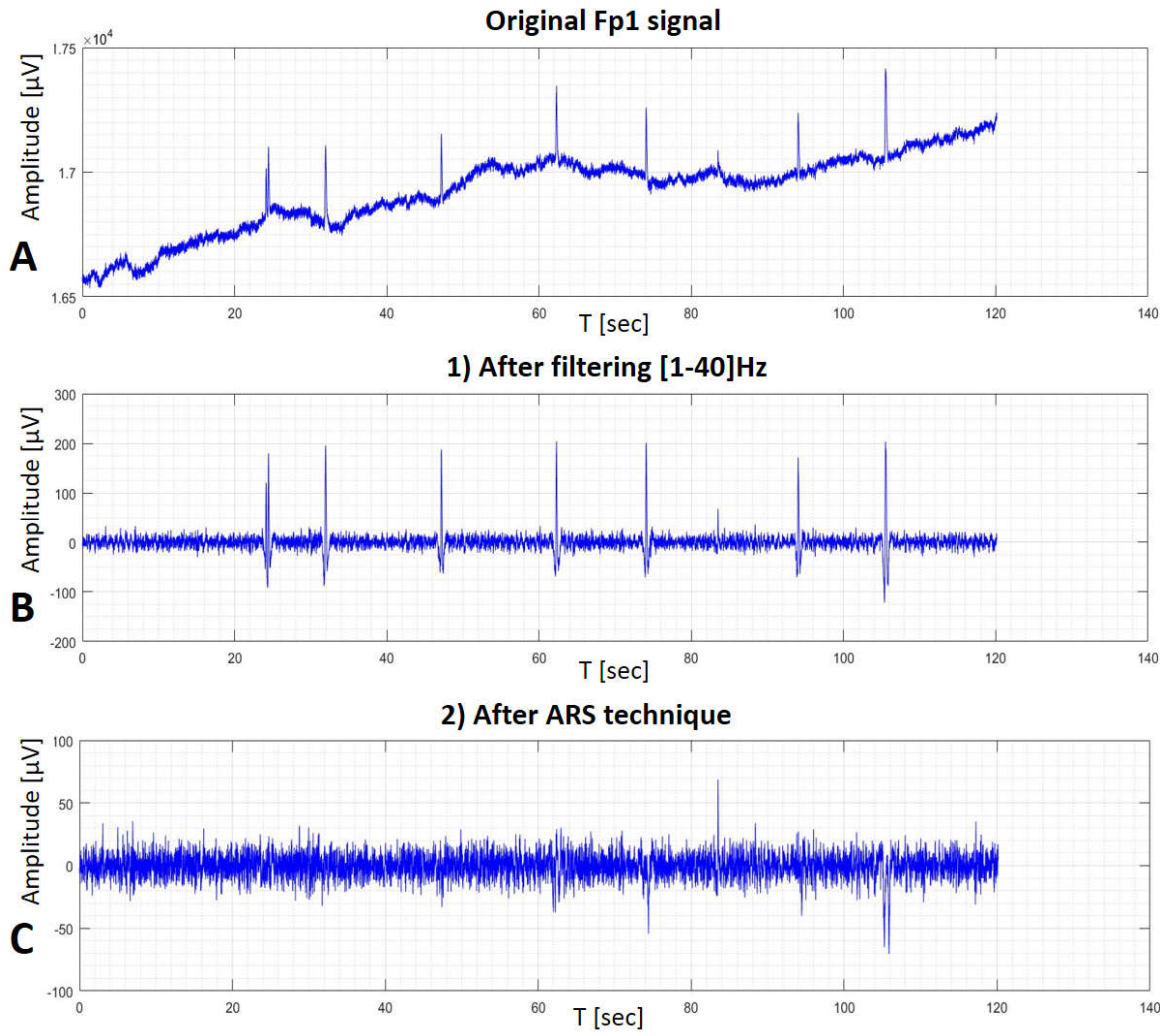

Figure 3.61: Example of EEG data preprocessing: (A) Recorded signal form the Fp1 electrode during a Rest acquisition, (B) filtered signal showing reduction in the DC and high frequency EEG components, (C) clean EEG signal after removal of ocular artifacts using ASR.

A Common Average Referencing (CAR) have been performed to enhance the signal to noise ratio. This method consists of computing the mean of the signal of all the electrodes and subtract it from every electrode. The Quick-20 EEG used in this study is equipped with 19 electrodes on the scalp providing 19 channels of information. So, the common noise contaminating the signals has been removed from each channel through the formula:

$$Channel\_CAR_i = Channel_i - \frac{\sum_{j=1}^{19} Channel_j}{19}$$

Where Channel_CAR$_i$ is the signal of the i-th channel obtained after the subtraction of the common noise.

The obtained signals are free of artifacts and ready for a future analysis to continue this study.

Chapter 4 Validations and Results

The following Chapter describes the validations of the acquisition GUI and of the developed algorithms and it presents all the results obtained from the evaluation of the subjects performance and the observations of their reports. The aims of these results are to provide a background of information to use in future studies. They can regard both the signals of interest on which conduct a more in depth analysis or indications of how to improve the acquisition platform to achieve better results.

The Section 4.1 summarises the performance of the Matlab GUI and describes a first attempt in the construction of a GUI 2.0 in Python to overcome its limitations. Section 4.2 and Section 4.3 present respectively the validations of the algorithm for the 2D reconstruction of the movement of the laparoscopic tool and the one for the blinking detection. Then, Section 4.4 treats the results of the tasks' performance evaluations with the developed scoring metric and other indicators while Section 4.5 reports all the observations that have been made on the subjects' reports.

4.1 GUI performance evaluation

The functioning of the GUI has been explained in Section 3.2.2. In the following Section, its features in terms of performance and limitations will be explored.

The critical part of the interface regards the acquisition cycle. In fact, all the other operations such as the participant information management or the initialization of the cameras don't have time constraints. On the other hand, the acquisition function have to ensure to maintain a real-time display of the laparoscopic camera video while frames from all the four cameras are sampled and saved into the correspondent files and the tunnel effect sound is played. As can be imagine, the Sampling Rate for those videos depends on the Matlab capacity to process videos and the time dedicated by the pc to all the other active processes (e.g. Cognionics and EyeTribeUI software for the respective signals acquisition).

The time required to complete a cycle in the acquisition loop has been monitored over time during simulations of real acquisitions using the TOC function of Matlab.

A cycle of the acquisition loop comprises:

1. A control to verify if the maximum time limit for the exercise has been reached.

2. A control to check the elapsed time from the previous sample. If it is equal or greater than 1/Fs where Fs is the output videos Frame Rate, samples from all the cameras are captured and written in the correspondent file.
3. A PAUSE to avoid the freeze of the laparoscopic video.
4. A control on the time elapsed from the beginning of the exercise to play the sound (tunnel effect) at the right moment.

Obviously, the maximum time required to complete the cycle occur when conditions 2, 3 and 4 are satisfied at the same time and all the other software required for signals acquisitions are running. In such conditions, the monitoring of the cycle duration over time has shown peaks of 0.16-0.17 seconds per cycle. The Frame Rate of the output videos has been adjusted based on this maximum duration.

All considered, this GUI allows video acquisitions at a maximum of 5Hz ($\Delta T = 0.2$ sec).

The GUI limitations can be summarized in:

- Matlab Image processing functions require more time with respect to other programming languages such as Python or C. This doesn′t allow the real-time manipulation of the laparoscopic video for the implementation of visual Tunnel Effects such as image rotation or the smoke effect.
- No multithreading approach has been used due to the difficulty and the limitations which make Matlab not suitable to deal with such a concept (except for the use of the parfor in other kinds of context). This could be the reason for the slightly perceivable delay in the laparoscopic video. Anyway, this delay is hardly perceivable and so, it doesn′t influence the subject performance.

Despite these limitations, this interface fulfils the requirements for this study, ensuring a solid acquisition system.

However, a new prototype of GUI has been developed in the last part of this study to overcome the limitations of the current version. It doesn't encompass all the functionality of the Matlab one but it constitutes a solid starting point for a next development of a 2.0 version of the system. Python 3.6 has been chosen as programming language due to its usability and high performance.

The layout of the new GUI has been created with Qt Designer. PyQt5 contains different modules such as QtCore, Qthread which have been used in Python to manipulate the

elements in the interface. The functionalities of the previous version that have been implemented in this prototype encompass:

- Participant information management
- Videos management

The main innovations regard the acquisition cycle. They consist in the use of:

- OpenCV library for video management.
- Multithreading. The QThread module of PyQt5 has been used to assign each camera to a different thread allowing to process the videos in parallel. Moreover, another thread has been use to write the beginning and end times (always in posixtime/unix scale) of each acquisition in a text file.

The two GUIs have been compared during similar operations such as: save participant information in an excel file, initialize the cameras and acquire the videos during the performance of a task.

The first impressions have been encouraging, showing an increase of the velocity for every operation in the prototype. Moreover, the very slight delay affecting the laparoscopic video in the Matlab GUI is no more present in the Python version.

These considerations make this prototype suitable for a future development and subsequent integration in a new version of the entire acquisition system.

4.2 Validation of the algorithm for the 2D motion reconstruction

A total of five tests have been made to validate the capacity of the algorithm to reconstruct the 2D movement of the laparoscopic tool. The 5^{th} is the result of all the reasoning on the previous ones. The use of the V channel in the HSV conversion of the image has been found to be more suitable for the squares detection with respect to the grayscale conversion. So, the validations have been conducted on that version.

Test 1:

The aim of this first test has been to assess how good was the estimation of the position of a fixed point on the ceiling along the video knowing the starting point. A small piece of black tape has been attached to the ceiling and a laser pointer parallel to the camera focal axis has been attached to the trocar. Then, a short video (about 13.4 seconds for a total of 67 frames) has been made moving the trocar and the reconstruction algorithm has applied to it.

Ten frames have been selected from the video and the following procedure has been applied:

1. Manual selection of the black tape position in the first image of the video to determine its 2D coordinates in the frame (its starting point).
2. Manual identification of the 2D coordinates of the tape in the ten selected frames (real 2D coordinates of the tape in the images).
3. Application of all the translational vectors and the rotational matrices retrieved from the algorithm to the starting point (from step 1) estimating the tape position in each frame.
4. Computation of the error (E) among the estimated positions of the tape in the selected frames and the manually detected ones (real positions).

The reconstruction algorithm has been applied in two conditions: without and with correction of the image distortion. Figure 4.1 represents the errors computed for all the selected frames in both conditions. On the x-axis has been reported the number of the frame and on the y-axis the correspondent error (pixel). No statistical difference has been observed among the two conditions.

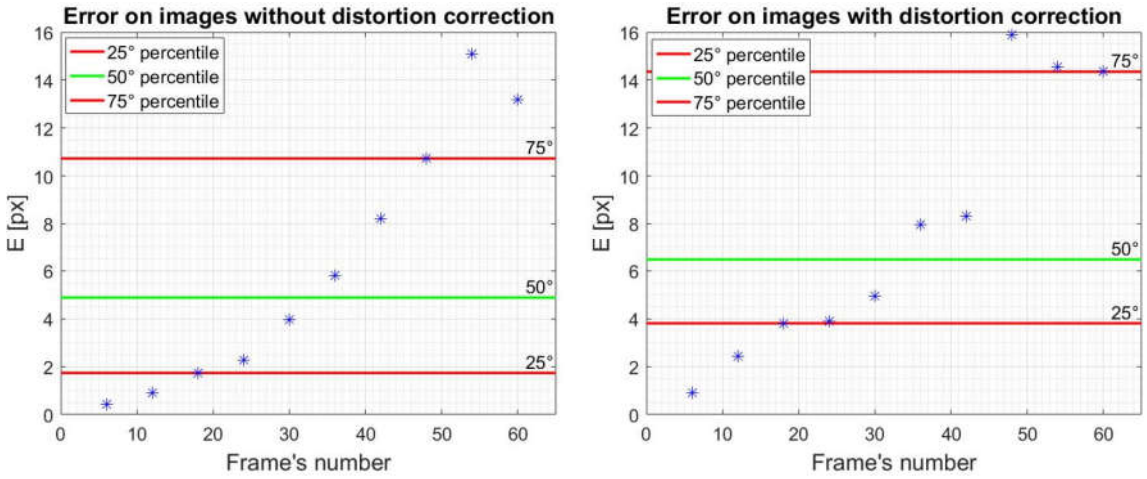

Figure 4.1: Errors among the estimated positions of the tape and the manually selected ones in the 10 selected frames. The left and right graphs represent the results respectively of the video without and with a correction of the image distortion (test 1). For each graph, the 25°, 50° and 75° percentiles are reported. No statistical difference have been observed.

The manual detection of the tape position in each frame can bring a maximum intrinsic error of 1-2 pixels. Anyway, the reconstruction error grows over time as can be evinced from the previous images.

This behaviour was expected because the estimated roto-translational transform to pass from one frame to the other is affected by an error. This frame by frame error is additive. This means that if all the roto-translational transforms have been applied to a starting point, the final estimated position will present an error equal to the frame by frame error multiplied by

the number of frames. This doesn't occur using for instance optical tracking systems where the estimation of the position of a marker doesn't depend on the previous position. However, the purpose of this algorithm is not to reconstruct correctly the exact trajectory of the tool but it is to estimate the entity of the frame by frame movements.

Test 2:

This second test has been made to verify the previous assertion. The same video and the same selected frames of the first validation have been used. For each i-th frame of the 10 selected ones, the following procedure has been adopted:

1. Manual identification of the 2D coordinates of the tape in the (i-1)th frame (starting point).
2. Manual identification of the 2D coordinates of the tape in the i-th frame (real position).
3. The translational vector and the rotational matrix found by the algorithm to pass from the (i-1)th frame to the i-th frame have been applied to the starting point (from step 1) of the tape in the (i-1)th frame in order to estimate its position in the i-th frame.
4. Compute the error between the estimated position of the tape (from step 3) in the i-th frames and real one (from step 2).

The reconstruction algorithm has been applied in two conditions: without and with correction of the image distortion. The results for the 10 selected frames have been summarized in Figure 4.2.

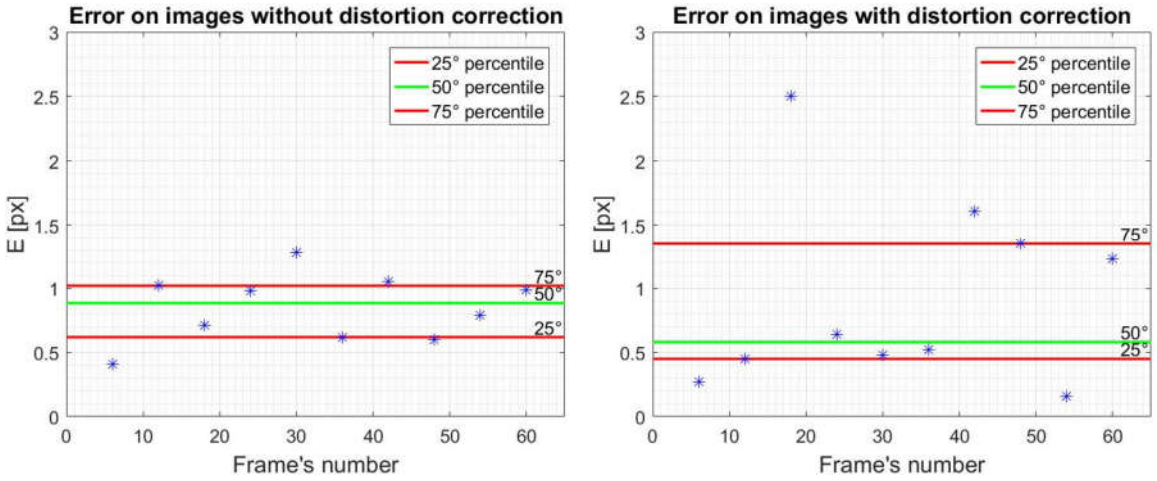

Figure 4.2: Error in the reconstruction of the tape position among ten couples of subsequent frames. The left and right graphs represent the results respectively of the video without and with a correction of the image distortion (test 2). For each graph, the 25°, 50° and 75° percentiles are reported. No statistical difference have been observed.

On the x-axis has been reported the frame's number in the video and on the y-axis the correspondent error (pixel). No statistical difference has been observed between the two conditions. The error is in general lower than 3px. Moreover, it is quite constant for the entire duration of the video confirming the initial affirmation.

Test 3:

This test aims at verifying if the entity of the movement between frames has an impact on the reconstruction error. Four black stripes have been located on the ceiling and the distance among them has been measured (Figure 4.3).

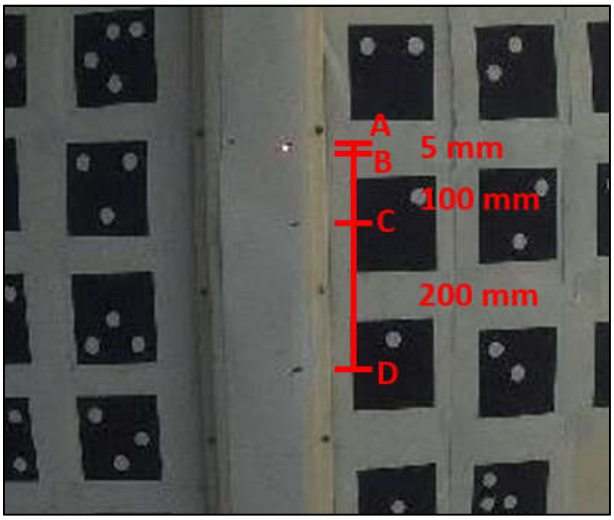

Figure 4.3: Disposition of the black stipes used for the test n°3

The laser pointer used in test 1 has been used to point toward each black stripe during the video registration. Seven frames have been selected from the video. They correspond to the moments in which the laser was pointing at the stripes in the following order:

1. Pointing at A
2. Pointing at B
3. Pointing at C
4. Pointing at D
5. Pointing at C
6. Pointing at B
7. Pointing at A

A new video has been mounted with only these frames. The reconstruction algorithm has been applied to the new video (only 7 frames) in two conditions: without and with correction of the image distortion.

For each i-th frame of the first 6 frames the following procedure has been adopted:

1. The real 2D position of the stripe pointed by the laser has been manually detected (starting point) in the i-th frame.
2. The roto-translational transform estimated by the algorithm to pass from the i-th frame to the (i+1)-th frame has been applied to the starting point (from step 1) to estimate the position of the same stripe in the (i+1)-th frame.
3. The real position of the stripe in the (i+1)-th frame has been manually detected and the error with the estimated position has been computed.

The obtained errors (Figure 4.4) show no statistical difference among the two conditions.

It is important to remark that in all this tests there is always the presence of the systematic error due to the manual detection of the real position of the target.

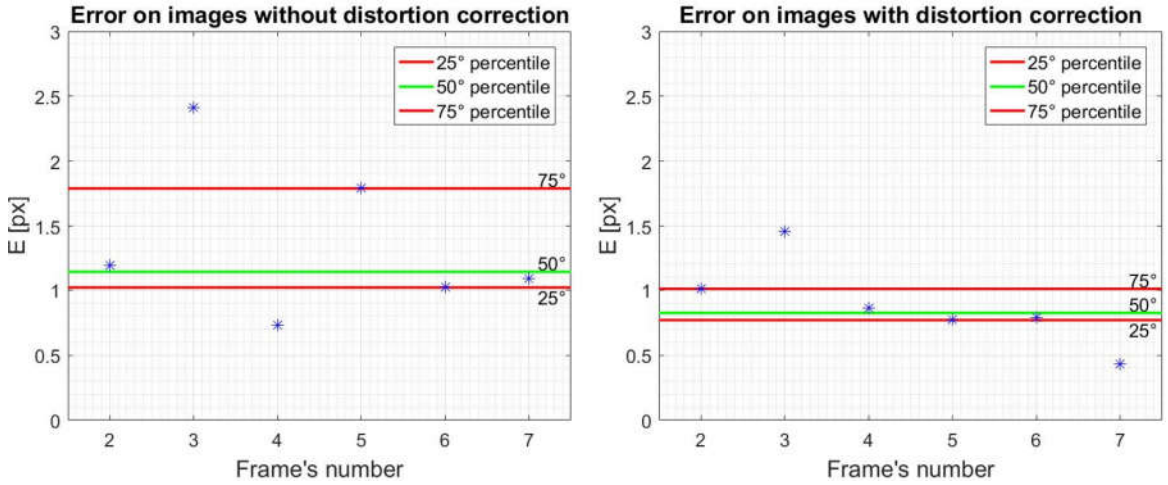

Figure 4.4: Error in the reconstruction of the stripe position among two subsequent frames in the video without (left) and with (right) correction of the distortion (test 3). For each graph, the 25°, 50° and 75° percentiles are reported. No statistical difference have been observed.

Test 4:

This test is similar to the 3rd. In this case a laser distance meter has been used to measure its distance from one wall of the room (Figure 4.5). The laparoscopic tool has been fixed at the distance meter. In this way, the instrument will follow the displacement of the distance meter changing the orientation of the trocar camera.

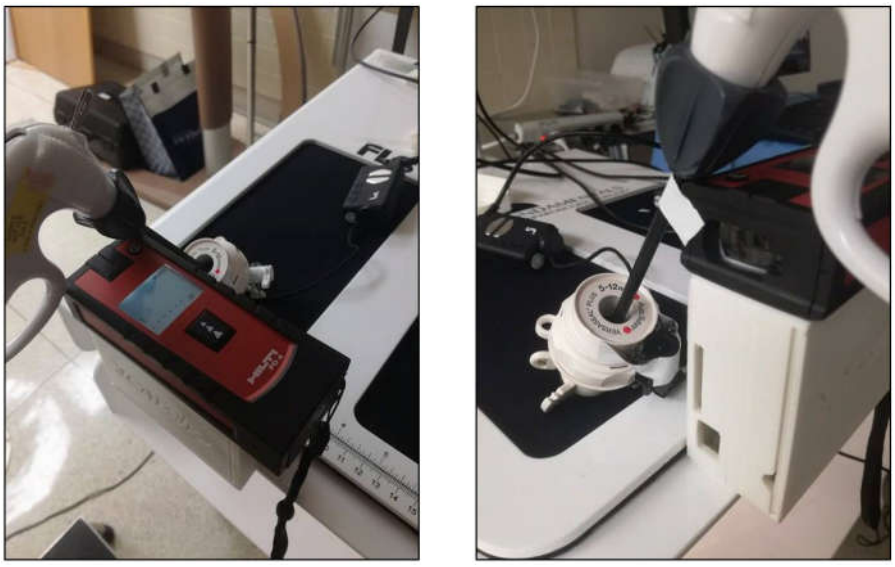

Figure 4.5: Laser distance meter fixed with the tool to meause the displacement of the instrument in two subsequent configurations with respect to the wall.

A total of four couples of images have been taken. For each one:

- The first image has been used as the reference position. It has been always taken with the trocar in vertical position.
- The second image has been taken after moving the distance meter together with the tool toward the wall.

The distances among the two positions of the distance meter in which the images have been captured are:

1. Among the 1st and 2nd frames: the distance meter has been moved of 7mm with the tool.
2. 3rd and 4th frames: 21 mm.
3. 5th and 6th frames: 38 mm.
4. 7th and 8th frames: 61 mm.

Based on trigonometry, it has been possible to estimate the displacement at the ceiling (dc) knowing the displacement of the distant-meter (d), the distance in height among the trocar pivot and the distant-meter (H) and the one among the pivot and the ceiling (Hc) (Figure 4.6).

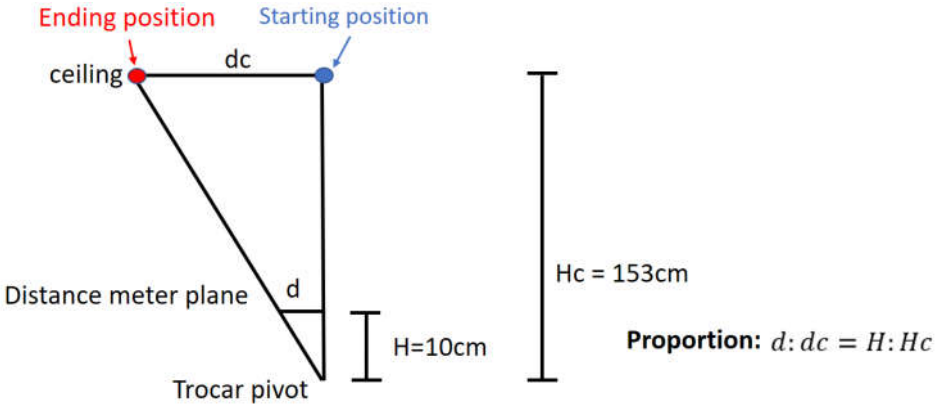

Figure 4.6: Schematic representation of the correspondent displacement seen on different planes. "d" is the displacement of the distance meter on its plane while "dc" is the correspondent one on the ceiling.

Therefore, the correspondent movement on the ceiling are:

1. 10.71 cm
2. 32.13 cm
3. 58.14 cm
4. 93.33 cm

The four couples have been mounted in video (8 frames). The algorithm for the reconstruction of the 2D motion of the tool has been applied to it in two conditions: without and with correction of the image distortion.

As for test 2, the error between the estimated and real positions of the black tape in the second frame of the each couple has been computed knowing its starting position (manually selected) in the first frame one.

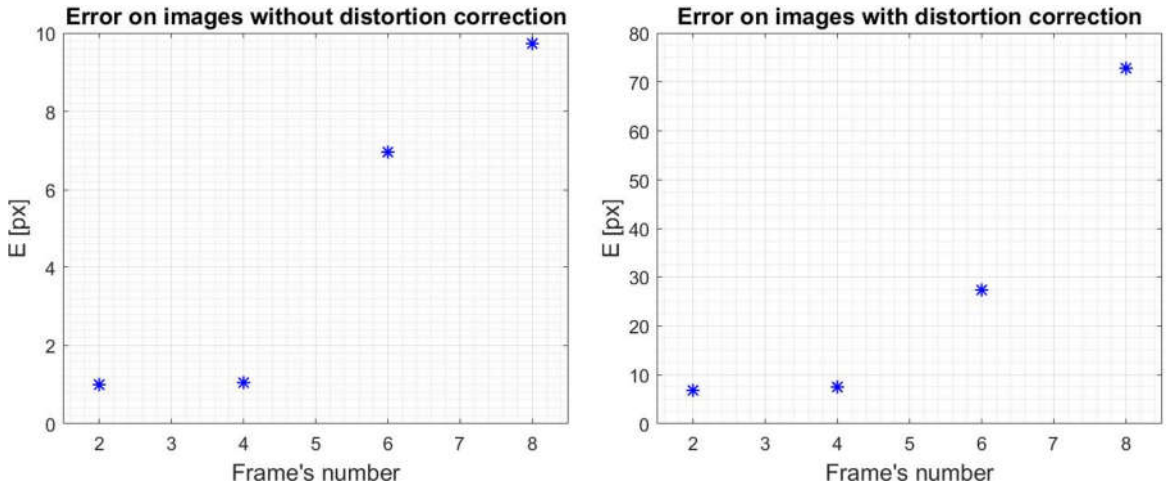

Figure 4.7: Error in the reconstruction of the tape position in the second frame of each of the four couples of images. The left and right graphs represent the results respectively of the video without and with a correction of the image distortion (test 4).

Figure 4.7 shows an increase of the error together with the entity of the displacement, in particular for the video in which the distortion of the image has been corrected.

A cause for this increase could be that in these four validation tests it has been tried to reconstruct the position of a fixed point on the ceiling. It could be close or far from the squares used to compute the roto-translational transforms depending from the tool's tilt. The evaluation of the error in this case is not properly corrected because it has been tried to reconstruct the movement of a point (black tape) that could be far from points (feature points of the pattern on the ceiling) used by the algorithm.

A last test has been conducted evaluating the error committed by the ICP registration algorithm in the estimation of the roto-translational transform. The projection of the tool rotational axis is always more or less at the center of the image. For this reason, the error in the reconstruction of its motion is well-represented by the error in the reconstruction of the feature points of the squares used in the ICP (close to the center of the image).

Test 5:

In this last test there is no manual detection. The evaluated error is directly the one made by the ICP function in the estimation of the roto-translational matrix to transform the cloud of points of i-th frame into the correspondent cloud of points of the (i+1)-th frame. The error has been computed for the four couples of frames used in Test 4. The procedure has been the following:

1. For each couple of frames the reconstruction algorithm estimates the squares in common that are closer to the center (as explained in Section 3.3.2). The feature points (corners and centroids) of these squares constitute the 'model' and 'data' points cloud used by the ICP function to estimate the roto-translational transform (R and T) among them.
2. R and T are affected by an error. In order to retrieve it, they have been applied to the "data" points cloud to estimate the 'model' one. The error is the difference among the points in the real 'model' cloud and in the estimated one.

The algorithm has been applied in two conditions: without and with correction of the image distortion. The bigger errors have been found for the 4^{th} couple that corresponds to the bigger displacement. For this couple, the ICP has used only features points from one common square on the ceiling. The errors in the reconstruction of all the points of the cloud have been reported in Figure 4.8.

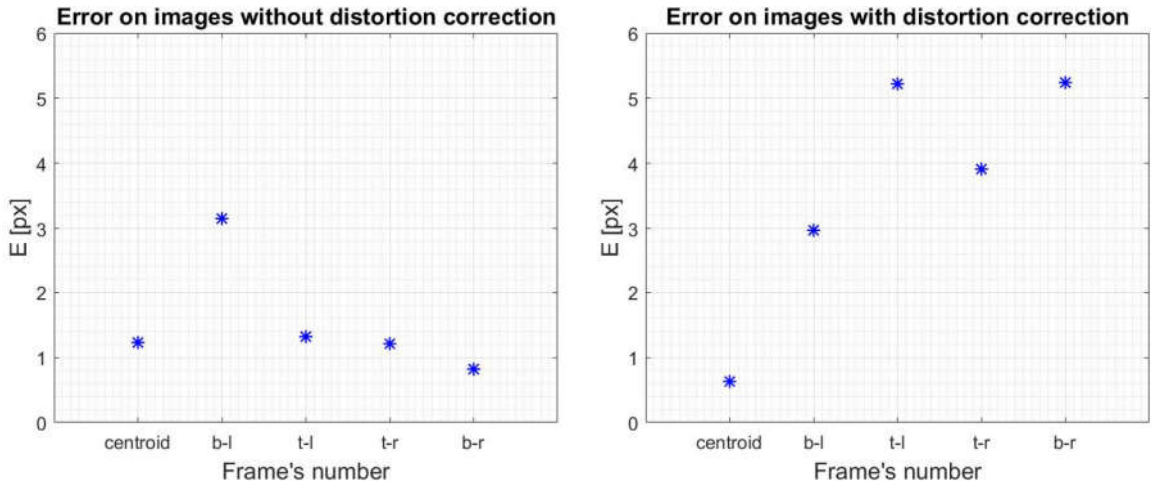

Figure 4.8: Errors in the reconstruction of each feature points used by the ICP algorithm to estimate the roto-translational transform between the frames of the 4th couple. The left and right graphs represent the results respectively of the frames without and with a correction of the image distortion (test 5).

The error seems to be lower for the original video (left graph) going above the 1.5 px only for displacement of the distance meter larger than 4 cm.

Considering all the four couples of frames, the Mean and the Std of the ICP registration error are respectively 0.81px and 0.67px for the original video and 2.29px and 1.47px for the corrected one.

Anyway, the errors in the original video remain under 4 px.

It is important to notice that all the errors estimated in the previous validations are errors computed on the ceiling plane. A small movement of the tool will appear as a big movement on the ceiling. The same concept can be applied to the error. An error of N pixels on the ceiling (ec) that correspond to M centimetres will correspond to a smaller error Z at the level of the tool tip (e) as can be seen in Figure 4.9.

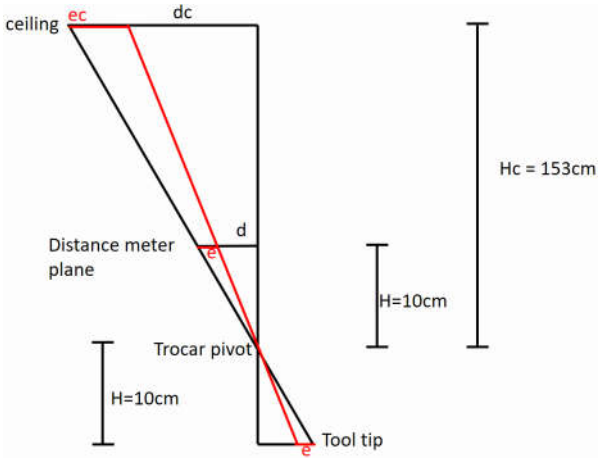

Figure 4.9: Schematic representation of the error on different planes

Considering the tip of the tool on a plane at 10cm below the pivot of the trocar and knowing that in the center part of the FOV the conversion coefficient is 0.22cm/px, the error at the level of the tip has been estimated through the proportion:

$$H{:}\,Hc = d{:}\,dc = e{:}\,ec$$

The correspondent of an error of 10 px on the ceiling is 2.2cm on the same plane. Then, 'e' can be computed as:

$$e = \frac{H}{Hc}ec = \frac{10cm}{153cm}2.2cm = 0.14cm$$

This error will change depending on the considered plane. It could be useful to consider the angle (α) that describes the distance (error) between the real and the estimated position. An example in provided in left part of Figure 4.10 where both the errors "ec" and "e" share the same angle α. In particular, α can be easily computed as part of a rectangular triangle. For an error of 10 px on the ceiling:

ec = 2.2 cm, Hc =153 cm $\qquad\qquad \alpha = arctg\left(\frac{ec}{H_c}\right) = 0.82°$

This case correspond to the maximum angle, in fact moving the base of the triangle (ec) on another location on the ceiling, the obtained angle will be lower (Figure 4.10 right).

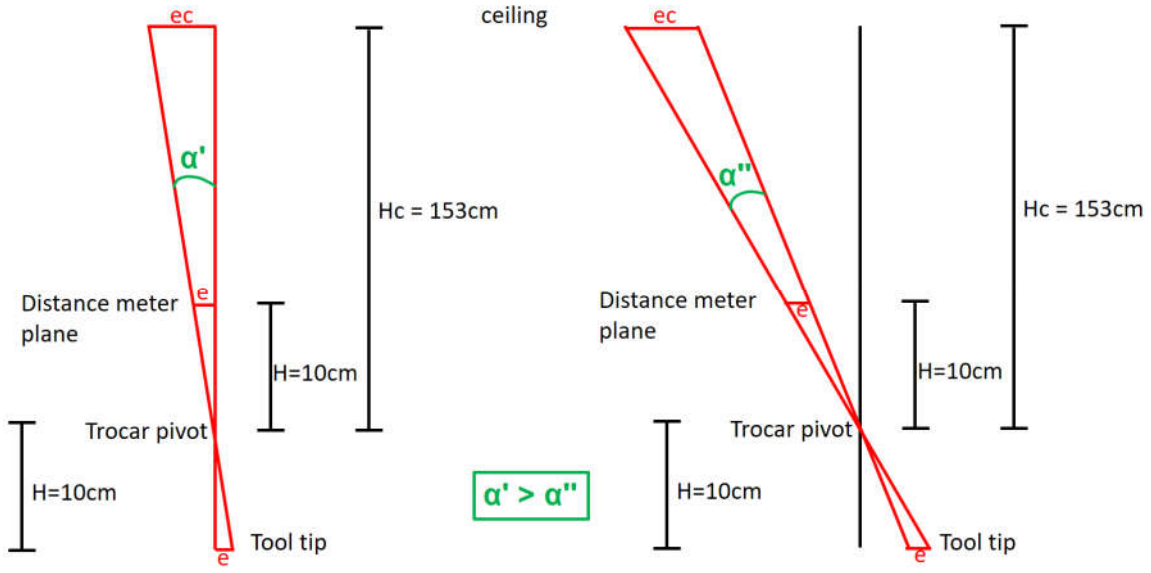

Figure 4.10: Schematic representation of the angle associated to the error. It is highlighted the difference in angle considering the error on the ceiling ('ec') estimated in a vertical position wrt to the pivot (α') or away from it (α''). The more 'ec' is far from the vertical position, the more alpha decreases.

The 5th test has shown that the algorithm has a better performance on a video where the correction of the distortion is not applied. In that condition, a maximum error of about 4 px has been found. The correspondent 'ec', 'e' and α are respectively 0.88cm, 0.06cm and

0.33°. These are the maximum errors affecting the system in the frame by frame 2D motion reconstruction for good quality images. A dangerous sources of errors regards the blurring of the images due to a very rapid movement that increase the probability of misdetections of the features points of the squares on the ceiling. In order to avoid it, a future improvement of the algorithm could imply something that is able to determine the level of blur in the frame and discard it if necessary.

4.3 Validation of the algorithm for the blinking detection

The frontal camera (face camera) integrated in the acquisition system has been used to validate the algorithm for the blinking detection. This camera has been placed in front of the subject in order to record his/her face and manually detect the number of real blinks. In practice, the information in its video of the performance have been used as ground truth. Different tests have been performed in order to validate and assess the reliability of the algorithm.

Test 1

A first brief acquisition has been made with only 4 blinks and one other kind of artifact (knit the brow), whose images have been displayed in Section 3.4 to explain the code. As it has been shown, the code has been able to detect all the blinks.

Test 2

A second longer video has been made to test how the code reacts to different blink conditions. Trying to control the blinking, the following behaviour has been assumed by the subject during the acquisition:

1. Normal blink looking at the screen
2. Turn the head on the left (looking away from the screen) and blink
3. Look down (away from the screen) and blink
4. Speak and blink (to check eventually influences of the speech in the eeg signal of Fp1 and Fp2)
5. Same as 4
6. Knit the brow and blink looking at the screen
7. Same as 6
8. Knit the brow, turn the head on the left and blink

9. Same as 8
10. Knit the brow, look down and blink
11. Normal looking at the screen

During the acquisition the head has also been turned towards the left and down without blinking in order to test also the effect of each movement alone. It must be noticed that this acquisition has been strongly affected by artifacts of different nature on purpose. In particular, the 7th blink has been done while turning the head becoming a very difficult one to detect (very weird movement).

In this test, the identification of the intervals of Eyes Not Captured (ENC) is more diversified. Apart from intervals with a duration that can be associated to a blink, the algorithm detected intervals with a duration equal to zero (single samples of ENC) and long intervals related to the period in which the subject was not looking at the screen.

The comparison among the video and the blinks detected by the algorithm has shown that the second has not been able to detect the 7th blink. Moreover, one false blink has been detected as real.

All the other blinks, also the ones while the subject was not looking at the screen, have been recognized as true by the only EEG.

Despite the error, this test has been performed in the worst conditions that could happen during an acquisition. In fact, during the performance the subject is for most of the time looking at the screen. Only in tasks that allow to exchange the instruments there are moments in which he/she could look somewhere else.

For this reason, it has been decided to test the algorithm on real performance in the next test.

Test 3

Here, the algorithm has been tested during real acquisitions (rest and pegs transfer) and the information of the frontal camera has been always used as validation.

From the face video of the 'Rest' acquisition a total of 10 blinks have been identified.

Figure 4.11 shows the blink candidates' intervals of the Eye Tracker. The green and black vertical bars represent the start and stop of each blink detected by the ET and the light blue asterisks represent the occurrences of the real blinks (from the ground truth). As can be seen, all the real blinks have bene correctly identified.

Figure 4.11: Gaze coordinates (x,y) vs time. The ground truth (magenta asterisks) completely match the ET candidates (vertical lines intervals)

The same of the EEG candidates which can be easily notices as simultaneous yellow lines on the two spectrograms (Figure 4.12A) and power vs time representations (Figure 4.12B). In the latter, the red, green, blue and magenta asterisk represent respectively: the eeg pre-candidates from the amplitude analysis, the pre-power candidates, the eeg's final candidates and the ground truth.

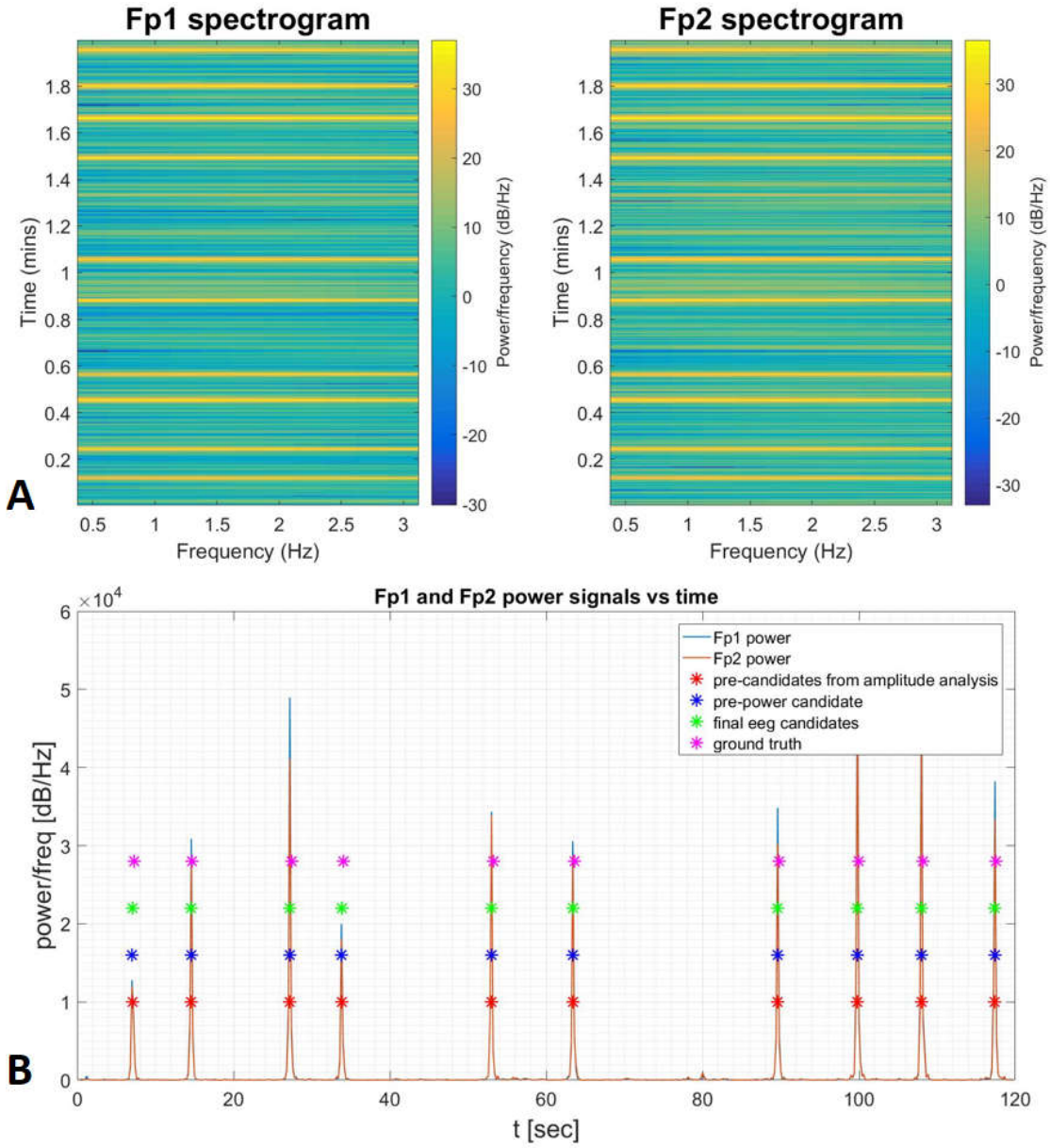

Figure 4.12: (A) the ten peaks power associated to the blinks can be easily seen on the Fp1 and Fp2 spectrograms in correspondence of the same times. The spectrogram of the signal has been computed for the range [0.5 3] Hz subdividing the signal in temporal window of 200 ms with an overlap of half-window among subsequent intervals. (B) Summing the contribute of all the freq ([0.5 3]Hz) in each window the total power vs time signal has been obtained for both the channels (Fp1 and Fp2). The two signals are almost overlapped and the 10 peaks are clearly visible. The red, blue, green and magenta asterisks represent respectively the eeg candidates from the amplitude analysis, the eeg power candidates, the eeg final candidates from a comparison of the previous two and the ground truth.

Therefore, from the comparison among the ET's and EEG's blink candidates all the true blinks have been detected (Figure 4.13).

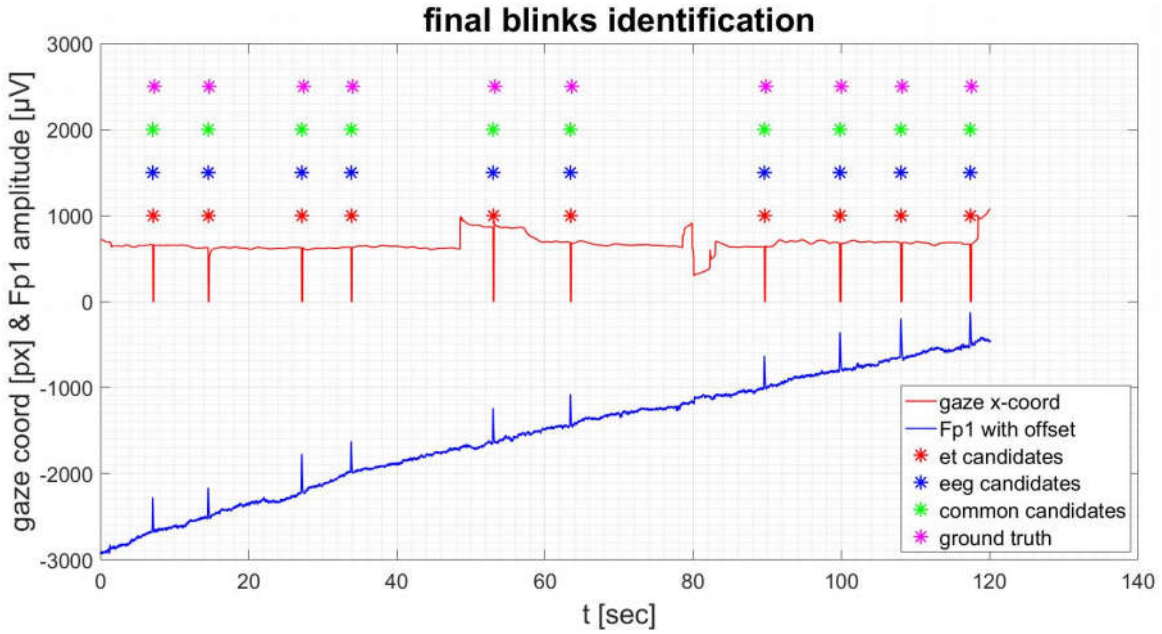

Figure 4.13: Final blink identification during the Rest in test 3. On the graph are reported Fp1 (with an offset) and gaze x-coord vs time. The red, blue, green and magenta asterisks are in correspondence of respectively the ET candidates, the EEG candidates, the common candidates and the ground truth.

The low movement of the head in this task (Rest) allows to have signals clear from other artifacts enhancing the performance of the algorithm.

For what concern the Pegs Transfer task, 2 blinks have been identified from the video. The Eye Tracker detected as true some false blink but the algorithm has been able to select only the true ones through the final comparison with the EEG candidates (Figure 4.14).

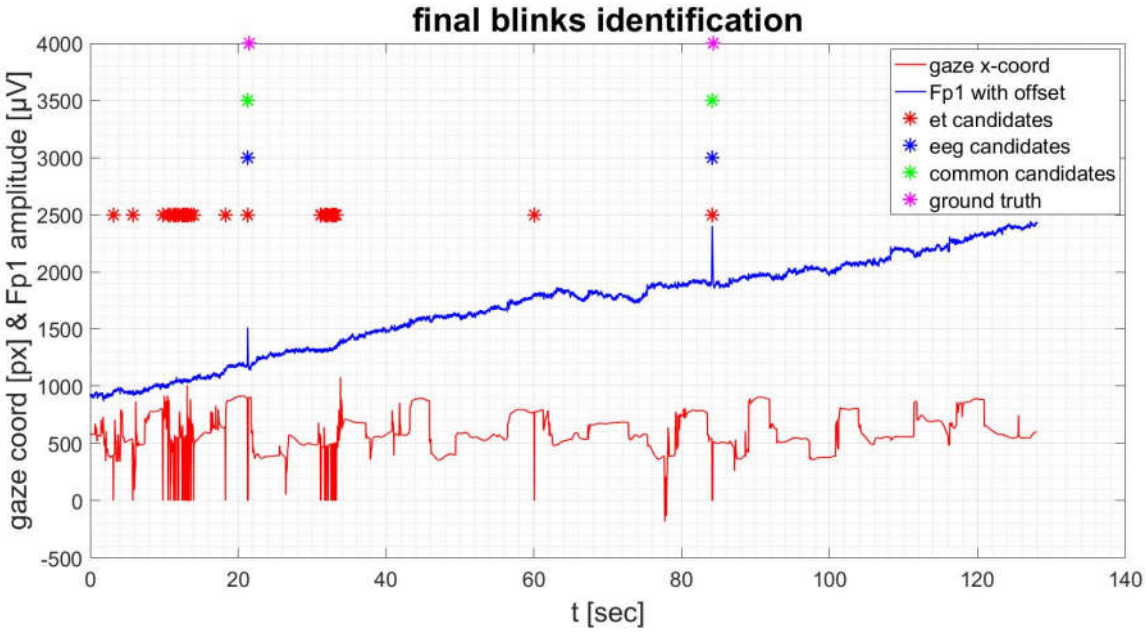

Figure 4.14: Final blink identification during the Peg Transfer in test 3. On the graph are reported Fp1 (with an offset) and gaze x-coord vs time. The red, blue, green and magenta asterisks are in correspondence of respectively the ET candidates, the EEG candidates, the common candidates and the ground truth.

In conclusion, in case of low movements of the head that don't corrupt the signals, the algorithm for the detection of the blinks has an accuracy of 100% providing a good estimation of the blink rate. Obviously, the more movements the subject makes, the more the signals from both the devices will be corrupted by artifacts decreasing the performance of the algorithm.

The usage of both ET and EEG allows to:

- Eliminate false positive from both the devices comparing the ET candidates with the ones from the EEG.
- Identify and eliminate EEG blink candidates which occur while the subject is not looking at the screen. They can be recognized because they occur during long intervals of eyes not captured identified by the ET. However, if for whatever reason also the blinks that happen in this condition are considered useful, they can be determined relying only on EEG signals.

The face camera has been kept for all the acquisition made in this study to conserve the ground truth. Moreover, it has been found useful to display the detected blinks on a final graph with signals from both the devices. From the observation of that graph, it is clear if

some parameters of the algorithm for the peaks detection have to be modified for a better estimation.

All the information extracted by the algorithm (i.e. blink rate, time occurrence of the blinking, periods in which the subject is not looking at the screen) have been saved in order to be used in the construction of the report with all the other signals.

4.4 Performance evaluation with the new FLS scoring metric

The new scoring metric described in Section 3.1 has been used to evaluate the performances of each subject by looking at the laparoscopic video of each task. This analysis has been conducted by the author of this work which is not a surgeon. However, the metric has been developed in collaboration with surgical Residents ensuring the usage of meaningful and objective criteria regarding the occurrence of events that can be easily identified on the video. Particular errors like the cut deviation from the circle have been assessed directly on the produced output (e.g. the gauze in the Circle Cut). Examples of performance's output have been reported in Figure 4.15 for the 2nd and the 3rd tasks.

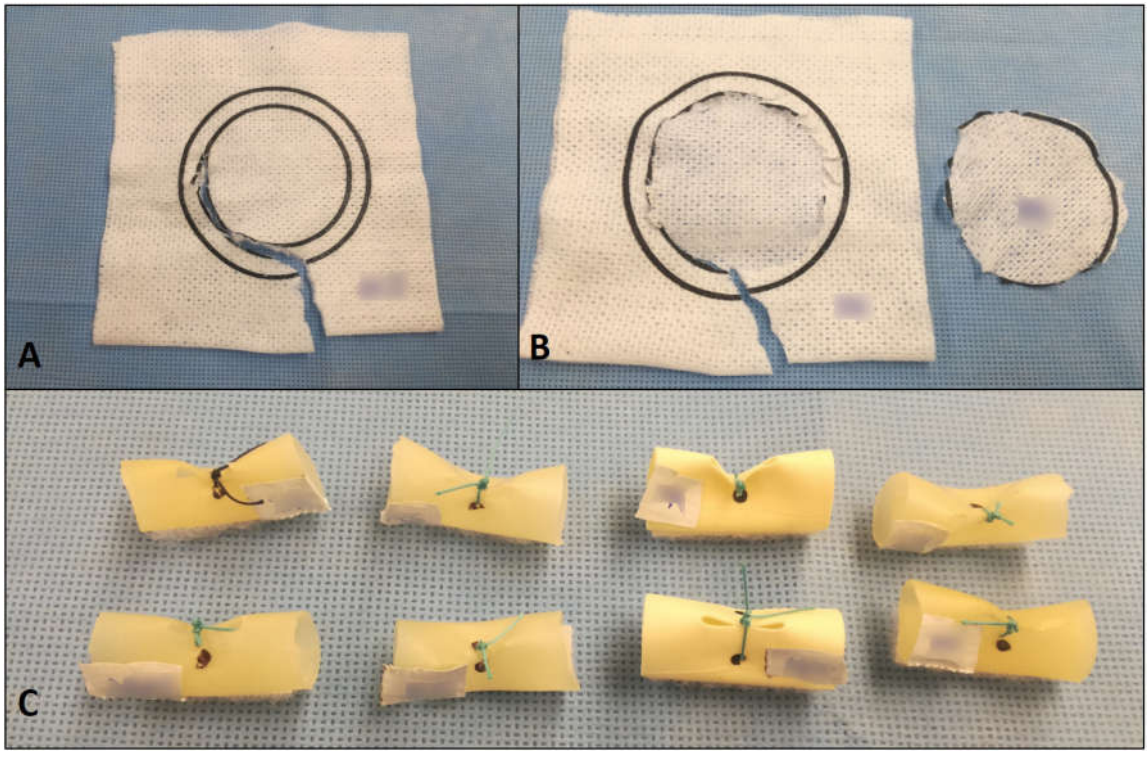

Figure 4.15: Some outputs from the Circle Cut and the Intracorporeal Knot tasks. (A) example of Beginner's result, (B) example of Expert's result, (C) all the penrose drains obtained from the Residents and the Experts.

The evaluation of the performance of all the 12 subject (4 Beginners (B), 5 Residents (R) and 3 Experts (E)) who participate to the study have been reported in Table 4.1. The scores of the singles tasks have been written in red while the last two line represent respectively the sum of the Peg Transfert's and Circle Cut's scores and the sum of all the three partial scores. No Beginners (B) have done the third exercise (Intracorporeal Knot). For this reason, a score equal to 0 has been assigned to them for that task and this will reflect on their final score (the sum of score of the three tasks) which make no sense to compare with the other categories' score.

INFO												
initials	Subj1	Subj2	Subj3	Subj4	Subj5	Subj6	Subj7	Subj8	Subj9	Subj10	Subj11	Subj12
category	B	B	B	B	R	R	R	R	R	E	E	E
PEGS (max score) = starting points	**700**	**700**	**700**	**700**	**700**	**700**	**700**	**700**	**700**	**700**	**700**	**700**
Completion time (sec)	154	156	300	232	95	112	206	228	82	115	118	92
# of not completed phases	0	0	1	1	0	0	0	0	0	0	0	0
# of small errors (object dropped but retrieved)	1	0	1	1	0	0	1	0	0	0	1	0
# of big errors (unretreivable object)	0	0	0	2	0	0	0	0	0	0	0	0
# of very big errors (no midair transfer)	0	1	0	0	0	0	0	0	0	0	0	0
pegs score	587	396	457	402	637	625	553	548	645	623	611	639
CIRCLE CUT (max score) = starting points	**700**	**700**	**700**	**700**	**700**	**700**	**700**	**700**	**700**	**700**	**700**	**700**
Completion time (sec)	300	300	300	300	244	192	300	300	240	291	81	297
# of not completed phases	2	3	4	3	0	0	0	2	0	0	0	0
# of small errors (the gauze comes out from the jumbo clip)	0	0	0	0	0	0	0	0	0	0	0	0
# of big errors (cut outside or inside the line by 2 mm)	0	1	0	0	3	4	3	0	2	1	4	2
circle cut score	300	150	100	200	387	372	350	300	440	456	446	402
INTRACORPOREAL KNOT (max score) = starting points	**700**	**700**	**700**	**700**	**700**	**700**	**700**	**700**	**700**	**700**	**700**	**700**
Completion time (sec)					449	179	562	315	323	151	152	151
# of not completed phases					0	0	0	0	0	0	0	0
# of small errors (more than one attempt in the needle insertion, detachment of the needle from the wire)					1	1	1	0	1	1	0	0
# of big errors (the knot comes apart, no hand exchange during subsequent throws)					0	0	0	0	1	0	0	0
# of very big errors (separation of the penrose drain from the velcro stripe, no double throw)					0	1	0	0	0	0	0	0
intracorporeal knot score	0	0	0	0	540	430	503	595	532	640	649	650
PEGS + CIRCLE SCORE (max score = 50pt)	**887**	**546**	**557**	**602**	**1024**	**997**	**903**	**848**	**1085**	**1079**	**1057**	**1041**
TOTAL SCORE (max score = 75 pt)	**887**	**546**	**557**	**602**	**1564**	**1428**	**1405**	**1443**	**1618**	**1719**	**1707**	**1690**

Table 4.1: Evaluation of the performance of 12 participants (4 B, 5 R, 3 E) with the new FLS scoring metric based on the analysis of the video of the performance. The score associated at each task is written in red. The last two lines represent respectively the sum of the score of the first two exercise and the sum of all of them. These scores are the same for beginners who didn't perform the third task.

Figure 4.16 gives a graphic representation of the scores in the two last line of the table maintaining the same colors in the table above. The 'light orange' bars represent the sum of the scores of task 1 and 2. Apart from Subj1, it is clear the difference among a Beginner performance and a subject from the surgical field. The differences are less evident between Residents and Experts which result to have a 'light orange' score similar to some Resident. However, looking at the 'dark orange' bars which represent the sum of all the scores, it results that the Experts have been assigned of the better scores. The 'dark orange' bars are not meaningful for Beginner cause they didn't do the third task (to which it has been assigned a score equal to zero).

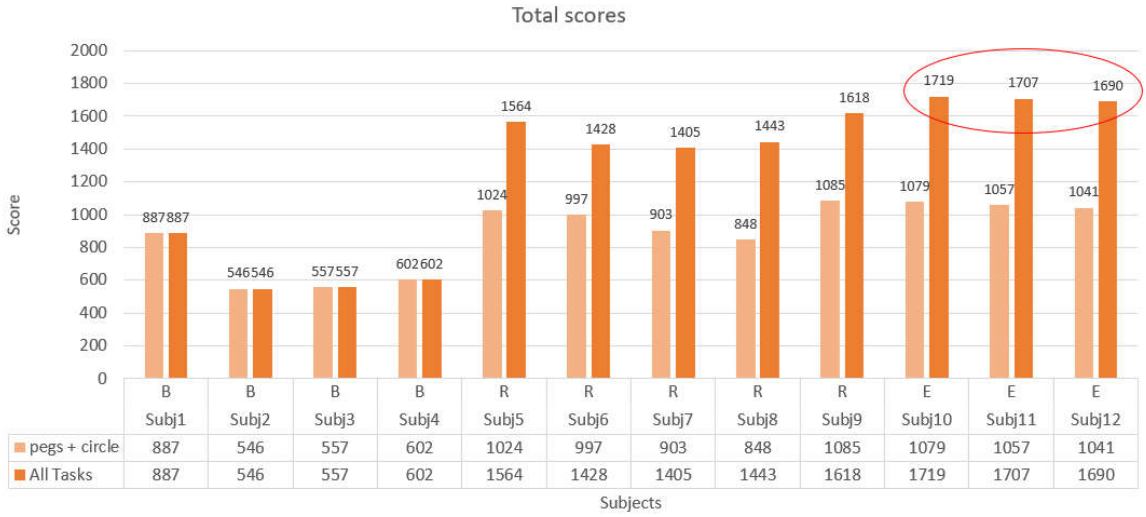

Figure 4.16: Representation of the two complex scores of the 12 participants. The 'light orange' one is the sum of the scores of Peg Transfer and Circle Cut while the 'dark orange' is the sum of all the three tasks. Each Beginner (B) shows equal scores because he/she has not done the 3rd task resulting in a contribute of 0 pts for that task. In the red circle have been highlighted the total scores of the Experts (E) which result to be the highest ones.

Figure 4.17 shows all the scores separated by exercise for a better understanding of the contribute of each of them in the final score. The same color notation of Table 4.1 has been maintained. Beginners show a drastic decrease in the performance of the second task. In particular, this explain the similarity of the 'light orange' score of Subj1 (B) with some Residents: this beginner has been able to complete the Peg task in a very good time and without mistakes ending to compensate the not so good score in the second task.

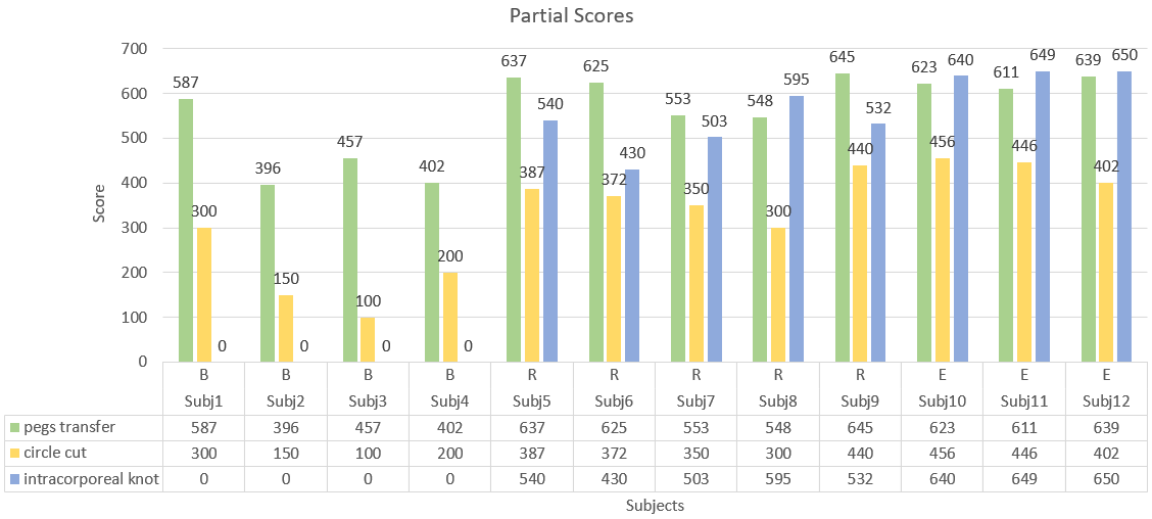

Figure 4.17: Representation of the scores of each task for the 12 participants

The main differences among Residents and Experts regard the third task, where the E have in general an higher score. The reasons of this difference have been searched in Table 4.1. Observing the notes about the Intracorporeal Knot, it is clear that the Expert have a much lower completion time with respect to Residents. Probably it is linked to the fact that they are more used to do similar tasks (knots) in the daily operations.

On the other hand, any relevant difference has been observed for the Circle Cut. In fact, two out of three Experts required the all time to complete the task while the one (Subj11) who did it faster, made more errors. Collecting impressions from the participants, it has emerged that the surgeons didn't feel very comfortable during the 2nd exercise because they said that in real operations they are used to have the camera closer to the area where they have to cut enhancing their precision. Probably this is the reason why, an exercise that in theory should be simpler that the third one, it turned out to be hardest one for Experts decreasing the differences with Residents score.

A more in depth analysis of the Intracorporeal Knot's phases has been conducted to assess difference in time completion of the two subsequent single throws changing hands. It has emerged that all Experts have been able to complete them very quickly and with no significant time differences (i.e. not depending on the hand) while this behaviour has been observed only on one Resident (Subj6) out of five. All the others present significantly different completion times for the single throw depending on the hand in use (e.g. 76 sec holding the needle with the left and 101 sec with the right for Subj8).

Overall, the new metric has remarked differences in the performances itself among participants of different categories. This difference is accentuated in the Circle Cut among B and the other two categories and in the Intracorporeal Knot among R and E. From subjects' impressions, it has been noted that the hardest exercise for R has been the third while for E, it has been the second. Finally, Experts have shown a better dexterity and ability in the use of both hand during same throws with different hands.

4.5 Preliminary analysis results

In this section have been reported the main observations from the participants' report. Refer to Table 3.4 and 3.5 for the legend of the symbols reported in the following figures. The tasks have been called with their name or with the following numeration:

- Task 0 = Rest

- Task 1 = Peg Transfer
- Task 2 = Circle Cut
- Task 3 = Intracorporeal Knot

Moreover, in the graphs subject of different expertise level have been named as follow:

- B = Beginner
- R = Resident
- E = Expert

It has been found that the ET can be source of useful information highlighting the capacity of some subjects in focusing into the exercise limiting the gaze dispersion. However this information must be related to the evaluation of the performance because it is not always true that a fast exercise with low gaze dispersion is linked to a good output. Correct ET data have been retrieved from 11 participants out of 12 because one of them wore glasses which don't allow the device to work properly.

The first task is suitable to observe the reaction to errors (e.g. drop of an object) from the gaze point of view. Figure 4.18 represents some examples of the Peg Transfer's gaze(x,y) plotted over time. This exercise consist basically in the transportation of objects from one side to the other and viceversa mainly in horizontal direction. For this reason, the gaze x-coordinate over time assumes a shape that is closed to a square wave. The high of the squares varies depending on how close are the pick-up and drop-off positions for each object but in general, the better is the performance, the more the curve is smooth and similar to a square wave (e.g. initial part of the last graph in Figure 4.18 , Subj12).

The red circles identify regions with the occurrence of small errors (indicated with blue triangles) which correspond to the drop of an object that the subject has been subsequently able to retrieve. The first two subjects in the figure (Beginners) show fast spikes on both x and y traces which induce to think to a loss of focus/concentration. On the other hand, a Resident (third row, Subj7) who experienced the same kind of error show a different reaction where the curves maintain their smoothness which can be linked to the maintenance of the focus and concentration.

The two blue circles represent two similar situation characterized by a noisy pattern. Both have been verified by looking at the laparoscopic and face videos of the performance. The first (Subj 3, B) has been caused by a loss of concentration at half exercise when the subject forgot to repeat the exercise moving all the objects to the original side of the pegboard until

the operator told him/her. The second (Subj 7, R) has been caused by an initial difficulty in transferring the object from one tool to the other. All these observations lead to the same concept: confident performances are characterized by smooth gaze signals while a noisy pattern is linked to difficult situations or loss of focus.

Finally, the green circle (Subj 12, E) identifies a change in the pattern of the gaze x-coord among the first and the second half of the exercise. This change remain constant for most part of the second half and it is due to a change in the technique. From the usual grasp, transfer and place an object before moving to the next one, the technique changes in: grasp an object, transfer it to the other tool, insert the other tool in the ring of another object, place the other one, pick-up the new one and on. This leads to an increase of speed besides a change in the pattern of the signal.

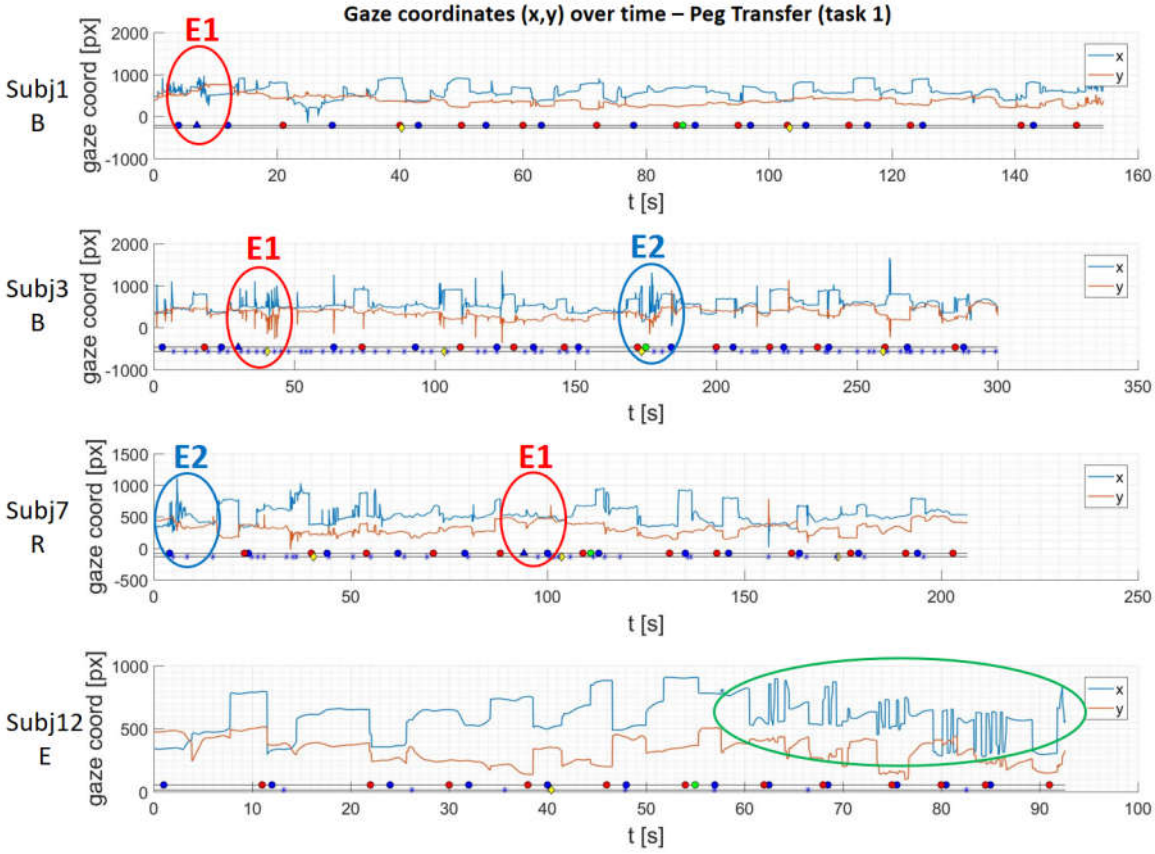

Figure 4.18: Examples of gaze coordinates (x,y) over time during the Peg Transfer of four different subjects. The red circle E1 identify the regions which contain errors (blue triangles). The spikes in the signals which characterized the reaction of Beginners (B) could be linked to a loos of concentration/focus. On the other hand Subj7 (R) maintains the focus during the error. The blue circles E2 represent respectively a loos of concentration for Subj3 and a difficulty during the transfer of an object for Subj7. Then, the green circle regards a change in the procedure technique for the entire 2nd half of the task.

On the other hand, the Circle Cut task is not suitable to see how the participant reacts to errors (e.g. cut deviations from the demarcated circle line) because they are assessed carefully at the end of the exercise by a direct examination of the gauze. Anyway, a smoother signal is always related to a confident performance. The same can be observed for the Intracorporeal Knot of which some examples have been reported in Figure 4.19. Looking at the three subjects in the image, it is clear as the first (Subj5, R) is the one characterized by a less smooth signal.

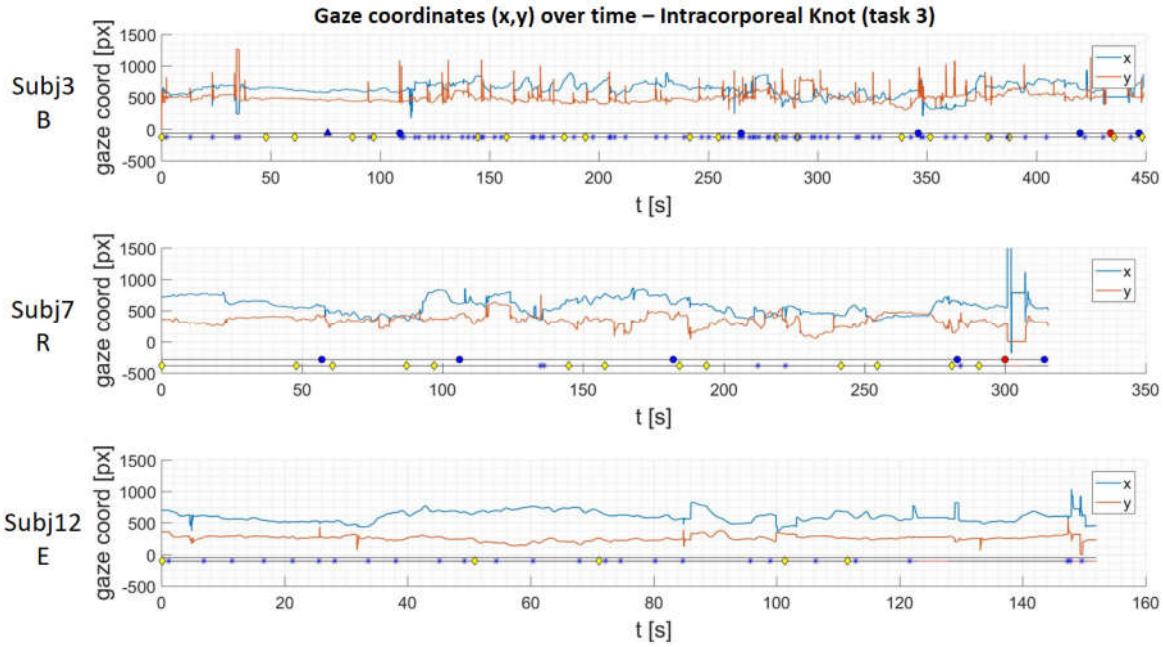

Figure 4.19: Examples of gaze coordinates (x,y) over time during the Intracorporeal Knot. In this task, a smoother signal is correlated to a better performance. In fact, both Subj8 (R) and Subj11(E) have received an high score in the task.

From a comparison with the scores of task 3 in Table 4.1 it has emerged that smoother signals are associated to a less number of error and higher scores. So, this could be linked to how confident is a subject with the task. The same cannot be said for task 2 which is an exercise aimed at testing precision. In fact, a faster and smoother exercise can be link either to a good performance or to a very fast performance without accuracy (e.g. not cut precisely along the line).

Another kind of representation on the same kind of information is based on the distribution of the gaze in the bi-dimensional space. Figure 4.20 reports some examples of the (x,y) points of gaze inside the screen during the Circle Cut. The exercise can be reconstruct over time referring to the color scale starting from blue and ending with dark red. Figure 4.20A

shows the difference among the three categories of participants where for the Beginner the difficulties are clear instead of the Resident and the Expert from which the final pattern represent a clear circle. Then, Figure 4.20B compares a Beginner and a Resident who have been able to cut only half a circle. The former (B) shows an higher gaze dispersion with respect the second (R).

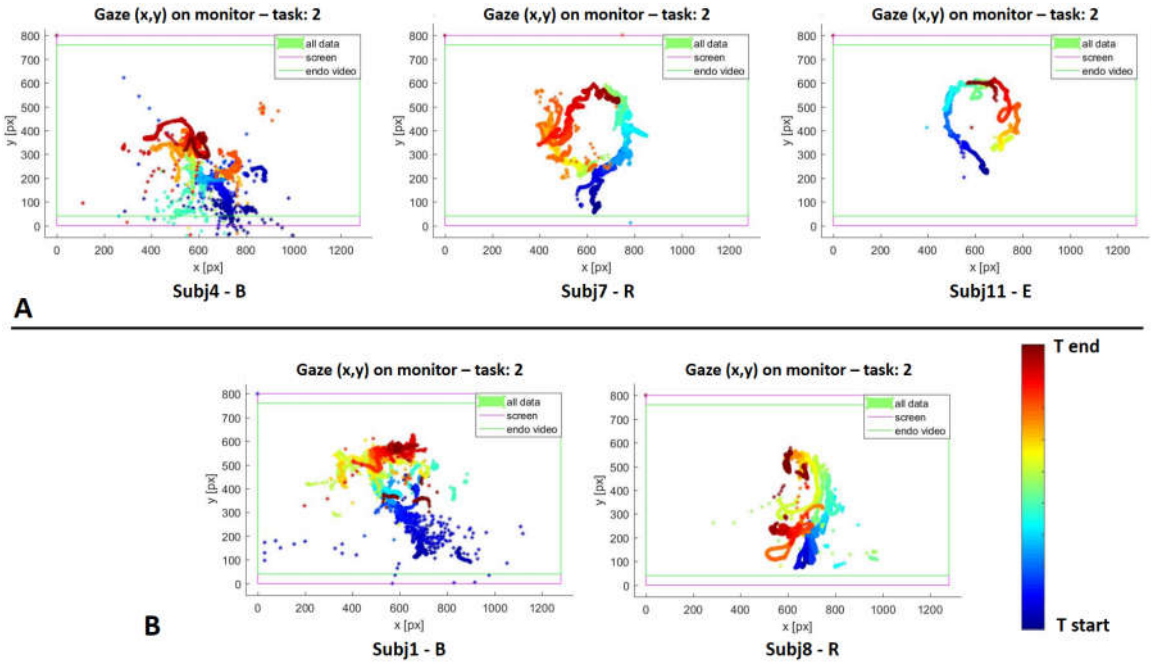

Figure 4.20: Examples of bidimensional representation of the gaze on the screen during the Circle Cut. The color scale has been used as timeline starting from blue. (A) comparison among Beginner, Resident and Expert: the focus of the last two allows to recognize a circle pattern on the graphs. (B) comparison among a Beginner and a Resident who have completed only 2/4 of circle: the R shows less dispersion of the gaze.

The gaze dispersion used to discriminate among Beginners and Resident in the Circle Cut, can be used to discriminate among Residents and Experts in the Intracorporeal Knot as it as can be seen in Figure 4.21. In fact, the graph of the Expert is way more focused on a specific area of the screen.

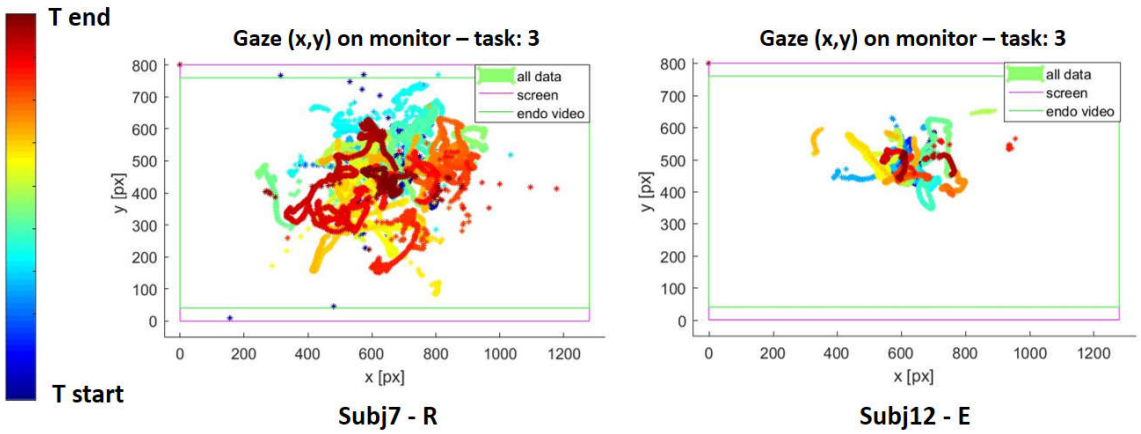

Figure 4.21: Examples of bidimensional representation of the gaze on the screen during the Intracorporeal Knot. The color scale has been used as timeline starting from blue. The Resident (left) shows a bigger dispersion with respect to the Expert (E) who has been very focus in a specific area.

These observations find confirmation in the analysis of the translations ([px]) among subsequent gaze positions. Figure 4.22 represents some examples of probability histograms of the module of gaze translations in px for task 2 and 3. Due to the long acquisitions and the kind of tasks the slow movements have the highest probability. Anyway, the focus in the image is toward the large movements area which can show differences among subjects in terms of economy of eye movement.

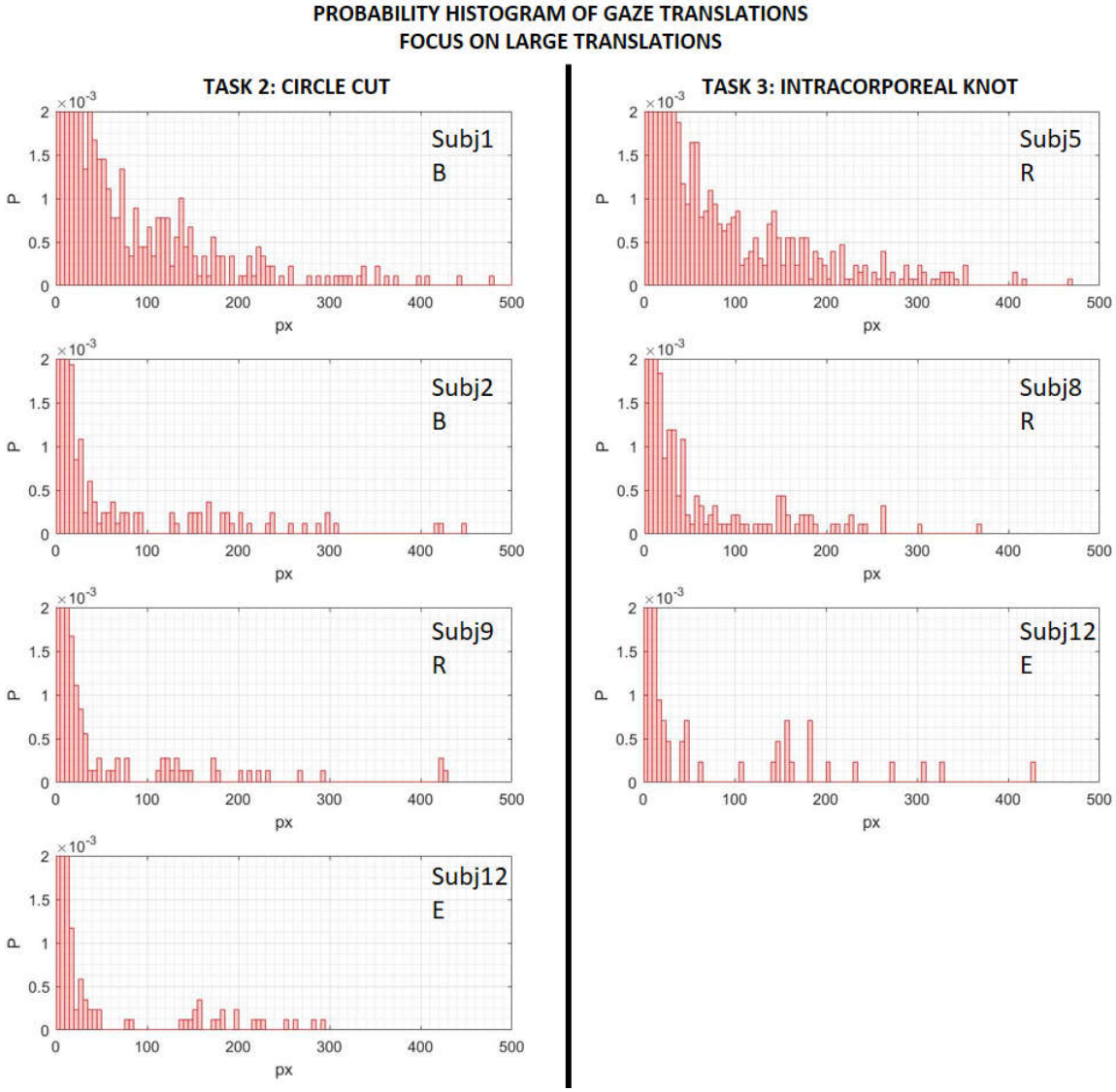

Figure 4.22: Examples of probability histograms of gaze translations of the Circle Cut (left) and Intracorporeal Knot (right). The graphs on the left show that a Beginner (B) presents an higher probability to compute big displacement with the gaze with respect to a Resident (R) or Expert (E). However, Subj2(B) presents pattern similar to a Resident mainly because the subject completed only ¼ of circle. The ones on the right show a distinction among Resident and Expert where the former generally present an higher probability to compute big displacement. Subj8 (R) has a graph similar to the one of the Expert and this could be linked to the good performance that he/she made.

The graphs in the first column (task 2) show an higher probability to compute large gaze displacement in Beginners with respect to Residents and Experts while the ones in the right column (task 3) show an higher probability in Residents with respect to Experts.

The graphs present also outliers like:

- Subj2 in the left column: the B has an histogram similar to the one of a R or E. Even if the participant has been very focused, it must be taken into account that he/she has been able to complete only ¼ of circle cut.
- Subj8 in the right column: the subject has an histogram similar to the one of an E. Looking at his/her score for the third task, it can be seen that he/she has the highest score among the R and it is closed to the one of an Expert. Therefore, in this case the similarity is due to a good performance.

The same deduction are reflected in the Mean and Std of the module of the translations of the gaze which have been reported in Table 4.2. The previous outliers have been highlighted with a red contour.

'Name'	Category	Task 2: Circle Cut		Task 3: Intracorporeal Knot	
		mean [px]	std [px]	mean [px]	std [px]
Subj1	B	5,5	29,6	NaN	NaN
Subj2	B	2,1	15,1	NaN	NaN
Subj3	B	3,8	24,7	NaN	NaN
Subj4	B	4,0	21,8	NaN	NaN
Subj5	R	3,0	16,6	5,6	24,8
Subj6	R	1,9	12,9	5,1	25,9
Subj7	R	1,8	10,5	3,9	19,9
Subj8	R	2,0	13,0	3,0	12,8
Subj9	R	2,2	12,9	5,4	25,3
Subj11	E	1,9	8,9	3,0	16,2
Subj12	E	1,8	10,1	2,4	14,1

Table 4.2: Table with an analysis of the signal of the gaze translations during the tasks. Mean and Std have been reported for the 2nd and the 3rd tasks. Both the parameters are generally higher for B wrt R and E in the Circle Cut. In the intracorporeal knot can be seen a difference among R and E where the former present the higher mean and std. In red have been highlighted two outliers respectively because of the completion of only ¼ of task (Subj2-B) and a very good performance (Subj8-R).

In general, the Mean variation [px] of the gaze and its STD [px] are lower for subject more focused. This means, R and E in the Circle Cut and E in the Intracorporeal Knot.

Another information obtained from the Eye Tracker are the pupils' dimensions. It has been observed a systematic increase of the pupils size from rest to exercise in all the participants. However, the dimensions are more or less constant during the exercise. This behaviour let think that it could be linked more to a condition of concentration than stress. Moreover, the

right pupil is always bigger than the left one for all the subjects but it seems to be related only to the position of the light source in the room.

For what concern the blinking retrieved from the multimodal analysis algorithm, it has been observed a systematic decrease of the blinking rate from rest to exercise as expected (i.e. due to the increase of focus/concentration). In particular, the average blinking rate among the 12 subjects is 20 blink/min with a Std of 13 blink/min during the rest phase. During the 3 tasks, the mean value decreases together with the Std respectively at 5 and 4 blink/min.

Moreover, it has been noticed an increase of the blinking during the more difficult phases of the exercise as it has happened for Subj5 in Figure 4.23. In that exercise there is a clear difference about the blink density (blue asterisks) between the first phase (first circle) and the three subsequent throw phases (2^{nd} , 3^{rd} and 4^{th} circles). In some subjects, an increase of the blinks has been also noticed toward the end or in the second half of an exercise. It is not clear if it could be due to fatigue or to a decrease in the concentration because the end is closer.

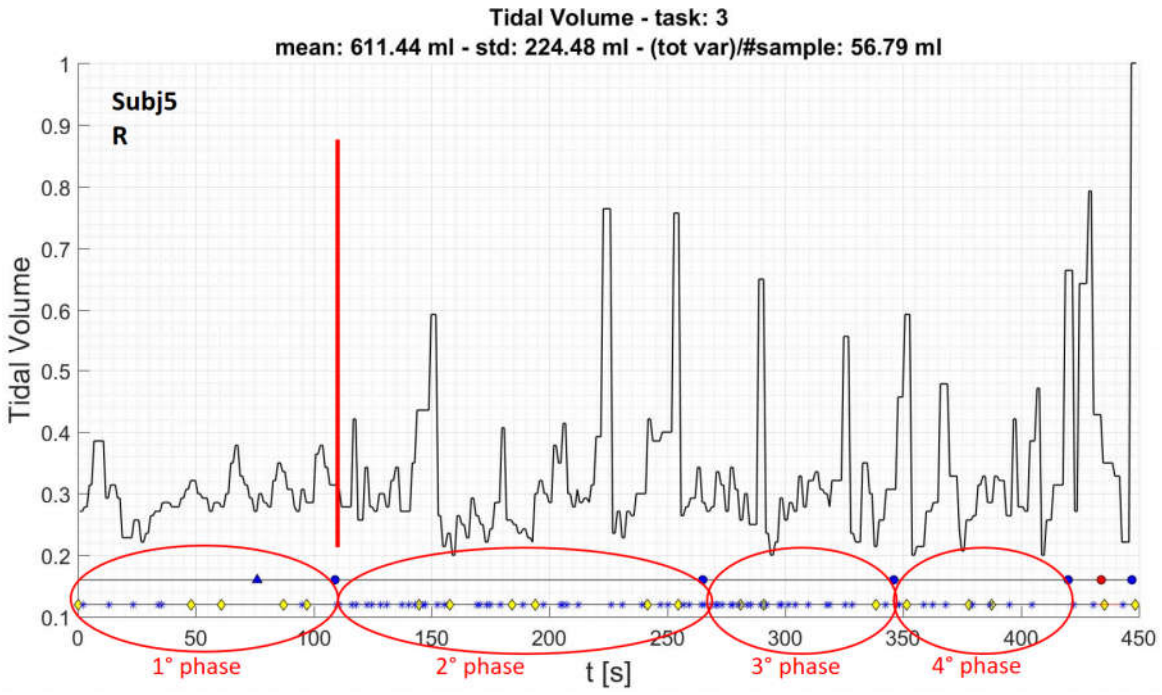

Figure 4.23: Tidal Volume of Subj5 (R) during the Intracorporeal Knot. The circles show an increase of the blink rate after the first phase (first circle = needle insertion). After this phase can be also observed an increase in the irregularity of the Tidal Volume which could be linked to discomfort.

Figure 4.23 represents also another change among the needle insertion (first phase) and the next phases which is the increase of the Tidal Volume variation. It has been found that the Tidal Volume tends to become more irregular during the more difficult exercise for the

subject. This means during the Circle Cut for Beginners and the Intracorporeal Knot for Residents.

During exercises which present a more regular Tidal Volume, it has been found that most of the subject tend to take deep inspiration during pauses. They can happen during the exchange of the instruments or among phases.

For what concern the information about the Heart Rate from the Hexoskin, at least one exercise for six participant presents a bad quality due to the amount of error in the signal detected by the device itself. From the observation of the remaining graphs no significant pattern has been found apart a general increase of the HR from rest to activity condition and a decrease of it in the second half of the Peg Transfer for two subjects. This could be linked to adaptation to the task or a more confidence derived from the use of the dominant hand.

Using the algorithm for the 2D motion reconstruction, it has been possible to obtain graphs as the ones represented in Figure 4.24. They are representations of the 2D motion of the tools in specific phases of the exercise. ‘A’ and ‘B’ regard the first half of the Peg Transfer while ‘C’ and ‘D’ represent the Circle Cut. The latter has been divided into segments to eliminate the time in which the tools have been exchanged. Anyway, all these graphs have not been able to provide any useful information as they are.

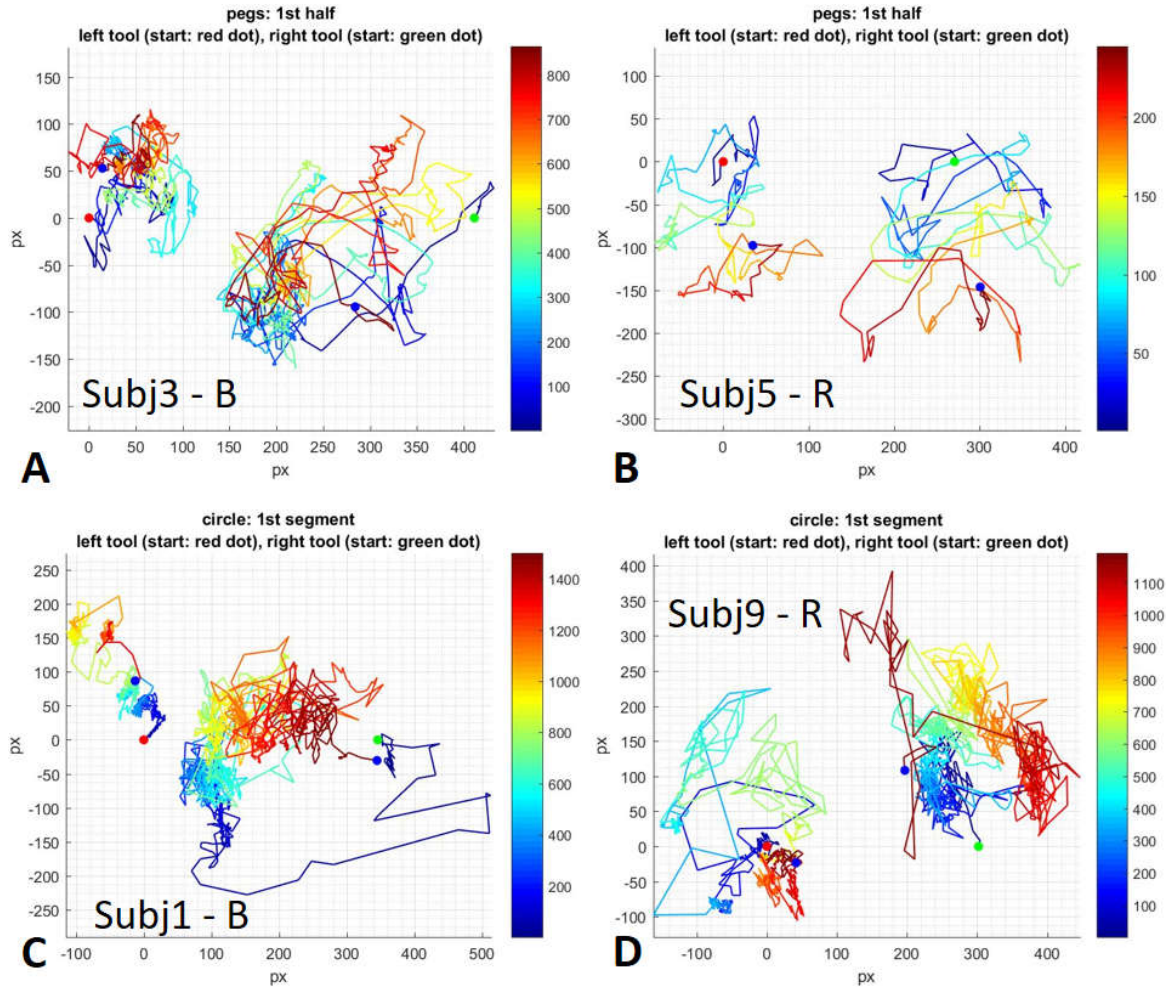

Figure 4.24: Examples of reconstruction of the 2D motion of the tools. (A) and (B) represent the first phase of the Peg Transfer of a Beginner and a Resident. (C) and (D) represent the Circle Cut of a B and a R: these are quite good representation because there was no tool exchange in these performances.

The presence of frames in which the algorithm has not been able to recognize the pattern on the ceiling or subsequent frames with no feature points in common could lead to an erroneous representation. But the exact reproduction of the motion was not the purpose of the algorithm. In fact, based on the acquire data, future studies about the smoothness curvature or other parameters can be conducted.

Finally, the introduction of the sound as Tunnel Effect had no effect on the participant. Everybody noticed it but they simply didn't care or asked about it at the end of the exercise. Probably a more invasive external event would be required to test the Attentional Tunnelling.

Chapter 5 Discussion and Conclusions

The present Chapter provides a discussion about the work. It has been divided in multiple sections, each of them treating a different topic that emerged during the study.
Section 5.1 deals with the functioning of the developed acquisition system and the level of acceptance by the medical community.
Section 5.2 treats the pro and cons of the blinking detection and motion reconstruction algorithm. Then, Section 5.3 discusses the observations made from the preliminary analysis of the data and Section 5.4 proposes ideas for future developments of the work.

5.1 Platform functioning and feedback from the medical community

The study aimed primarily to develop a multisensory platform with different sources of information to move toward a new way of conducting training in the laparoscopic field. This approach has been based on the hypothesis that subjects with different level of expertise perform the tasks differently, not only in terms of number of errors and completion time but also in terms of concentration, physiological reactions, mental load and stress. The latter can be defined as the response by the body to a stimulus which interferes with the normal physiologic status. This physical, mental, or emotional tension of a subject decreases his/her feeling of being in control of the situation.
The decision to include a large gamma of instruments faces the impossibility of knowing a-priori which are the signals of interest. Moreover, the devices have been selected to allow a non-invasive signal acquisition to not create discomfort for the participant.
Among the instrumentation, the Hexoskin shirt has been found to not guarantee always good quality measures. The main limitation of such a device is related on how well the shirt fits on the subject. A bad adherence of the sensors to the skin or their wrong placement could affect badly the measurements. Moreover, if the sensors are casually touched by the subject during the performance, their signal will be disturbed.
A part from the quality of the Hexoskin data, the acquisition system developed in this work guarantees a robust data acquisition and it has received positive feedback from all the participant of the surgical field who tested the platform. They manifested their enthusiasm for the different kind of training, especially Residents who were curious to see which are the differences among them and the experts.

The Matlab GUI allows the management of the acquisitions and the display of a real-time video which not degrades over time. Moreover, the algorithm based on the UNIX time allows to record signals separately from different devices for a post-acquisition extraction and synchronization. The main limits regard the videos recording at a maximum of 5 Hz and the possibility to perturbate the exercise with external events. The second have been limited to the only sound occurrences due to the impossibility to manipulate the laparoscopic video with Matlab without introducing noticeable delays in the real-time video.

5.2 Eye blinking detection and tool 2D motion reconstruction

The developed algorithm for the blink detection has shown good performances and reliability in this study. The main advantage of this method over other blink detection methods is the usage of two devices at the same time. These multimodal analysis allows to overcome the limitations affecting the single devices given by the possibility to move the head in the space and the eyes out of the monitor during the exercises. The detection of the blinks on the EEG's Fp1 and Fp2 signals has confirm the possibility to detect them directly over the amplitude signals of the most influenced electrodes and based on the power analysis experience in different studies [29], [32]. However, the optimum parameters used by the algorithm in those analysis have been found to vary among subject. Displaying a graph of the signals, the operator can understand if an adjustment of those parameter is necessary to improve the blinking detection.

The performance of the algorithm has been found to decrease when the subjects moves the whole body for example during the exchange of the instruments which can bring him/her on the edge of the tracking volume of the ET and can induce lots of movement artifacts on the dry EEG.

The new algorithm for the 2D reconstruction of the movement of the tools has shown to enhance the method on which the Smart Trocars are based. One of its main advantages is the chance to eliminate the dependency from the color in the detection of the shapes on the ceiling which could be difficult or bias depending on the kind of ambient illumination. Moreover the identification of common shapes on subsequent frames ensures to compare always correspondent cloud of points in the ICP. The main drawback of the method is the dependency on the quality of the image. Blurred images linked to very fast movements of the tool badly affects the segmentation and the correct identification of the feature points

(i.e. corners and centroids) of the segmented shapes and the classification of their inside geometrical patterns. A method for the recognition of corrupted frames (e.g. due to blur) should be included to avoid the use of such frames in the reconstruction decreasing the errors in the estimation of the movement.

5.3 Preliminary analysis discussion

The introduction of the new scoring metric had the purpose to extend the evaluation to subjects which are not from the surgical field (i.e. Beginners) and to increase the set of evaluation criteria. It is based on the analysis of the video of the performance of the subject. Its usage for the evaluation of the performance of the 12 participants has highlighted different scores based on the expertise level as it has bene shown in Table 4.1. In particular, from the data reported in Figure 4.17 , the Circle Cut has been found to be the task that better highlights the differences among Beginners and the other categories while the Intracorporeal Knot differentiates between Residents and Experts. These differences have been confirmed by the preliminary analysis conducted mainly on the ET and the Hexoskin signals. The former has shown that an higher capacity to focus and a lower gaze dispersion are associated to better performance in exercises which don't require a diffuse movement of the eyes. For instance in the Intracorporeal Knot, Residents with a score similar to an Expert's one have been characterized by similar level of gaze dispersion. However, it is not completely true for exercises aimed to assess the precision as the Circle Cut where a fast and smooth gaze have not always been correlated to good results. This remarks the necessity to combine the analysis of these signals with an evaluation of the performance itself to not achieve misleading conclusions underlined in other studies. Moreover, the observation of the gaze position over time in the Peg Transfer has pointed out a difference in how subjects react to errors. Beginners show a loose of concentration/focus that has been confirmed by looking at the face video. On the other hand Residents maintain the focus on the task.

The observation of the of the heart rate and RR intervals have revealed the presence of errors in about 1/3 of the acquisitions despite the check of the quality at the beginning of each task. This could be linked to the not perfect adhesion of the sensors on the skin or to collision during the movement of the subject. For this reason, a change in the setup or new device will be required to improve the quality of the heat activity signals. On the other hand, the observation of the patterns of the respiratory activity signals such as the Tidal Volume has

shown an increase of the variability during the most difficult phases make it suitable for a future investigation.
Similarly for the blinking rate, that apart the drastic decrease from rest to exercise, shows local increases during discomfort phases. On the contrary, the pupil dimension has not been found to be a good indicator in this study. In fact, it is characterized by an increase of the size from rest to task but the signal is quite constant over time with no correlation with specific situation, phases or events.
Finally, the use of the sound to test the Attentional Tunnelling has not given any result; the subjects noticed it without any influence on the performance.

5.4 Future developments

In conclusion, this work has touched different topics from the development of a new acquisition system to the realizations of algorithms for the detection of the eye blinking and the reconstruction of the 2D motion of the tool and the conduction of a preliminary analysis on a subset of acquired data. In the previous sections of this chapter, pro and cons, limitations and observations about the different components of the study have been explained. Here, new ideas and possible developments will be proposed in the following points:

- Introduce a new device in the acquisition system for the monitoring of the heart activity. It should guarantee the adherence of the sensors to the skin and be less subject to the motion of the participant which were the main problems affecting the Hexoskin smart cloth. Moreover, it should be easy to wear, non-limit the movement and allow a check of the quality prior usage. In this way, it will be possible to acquire reliable data about the heart activity such as the Heart Rate, the RR peaks and it will also decrease the time required for the preparation of the participant.
- Finish the realization of the new GUI written in Python to increase the performances of the acquisition system and allow the implementation of different kind of Tunnel Effects. In particular, external perturbations like the sudden rotation of the laparoscopic video or the appearance of smoke in the video could represent good simulations of real events in the OR (e.g. during procedure which imply to burn the tissues) and it could be interesting to see how subject with different expertise level react to them.

- Improve the reconstruction algorithm of the 2D movement of the tool including an algorithm that recognizes blurred frames to eliminate them from the analysis decreasing the errors.
- Extend the number of the participants for all the three categories to conduct the analysis on a wider dataset.
- Conduct a more in depth analysis on both the interesting signal observed in this preliminary study and the other signals. Among the seconds in particular, the EEG, cleaned with the method proposed in this work, could be studied analysing the Alpha, Beta and Theta powers. Moreover, studies of smoothness and curvature can be applied to the reconstructed movement of the tool.

The wish of the author is that this native study will be followed by a more in depth analysis of the signals aimed at finding parameters which can be include in the evaluation of the FLS performance, extending the idea of surgical training to the monitoring of the mental, physical and emotional status of the trainee.

More in general, the hope is that this study may be an inspiration for the introduction of this wider idea of training also in other fields of the research world.

Appendix A Matrix of the synchronized data

The data mat produced is a 5x7 cell matrix (Fig A.1) in which the first row is occupied by the column headers. Data are subdivided by task (rows) and by device (columns).

all_data

5x7 cell

	1	2	3	4	5	6	7
1	'info'	'exercise'	'synch'	'smart t...	'eye tra...	'hexosk...	'eeg'
2	2x13 cell	0	3x5 cell	[]	2x14 cell	2x23 cell	2x29 cell
3	2x13 cell	1	4x6 cell	2x11 cell	2x14 cell	2x23 cell	2x29 cell
4	2x13 cell	2	6x6 cell	2x11 cell	2x14 cell	2x23 cell	2x29 cell
5	2x13 cell	3	16x6 cell	2x11 cell	2x14 cell	2x23 cell	2x29 cell

Fig A.1: Example of output cell matrix from the data pre-processing (extraction and synchronization) phase. Data are subdivided by task and by device.

“Info” column

Each row contains info of the participant from the excel file:

1. Name: initials of the participant
2. Rec date: recording date
3. Category: Beginner (B), Resident (R) or Expert (E)
4. R or L handed
5. Age
6. Sex
7. Years of practice
8. Weight [pound]
9. Height [ft in]
10. Rest dev info: list of the devices used in the acquisition
11. Pegs dev info: list of the devices used in the acquisition
12. Circle dev info: list of the devices used in the acquisition
13. Knot dev info: list of the devices used in the acquisition

“exercise” column

Each row contains the identifier of the exercise:

- 0 = Rest
- 1 = Peg Transfer
- 2 = Circle cut
- 3 = Intracorporeal knot

“synch” column

Each row contains the synch time (trigger information). It is a nx5 or nx6 mat (Fig A.2) structured as follows:

all_data(3, 3)

1	2	3	4	5	6
[]	[]	[]	[]	[]	[]
[]	0	2.2726e-04	[2017,9,1,15...	1.5043e+12	[]
[]	1	40.2915	[2017,9,1,15...	1.5043e+12	'beep1'
[]	1	103.4132	[2017,9,1,15...	1.5043e+12	'beep2'
[]	100	154.4101	[2017,9,1,15...	1.5043e+12	[]

Fig A.2: example of data cell in the "synch" column of the pre-treated data matrix in Fig A.1.

- The second column can be:
  - 0: beginning of the recording
  - 1: on recording. It corresponds to a tunnel effect event.
  - 100: end of the recording
- The third is "toc"
- The forth is the "clock" (current data&hour)
- The fifth is the time in ms extracted using java.lang.System.currentTimeMillis: Returns the current system time in milliseconds since January 1, 1970 00:00:00 UTC
- The sixth (not always present) contains strings to describe the specific tunnel effect

"smart traj" column

Each row contains a 2x11 cell (Fig A.3) with respectively:

1. Left trocar trajectory time: cell of a time vector
2. Right trocar trajectory time: cell of a time vector
3. Left trocar translational vector: cell of (x,y) components
4. Right trocar translational vector: cell of (x,y) components
5. Left trocar rotational matrix vector
6. Right trocar rotational matrix vector
7. % of Left trajectory: it is the percentage of the image vector that has been converted into traj
8. % of Right trajectory: it is the percentage of the image vector that has been converted into traj
9. L feature selection quality: vector which shows how far from the center where the features used to compute the rototranslational matrix among subsequent frames. From left to right, the distance from the center of the image increases. The last element indicates the subsequent frames in which some features have been recognized but were not the same (impossible to compute the traj).
10. R feature selection quality: same
11. All t: the track with the time associated to all the frames.

all_data(3, 4)

1	2	3	4	5	6	7	8	9	10	11
'L time'	'R time'	'L transl'	'R transl'	'L rot'	'R rot'	'% L transl'	'% R transl'	'l feature sel...	'r feature se...	'all t'
1x747 cell	*1x773 cell*	*2x747 double*	*2x773 double*	*2x2x747 dou...*	*2x2x773 dou...*	96.6365	100	*1x18 double*	*1x18 double*	*1x773 cell*

Fig A.3: example of data cell in the "smart traj" column of the pre-treated data matrix in Fig A.1.

“eye tracker” column

Each row contains a 2x14 cell (Fig A.4) with 14 cells containing the features extracted from eye.txt for each exercise. These are respectively:

1. Avg x: smoothed gaze x-coordinate in pix
2. Avg y: smoothed gaze y-coordinate in pix
3. Left x: smoothed x-coord of the left eye
4. Left y: smoothed y-coord of the left eye
5. Pupil center left x: pupil x-coordinate normalized of the left eye
6. Pupil center left y: pupil y-coordinate normalized of the left eye
7. Pupil size left: pupil size of the left eye
8. Right x: smoothed x-coord of the right eye
9. Right y: smoothed y-coord of the right eye
10. Pupil center right x: pupil x-coordinate normalized of the right eye
11. Pupil center right y: pupil y-coordinate normalized of the right eye
12. Pupil size right: pupil size of the right eye
13. Time and date of the acquisition of the sample
14. Posixtime: time occurrence of each sample that has the same time reference of all the data from the other devices. It is the time that is used to synchro these data with all the others.

all_data{3, 5}

1	2	3	4	5	6	7	8	9	10	11	12	13	14
'avg x'	'avg y'	'left x'	'left y'	'p center l x'	'p center l y'	'p size left'	'right x'	'right y'	'p center r x'	'p cent...	'p size ...	'tim...	'posixtime [ms]'
4636x1 ...	4636x1 ...	4636x1 ...	4636x1 ...	4636x1 dou...	4636x1 dou...	4636x1 dou...	4636x1 ...	4636x1 ...	4636x1 dou...	4636x1 ...	4636x1...	463...	4636x1 double

Fig A.4: example of data cell in the “eye tracker” column of the pre-treated data matrix in Fig A.1.

“hexoskin” column

Each row contains a 2x23 cell (Fig A.5). The columns represents respectively:

1. Time 1Hz [ms]: in posixtime
2. HR [bpm]: corrected based on quality. Correction: if an errors occurs, the HR value of the correspondent sample is set equal of at the previous detected value.
3. HR quality [na]
4. BR [rpm]: corrected based on quality. Correction: if an errors occurs, the BR value of the correspondent sample is set equal of at the previous detected value.
5. BR quality [na]
6. Minute Ventilation [ml/min]
7. Tidal Volume [ml]
8. Time NN [ms] : in posixtime
9. NN intervals [s]
10. Time 256Hz [ms] : in posixtime
11. ECG lead I [mV]
12. Time 128Hz [ms] : in posixtime
13. Abdominal respiration [na]
14. Thoracic respiration [na]

15. Time RR [ms] : in posixtime
16. RR intervals [s]
17. RR quality [na]
18. blank. *The following columns are data obtained from an analyses of the previous data*
19. HR errors detected: count of the error in the quality vector of the specific exercise
20. HR errors detected %: percentage of the previous value
21. BR errors detected: count of the error in the quality vector of the specific exercise
22. BR errors detected %: percentage of the previous value
23. Nn over rr %: ratio among the length of NN interval and RR interval vectors. It gives an idea of the quality of the QRS detection.

	1	2	3	4	5	6	7	8	9	10	11
1	'time 1HZ [ms]'	'HR [bpm]'	'HR quality [na]'	'BR [rpm]'	'BR quality...	'Min Ventilation [ml/min]'	'Tidal Volume raw [ml]'	'time NN [ms]'	'NN interval [s]'	'time 256Hz [ms]'	'ECG lead I [mV]'
2	*120x1 double*	*120x1 do...*	*120x1 double*	*120x1 d...*	*120x1 dou...*	*120x1 double*	*120x1 double*	*165x1 double*	*165x1 double*	*30743x1 double*	*30743x1 double*

	12	13	14	15	16	17	18	19	20	21	22	23
1	'time 128Hz [ms]'	'abdominal resp...	'thoracic resp...	'time RR [ms]'	'RR interval [s]'	'RR quality'	[]	'HR errors...	'HR errors detected %'	'BR errors ...	'BR errors detected ...	'nn over rr %'
2	*15371x1 double*	*15371x1 double*	*15371x1 dou...*	*170x1 double*	*170x1 double*	*170x1 dou...*	[]	1	0.8333	0	0	97.0588

Fig A.5: example of data cell in the "hexoskin" column of the pre-treated data matrix in Fig A.1.

"eeg" column

Each row contains a 2x29 cell (Fig A.6). The columns represents respectively:

- From the 1st to the 20th: the 20 channel signals
- From the 21st to 23rd: accelerations signals
- 24th: peak counter
- 25th: trigger events
- 26th: time vector in the complete and original eeg track [ms]
- 27th: posixtime (used for synchronization of each signals with all the data from the other devices)
- 28th: principal info (2x4 cell)
    - Sample rate
    - N of channels
    - Exercise starting index in the original and complete track
    - Exercise ending index in the original and complete track
- 29th: eeg data in the struct format which is readable by the EEGLAB toolbox

all_data{5, 7}

	1	2	3	4	5	6	7	8	9	10	11	12	13	14	15	16	17	18	19	20	21	22	23	24	25	26	27	28	29
1	'F7'	'Fp1'	'Fp2'	'F8'	'F3'	'Fz'	'F4'	'C3'	'Cz'	'P8'	'P7'	'Pz'	'P4'	'T3'	'P3'	'O1'	'O2'	'C4'	'T4'	'A2'	'ACC0'	'ACC1'	'ACC2'	'Pack...	'TRIGGER'	'time...	'posixtime [ms]'	'principal info'	'eeg ex struct'
2	*1x...*	*1x1...*	*1x1...*	*1x...*	*1x...*	*1x...*	*1x...*	*1x...*	*1x...*	*1x...*	*1x...*	*1x...*	*1x...*	*1x...*	*1x...*	*1x...*	*1x...*	*1x...*	*1x...*	*1x...*	*1x16...*	*1x16...*	*1x16...*	*1x16...*	*1x1616...*	*1x16...*	*1x161618 dou...*	*2x4 cell*	*1x1 struct*

Fig A.6: example of data cell in the "eeg" column of the pre-treated data matrix in Fig A.1.

BIBLIOGRAPHY

[1] Eurostat, "Surgical operations and procedures statistics," 2017. [Online]. Available: http://ec.europa.eu/eurostat/statistics-explained/index.php/Surgical_operations_and_procedures_statistics#Increasing_and_decreasing_surgical_operations_and_procedures.

[2] iDataResearch, "3.5 Million Laparoscopic Procedures Performed in the US Across 12 Procedure Types According to iData Procedure Tracker," 2017. [Online]. Available: https://idataresearch.com/3-5-million-laparoscopic-procedures-performed-us-across-12-procedure-types-according-idata-procedure-tracker/.

[3] C. Robinet, "Operative Room awareness with the Smart Trocar: innovative laparoscopic surgery," no. August, 2015.

[4] J. Finkelstein, E. Eckersberger, H. Sadri, S. S. Taneja, H. Lepor, and B. Djavan, "Open Versus Laparoscopic Versus Robot-Assisted Laparoscopic Prostatectomy_The European and US experience," vol. 12, no. 1, 2010.

[5] N. Mortensen, "Does laparoscopic surgery spell the end of the open surgeon?," 2003.

[6] J. Seok, P. G. Choi, and K. Hoon, "S052 : a comparison of robot-assisted , laparoscopic , and open surgery in the treatment of rectal cancer," pp. 240–248, 2011.

[7] G. H. Ballantyne, "Robotic surgery , telerobotic surgery , telepresence , and telementoring Review of early clinical results," pp. 1389–1402, 2002.

[8] B. Morris, M. Hons, and P. C. Physician, "Robotic Surgery : Applications , Limitations , and Impact on Surgical Education," *MedGenMed*, vol. 7, no. 3, pp. 1–9, 2005.

[9] Providence Health Team, "Laparoscopic and robotic surgery: What's the difference?," 2015.

[10] S. A. Mir, J. A. Cadeddu, J. P. Sleeper, and Y. Lotan, "Cost Comparison of Robotic, Laparoscopic, and Open Partial Nephrectomy," vol. 25, no. 3, pp. 447–453, 2011.

[11] SAGES, "Fundamentals of Laparoscopic Surgery," pp. 3–5, 2008.

[12] L. M. Brunt, "Celebrating a decade of innovation in surgical education," 2014.

[13] G. M. Fried, "FLS Assessment of Competency Using Simulated Laparoscopic Tasks," *J. Gastrointest. Surg.*, no. May 2007, pp. 1–7, 2008.

[14] S. Arora, N. Sevdalis, D. Nestel, and M. Woloshynowych, "The impact of stress on surgical performance : A systematic review of the literature," *Surgery*, vol. 147, no.

3, p. 318–330.e6, 2010.

[15] MedicineNet.com, “Medical Definition of Stress,” 2016. [Online]. Available: https://www.medicinenet.com/script/main/art.asp?articlekey=20104.

[16] FLS program, “Bulletin of information,” pp. 1–6, 2012.

[17] FLS program, “FLS Manual Skills Written Instructions and Performance Guidelines,” no. February, 2014.

[18] E. M. Ritter and D. J. Scott, “Design of a Proficiency-Based Skills Training Curriculum for the Fundamentals of Laparoscopic Surgery,” pp. 107–112, 2007.

[19] G. Sroka *et al.*, “Fundamentals of Laparoscopic Surgery simulator training to proficiency improves laparoscopic performance in the operating room — a randomized controlled trial,” *AJS*, vol. 199, no. 1, pp. 115–120, 2010.

[20] L. Beyer *et al.*, “Impact of laparoscopy simulator training on the technical skills of future surgeons in the operating room : a prospective study,” *AJS*, vol. 202, no. 3, pp. 265–272, 2011.

[21] A. O. Castellvi, L. A. Hollett, A. Minhajuddin, and D. C. Hogg, “Maintaining proficiency after Fundamentals of Laparoscopic Surgery training : A 1-year analysis of skill retention for surgery residents,” *Surgery*, vol. 146, no. 2, pp. 387–393, 2009.

[22] P. G. Gauger *et al.*, “Laparoscopic simulation training with proficiency targets improves practice and performance of novice surgeons,” *AJS*, vol. 199, no. 1, pp. 72–80, 2010.

[23] H. Hur, D. Arden, L. E. Dodge, B. Zheng, and H. A. Ricciotti, “Fundamentals of Laparoscopic Surgery : A Surgical Skills Assessment Tool in Gynecology,” *JSLS*, pp. 21–26, 2011.

[24] L. S. Feldman, J. Cao, A. Andalib, and S. Fraser, “A method to characterize the learning curve for performance of a fundamental laparoscopic simulator task : Defining ‘“ learning plateau ”’ and ‘“ learning rate ,”’” *Surgery*, vol. 146, no. 2, pp. 381–386, 2009.

[25] N. Sharma and T. Gedeon, “Objective measures , sensors and computational techniques for stress recognition and classification : A survey,” *Comput. Methods Programs Biomed.*, vol. 108, no. 3, pp. 1287–1301, 2012.

[26] U. R. Acharya, Æ. K. P. Joseph, N. K. Æ. Choo, M. Lim, and Æ. J. S. Suri, “Heart rate variability : a review,” *Med Bio Eng Comput*, pp. 1031–1051, 2006.

[27] Task Force of The European Society of Cardiology and The North American Society of Pacing and Electrophysiology, “Heart rate variability Standards of measurement, physiological interpretation, and clinical use,” pp. 354–381, 1996.

[28] R. K. Dishman, Y. Nakamura, M. E. Garcia, R. W. Thompson, A. L. Dunn, and S. N. Blair, “Heart rate variability , trait anxiety , and perceived stress among physically fit men and women,” *Int. J. Psychophysiol.*, 2000.

[29] M. Haak and B. C. Interface, “Detecting stress using eye blinks and brain activity from eeg signals.”

[30] R. H. V. D. S. Olivier and Æ. C. D. P. Van Hullenaar, “Ergonomics , user comfort , and performance in standard and robot-assisted laparoscopic surgery,” *Surg. Endosc.*, pp. 1365–1371, 2009.

[31] R. Berguer, W. D. Smith, and Y. H. Chung, “Performing laparoscopic surgery is significantly more stressful for the surgeon than open surgery,” *Surg. Endosc.*, pp. 1204–1207, 2001.

[32] P. Manoilov, “EEG Eye-Blinking Artefacts Power Spectrum Analysis,” pp. 1–5, 2006.

[33] T. Partala and V. Surakka, “Pupil size variation as an indication of affective processing processing,” *Int. J. Hum. Comput. Stud.*, no. July, 2003.

[34] M. Yuliya Y. Yurko, P. Mark W. Scerbo, M. Ajita S. Prabhu, B. Christina E. Acker, and P. Dimitrios Stefanidis, MD, “Higher Mental Workload is Associated With Poorer Laparoscopic Performance as Measured by the NASA-TLX Tool,” vol. 5, no. 5, pp. 267–271, 2010.

[35] A. C. Satoru Tokuda, Goro Obinata, Evan Palmer, “Estimation of mental workload using saccadic eye movements in a free-viewing task in a Free-Viewing Task,” *EMBC*, no. August, 2011.

[36] M. W. Scerbo, R. C. Britt, and D. Stefanidis, “Differences in mental workload between traditional and single- incision laparoscopic procedures measured with a secondary task,” *Am. J. Surg.*, vol. 213, no. 2, pp. 244–248, 2017.

[37] S. Arora, T. Tierney, N. Sevdalis, A. Darzi, and R. Kneebone, “The Imperial Stress Assessment Tool (ISAT): A Feasible , Reliable and Valid Approach to Measuring Stress in the Operating Room,” *World J. Surg.*, pp. 1756–1763, 2010.

[38] R. Nicolas, F. Dehais, E. Rachelson, C. Thooris, S. Pizziol, and C. Tessier, “Formal

Detection of Attentional Tunneling in Human Operator – Automation Interactions," *IEEE*, vol. 44, no. 3, pp. 326–336, 2014.

[39] G. Durantin, J. Gagnon, S. Tremblay, and F. Dehais, "Using near infrared spectroscopy and heart rate variability to detect mental overload," *Behav. Brain Res.*, vol. 259, pp. 16–23, 2014.

[40] G. Toti, M. Garbey, V. Sherman, B. L. Bass, and B. J. Dunkin, "A Smart Trocar for Automatic Tool Recognition in Laparoscopic Surgery," 2015.

[41] Mobius, "Instruction Manual for the Mobius ActionCam Video-Out."

[42] A. Al-rahayfeh and M. F. Member, "Eye Tracking and Head Movement Detection : A State-of-Art Survey," *IEEE J. Transl. Eng. Heal. Med.*, no. November, 2013.

[43] TheEyeTribe, "Eye Tracking." [Online]. Available: http://aws-website-theeyetribe-lbmoo.s3-website-us-east-1.amazonaws.com/dev.theeyetribe.com/dev.theeyetribe.com/general/index.html.

[44] Hexoskin Website, "Hexoskin smart shirt specifications." [Online]. Available: https://www.hexoskin.com/pages/health-research.

[45] Hexoskin, "Hexoskin API Documentation." .

[46] A. P. Buccino, "Development of a hybrid EEG-NIRS Brain-computer interface for multiple motor tasks," no. August, 2015.

[47] Cognionics, "Quick-20 Dry EEG Headset Datasheet."

[48] BioNumbers, "Average duration of a single eye blink." [Online]. Available: http://bionumbers.hms.harvard.edu/bionumber.aspx?id=100706&ver=0.

[49] N. Aroua, "Using Wireless dry EEG System to Detect Mental Workload during Mental Arithmetic," 2016.